ANALYSIS OF THE PROPAGATION OF UTERINE ELECTRICAL ACTIVITY APPLIED TO PREDICT PRETERM LABOR

Mahmoud Hassan

▶ To cite this version:

HAL Id: tel-01368042
https://hal.archives-ouvertes.fr/tel-01368042

Submitted on 18 Sep 2016

Mahmoud Hassan

« Université de Technologie de Compiègne (UTC, France) Reykjavik University (RU, Islande)/ »

<u>Titre</u> :

Etude de la propagation de l'activité électrique utérine dans une optique clinique : Application à la détection des menaces d'accouchement prématuré.

Thèse soutenue le 7 Juin 2011, devant les membres du jury :

<u>Jury :</u>

Thierry Denoeux (Président)
Prof., Université de Technologie de Compiègne (UTC) - Compiègne, France
Catherine Marque (Directrice de thèse)
Prof., Université de Technologie de Compiègne (UTC) - Compiègne, France
Brynjar Karlsson (C-directeur de thèse)
Assistant Prof., Háskólinn í Reykjavík (HR) – Reykjavik, Iceland
Lotfi Senhadji (Rapporteur)
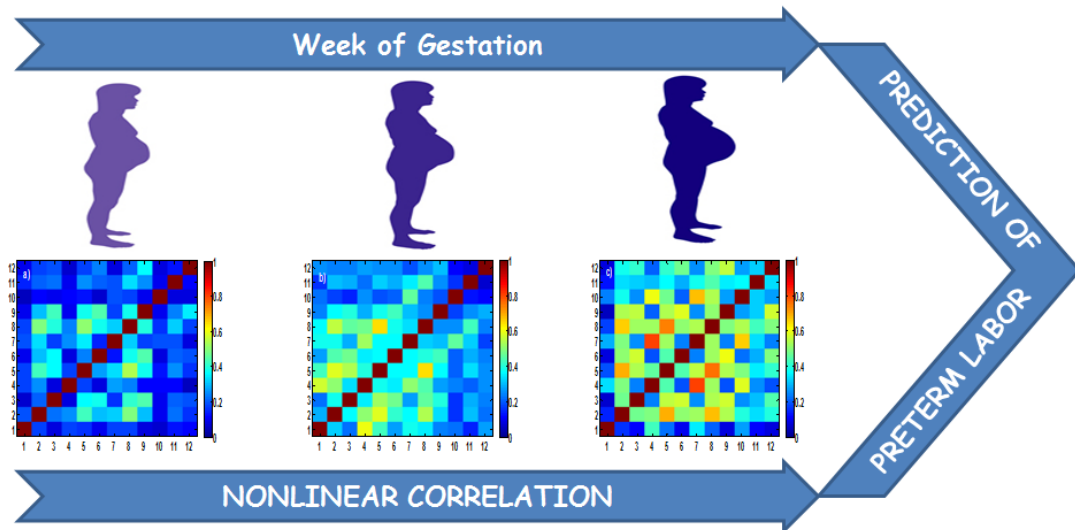*Prof., LTSI, Université de Rennes1- Rennes, France.*
Sergio Cerutti (Rapporteur)
Prof., Politecnico di Milano- Milano, Italy
Sofiane Boudaoud (Examinateur)
Assistant Prof., Université de Technologie de Compiègne (UTC)-France

ANALYSIS OF THE PROPAGATION OF UTERINE ELECTRICAL ACTIVITY APPLIED TO PREDICT PRETERM LABOR

Mahmoud HASSAN

Thierry Denoeux (*president*)

Prof., Université de Technologie de Compiègne (UTC) - Compiègne, France

Catherine Marque (*Supervisor*)

Prof., Université de Technologie de Compiègne (UTC) - Compiègne, France

Brynjar Karlsson (*Supervisor*)

Assistant Prof., Háskólinn í Reykjavík (HR) – Reykjavik, Iceland

Lotfi Senhadji (*Reviewer*)

Prof., LTSI, Université de Rennes1- Rennes, France.

Sergio Cerutti (*Reviewer*)

Prof., Politecnico di Milano- Milano, Italy

Sofiane Boudaoud (*Examiner*)

Assistant Prof., Université de Technologie de Compiègne (UTC)-France

To…

Résumé en français

Titre

Etude de la propagation de l'activité électrique utérine dans une optique clinique : Application à la détection des menaces d'accouchement prématuré

Introduction:

Il reste beaucoup de questions ouvertes concernant le fonctionnement de l'utérus humain. L'une de ces questions est comment l'utérus fonctionne en tant qu'organe organisé pour générer une contraction synchrone et expulser un nouvel être humain dans ce monde ? Si nous ne comprenons pas comment l'utérus fonctionne, quand il fonctionne normalement, il est évident que nous ne serons pas en mesure d'intervenir ou de prévoir quand, avec parfois des conséquences tragiques, il ne fait pas son travail correctement et qu'un enfant nait avant d'être prêt !

Le but de notre recherche est de comprendre ce que l'activité électrique de l'utérus peut nous apporter sur la prévention du risque de naissance prématurée, de mieux comprendre comment fonctionne l'utérus et de bénéficier de ces connaissances pour développer un outil qui peut être utilisé pour la détection de l'accouchement et la prédiction du travail prématuré.

Cette idée d'utiliser l'activité électrique détectée à la surface de l'abdomen (ou électrohystérogramme EHG) pour prédire un accouchement prématuré n'est pas nouvelle et beaucoup de travaux ont déjà été mis en œuvre. La nouvelle approche dans ce travail n'est pas d'utiliser le signal recueilli par un ou deux endroits isolés sur l'abdomen de la future mère, mais de cartographier la propagation des signaux et d'explorer l'auto organisation des contractions. Nous utilisons donc une matrice d'électrodes pour nous donner une image beaucoup plus complète de l'organisation et du fonctionnement de l'utérus.

L'accouchement est le processus physiologique par lequel le fœtus est expulsé de l'utérus vers le monde extérieur. Il est défini comme la survenue de contractions utérines régulières accompagnées de l'effacement du col et de la dilatation cervicale. Dans le travail normal, les contractions de l'utérus et la dilatation du col sont précédées par des changements biochimiques du tissu conjonctif du col utérin.

Le travail prématuré, défini comme le travail avant la fin de la 37e semaine de gestation, est toujours la complication obstétricale la plus fréquente pendant la grossesse, avec 20% de toutes les femmes enceintes à haut risque d'accouchement prématuré. Aux États-Unis, plus d'un demi-million de bébés sont nés prématurément chaque année. Les soins intensifs néonataux coûtent 500 $ par jour, ce qui constitue des dépenses de plus de 4 milliards de dollars chaque année. En outre, le travail prématuré est la cause principale pour 85% de la mortalité infantile et pour 50% des troubles neurologiques infantiles (2009). La naissance prématurée peut survenir après soit un travail spontané avec membranes intactes, soit une rupture prématurée des membranes, soit un déclenchement du travail ou un accouchement par césarienne pour indication maternelle ou fœtale (Denney et al., 2008). La pathogénie du travail prématuré spontané n'est pas bien comprise. Les contractions prématurées spontanées peuvent être provoquées par une activation précoce du processus normal du travail ou par d'autres causes pathologiques inconnues (Denney et al., 2008; Leman et al., 1999)

Une des clés pour traiter efficacement le travail prématuré est sa détection précoce. Si le travail prématuré est décelé tôt, les médecins peuvent tenter d'arrêter le processus de travail, ou en cas d'échec, sont mieux préparés à gérer le nouveau-né prématuré.

Le développement de méthodes efficaces pour prévenir l'accouchement prématuré dépend de la compréhension des mécanismes qui déclenchent le travail. La tâche la plus difficile et importante aujourd'hui pour des médecins en soins de maternité est sans aucun doute le diagnostic du travail. Savoir que le vrai travail (qui aboutira à l'accouchement) a commencé, ainsi que prédire quand il va commencer, est important pour toutes les grossesses, normales et pathologiques. D'autre part, la prévision précise et le diagnostic du travail prématuré spontané permettrait également aux cliniciens de débuter le traitement chez des femmes en vrai travail, et d'éviter les traitements inutiles ainsi que l'hospitalisation chez les femmes qui ont simplement des contractions prématurées, mais qui ne sont pas en vrai travail. La prévision du travail pour les grossesses normales est aussi très importante car elle permettrait de réduire les hospitalisations, les interventions et les dépenses inutiles.

L'électrohysterographie (EHG) est la mesure non invasive de l'activité électrique sous-jacente de l'utérus. Le premier signal EHG rapporté dans la littérature a été mesurée en 1931 par la déviation d'une aiguille galvanométrique au cours d'une contraction utérine (Bode, 1931). De nombreuses études ont prouvé que l'enregistrement externe de l'activité électrique de l'utérus pendant les contractions peut être une alternative intéressante aux enregistrements

traditionnels de surveillance de la grossesse. En outre, au cours des dernières années, l'EMG utérin est devenu l'objet de nombreuses études, et s'est avéré très intéressant, car il offre un meilleur aperçu de la progression de la grossesse et du début du travail (Devedeux et al., 1993; Garfield et al., 2002; Garfield et al., 1998b). Ainsi, ce signal, détecté aussi tôt que 18 semaines de gestation, peut fournir une méthode non-invasive plus objective et plus précise que les méthodes actuelels (tocographie externe) pour le suivi des grossesses et la prédiction du travail (Devedeux et al., 1993). Ainsi, le signal EHG peut non seulement remplacer les méthodes invasives ou inexactes qui sont actuellement employées pour la surveillance des contractions pendant la grossesse ou le travail, mais pourrait également fournir un outil pour prédire l'accouchement.

Les études ont souvent été focalisées sur le développement de techniques de traitement du signal dédiées, qui permettent la détection et l'interprétation de paramètres de pertinence clinique. De nombreux paramètres dérivés du signal EHG ont été considérés, tant dans l'espace tempotel (Marque et al., 1986; Verdenik et al., 2001) que spectral (Garfield et al., 2005; Maner et al., 2003; Marque et al., 1986). Des études cliniques de grande envergure sont nécessaires pour comprendre la relation existant entre les paramètres dérivés du signal EHG et les processus conduisant à la contractilité utérine, ce qui reste un défi considérable.

Les phénomènes physiologiques sous-jacents au travail (prématuré ou à terme) restent mal compris. Il est bien connu que la contractilité utérine dépend de l'excitabilité des cellules utérines mais aussi de la propagation de l'activité électrique à l'utérus entier (Devedeux et al., 1993).

Ces deux aspects, l'excitabilité et la propagation, influencent à la fois sur le contenu spectral de l'EHG, composé principalement de deux composantes fréquentielles, traditionnellement dénommée FWL (Fast Wave Low) et FWH (Fast Wave High). Ces composants fréquentielles sont supposées être liées à la propagation et à l'excitabilité de l'utérus, respectivement (Devedeux et al., 1993).

La majorité des méthodes utilisées dans la littérature pour la prédiction du travail prématuré utilisent le plus souvent l'analyse du contenu haute fréquence de l'EHG. Certaines modifications des caractéristiques des signaux EHG a été observé lors de l'accouchement. Les potentiesl d'actions responsables de contractions ont été signalés comme plus fréquentes et leur durée plus constante dans le travail (Maner and Garfield, 2007). Une augmentation de

l'amplitude et de la fréquence des signaux EHG, évaluée par l'analyse du spectre de puissance, a également été observée avant le travail (Maner et al., 2003).

Ces méthodes ne sont cependant pas utilisées en pratique courante actuelle en raison d'une forte variance des résultats obtenus et d'un taux de prédiction insuffisant. Prendre en compte à la fois les informations d'excitabilité et de propagation pourrait aider à augmenter la capacité de prédiction de l'EHG pour l'identification des menaces d'accouchement prématuré.

A notre connaissance, seule l'étude de Lucovnik et al. (Lucovnik et al., 2011) s'est concentrée sur la caractérisation de la propagation de l'activité électrique pour la détection et la prédiction du travail prématuré. Leurs résultats sont certes importants et très encourageants. Mais ils ne se sont appuyés, dans l'étude présentée, que sur une évaluation approximative de la vitesse de propagation apparente. L'objectif de ce travail est l'analyse de la propagation de l'activité électrique utérine en vue d'une application clinique.

Notre contribution à ce domaine s'articule autour de quatre thèmes principaux:

 1. **Analyse Monovariée**: utilisation de techniques Monovariées pour étudier les caractéristiques non linéaires des signaux EHG ; test de la capacité de ces méthodes à classifier les signaux de grossesse et d'accouchement.

2. **Analyse Bivariée**: utilisation des méthodes de détection des relations entre les signaux enregistrés à différents endroits pour une contraction donnée. Les relations d'amplitude et de phase seront explorées dans le domaine temporel et temps-fréquence.

3. **Analyse multivariée**: exploitation des enregistrements multicanaux des signaux EHG, par modélisation autorégressive à plusieurs variables, pour tenir compte de toutes les connexions possibles entre les signaux disponibles.

4. **Débruitage des signaux EHG monopolaires**: un véritable défi est la contamination des signaux EHG monopolaires par différentes sources de bruit. Nous visons ici à développer un algorithme qui peut éliminer les artefacts des signaux EHG monopolaires afin d'obtenir un rapport signal / bruit suffisant pour utiliser ces signaux dans l'analyse de la propagation.

Objectifs de thèse et de l'organisation du manuscrit

L'objectif global de cette thèse est d'étudier le phénomène de propagation de l'activité utérine contractile de l'utérus. Les résultats attendus seront utilisés à la fois à enrichir les

connaissances scientifiques dans ce domaine et d'essayer d'améliorer les performances de la prédiction de la prématurité chez les femmes.

Dans cet objectif, basé sur les travaux sur l'EEG (électroencéphalogramme), nous avons exploré la possibilité d'analyser la synchronisation des différentes parties de l'utérus à différents moments pendant la grossesse et le travail. Le nombre de méthodes disponibles pour analyser les relations entre signaux a fortement augmenté au cours des dernières années. Ces méthodes peuvent être divisées en deux types selon les suppositions sous-jacentes de la dépendance entre les signaux: (i) les méthodes linéaires comprennent la corrélation croisée linéaire et la fonction de cohérence (ii) les méthodes non linéaires comprennent le coefficient de corrélation non linéaire, la synchronisation de phase et les méthodes issues de la physique et la théorie du chaos. De plus, il y a une forte probabilité que les relations entre les signaux utérins sont non stationnaires, en particulier dans le cas des signaux de travail. Pour cette raison, une partie de notre analyse des relations EHG est consacrée à l'approche temps-fréquence en utilisant la transformée en ondelettes, afin de respecter autant que possible la non stationnarité des signaux.

La monographie est organisée comme suit:

• **Dans le chapitre 1**, nous présentons un bref état de l'art sur les aspects anatomique et physiologique de l'activité utérine. Ensuite, nous décrivons les différentes études de propagation qui ont été faites dans le passé ainsi que le protocole expérimental utilisé pour obtenir les signaux utilisés dans ce travail.

• **Dans le chapitre 2**, nous analysons les caractéristiques non linéaires des signaux utérins pendant la grossesse et le travail. Trois méthodes non linéaires, la réversibilité du temps, l'entropie approximative et la correntropy, sont comparées sur des signaux synthétiques. La comparaison a démontré la supériorité de la réversibilité du temps pour la détection de la linéarité et la non-linéarité des différents signaux. Ensuite, la méthode avec la plus haute performance (réversibilité du temps) est appliquée à des signaux réels EHG. Les résultats ont montré que les contractions utérines pendant la grossesse sont réversibles, alors que des contractions de travail sont temporellement irréversibles. Les résultats obtenus montrent que la réversibilité du temps pourrait devenir un outil puissant pour distinguer entre les contractions pendant grossesse et les contractions de l'accouchement dans une optique clinique.

• **Dans le chapitre 3**, nous présentons les méthodes permettant l'analyse des relations linéaires et non linéaires entre signaux. Les résultats obtenus par l'application de ces méthodes pour étudier la différence de synchronisation entre la grossesse et le travail montrent que les signaux durant l'accouchement sont plus corrélés que les signaux de grossesses. De plus, l'évolution de la synchronisation avec le terme a montré une augmentation de la corrélation en amplitude et une désynchronisation en phase en passant de grossesse à l'accouchement. L'utilisation des enregistrements multicanaux lors de l'analyse de cette synchronisation a démontré une plus grande efficacité de ces méthodes appliquées à tous les canaux que lorsqu'un seul canal est utilisé. Puis nous avons étudié les relations entre les contractions utérines dans le domaine temps-fréquence (TF). Nous avons utilisé des méthodes estimées à partir de la transformée en ondelettes pour calculer séparément ou simultanément l'amplitude TF et/ou la relation de phase. Nous proposons également une méthode basée sur les données des 'surrogates' pour obtenir de la significativité de la relation détecté. Les résultats ont montré une plus grande cohérence dans les basses fréquences que les hautes fréquences des signaux EHG, soutenant l'hypothèse que les basses fréquences ont une relation plus forte à la propagation que les hautes fréquences. En plus, les résultats ont confirmé les observations de l'augmentation de corrélation d'amplitude et de synchronisation de phase, passant de la grossesse à l'accouchement.

En gros, les résultats ont montré que toutes les méthodes de 'détection de relation entre les signaux' peuvent être des outils puissants pour classer les contractions de grossesse et d'accouchement.

• **Le chapitre 4** est consacré à l'analyse multivariée des signaux multicanaux utérins. Nous avons testé le modèle autorégressif multivariée (MVAR) sur des signaux synthétiques et réels, et proposé une version préliminaire d'adaptation (W-MVAR). Le modèle proposé a été testé sur des signaux synthétiques ainsi que des signaux réels. Sur les signaux synthétiques, W-MVAR a présenté de meilleures performances pour la détection des relations entre les signaux lorsque les caractéristiques non-stationnaires sont présentes dans les signaux.

L'application de la MVAR et W-MVAR sur les signaux EHG a clairement démontré que le W-MVAR est beaucoup plus efficace dans la différenciation des signaux grossesse et l'accouchement que le MVAR.

• **Dans le chapitre 5**, nous présentons un nouvel algorithme de débruitage des signaux EHG monopolaire. Tous les travaux présentés dans les chapitres précédents a été fait en utilisant

des signaux bipolaires. Ces signaux ont donné de bons résultats, mais présentent des limites pour les études sur la localisation ou la directivité de l'activité utérine. Une combinaison entre la Séparation aveugle de sources fondée sur la corrélation canonique (BSS_CCA) et la Décomposition en Mode Empirique pour le débruitage du signal EHG est proposée dans ce chapitre et y est quantitativement et qualitativement analysé. La méthode consiste en deux étapes. Tout d'abord, BSS_CCA a été utilisé pour extraire les bouffes utérines en présence de bruit de forte intensité dans la même bande de fréquence que le signal. Ensuite, les signaux sont donnés un dernier «nettoyage» en appliquant EMD. Les résultats ont montre que notre algorithme est très efficace pour éliminer les différents sources de bruits contaminant les signaux EHG.

Les premiers essais d'analyse de synchronisation sur ces signaux monopolaires débruités sont ensuite présentée une augmentation de la corrélation avec le terme (ce qui confirme les résultats obtenus par les signaux bipolaires) mais aussi une vue spatiale des zones de fortes corrélation qui pourrait être utilisé pour la localisation de l'activité électrique uterine.

• Une discussion et des conclusions générales à cette thèse sont données dans le **chapitre 6**, avec des propositions pour les travaux futurs.

Les résultats obtenus dans cette thèse ont été publiés dans 4 articles de revues et 10 comptes rendus de conférence.

Contents

Chapter 0 Introduction

There are many open questions concerning the functioning of the human uterus. One of these open questions concerns exactly how the uterus operates as an organ to perform the very organized act of contracting in a synchronized fashion to expulse a new human into this world. If we don't understand how it works when it is working normally, it is obvious that we will not be as capable of intervening or preventing when, sometimes with tragic consequences, it does not do its job properly and a child is born before it is ready.

The aim of our research is to be able to understand what the electrical activity of the uterus can tell us about the risk of premature birth, to understand better how the uterus works and to benefit from these understanding to find tool that can be used for labor detection and prediction of preterm labor.

This idea of using the externally detected electrical activity of the uterus (electrohysterogram or EHG) to predict preterm labor is not new and lot of work has already been put into it. The novel approach in this work is not to use the signal collected from one or two isolated places on the expectant mother's abdomen but to map the propagation of the signals and to investigate the auto organization of the contractions. We therefore use a matrix of electrodes to give us a much more complete picture of the organization and operation of the uterus as pregnancy reaches its conclusion.

Labor is the physiologic process by which a fetus is expelled from the uterus to the outside world and is defined as regular uterine contractions accompanied by cervical effacement and dilatation. In the normal labor, the uterine contractions and cervix dilatation are preceded by biochemical changes in the cervical connective tissue.

Preterm labor, defined as labor before completing the 37th week of gestation, is still the most common obstetrical complication during pregnancy, with 20% of all pregnant women at high risk of preterm labor. In the United States, more than half a million babies -that's 1 over 8- are born premature each year. At $500 a day for neonatal intensive care, this constitutes expenditure well over $4 billion each year. Also, preterm labor accounts for 85% of infant mortality and 50% of infant neurologic disorders (2009). The premature birth can occur after spontaneous labor with intact membranes, preterm premature rupture of the membranes, as

well as labor induction or caesarean delivery for maternal or fetal indications (Denney et al., 2008). The pathogenesis of spontaneous preterm labor is not well understood: spontaneous preterm contractions may be caused by an early activation of the normal labor process or by other (unknown) pathological causes (Denney et al., 2008; Leman et al., 1999).

One of the keys to treat efficiently preterm labor is its early detection. If preterm labor is detected early, medical specialists can attempt to stop the labor process, or if unsuccessful, are better prepared to handle the premature infant.

The development of effective methods to prevent preterm birth depends upon the understanding of the mechanisms that initiate labor. Perhaps the most difficult and important task facing medical practitioners in maternity care today is the diagnosis of labor. Knowing that true labor (which will lead to delivery) has begun, as well as predicting when it will start, is important for both normal and pathological pregnancies. On the other hand, accurate prediction and diagnosis of spontaneous preterm labor will also allow clinicians to start any necessary treatment earlier in women with true labor, and avoid unnecessary treatment and hospitalization in women who are simply having preterm contractions, but who are not in true labor. Even noticeable dynamic cervical change may not be an accurate indicator of true labor, as a large percentage of women with established cervical change do not deliver preterm when not treated with tocolytics (Linhart et al., 1998). Prediction of labor in normal pregnancies is very important as well as it can minimize unnecessary hospitalizations, interventions and expenses.

Electrohysterography (EHG) is the noninvasive measurement of the electrical activity underlying uterine contractions. The first EHG signal ever reported in the literature was measured in 1931 as the deflection of a galvanometric needle during a uterine contraction (Bode, 1931). Many studies have proved that the external recording of the electrical activity of the uterus during contractions can be an attractive alternative to traditional recordings for pregnancy monitoring. Furthermore, over the last years, uterine EMG has become the object of many studies, and has been proven to be of interest as it offers a better insight into the progression of pregnancy and the onset of labor (Devedeux et al., 1993; Garfield et al., 2002; Garfield et al., 1998b). Thus, this signal, detected as early as 18 weeks of gestation, may provide a non-invasive, more objective and accurate method for pregnancy monitoring and prediction of labor (Devedeux et al., 1993). Thus, EHG may not only replace the invasive or inaccurate methods that are currently employed for contraction monitoring during pregnancy and labor, but could also be an alternative tool for predicting delivery.

The studies have often been focused on the application of the EHG into a useful clinical application. More precisely, the researches concentrate on developing dedicated signal analysis techniques that permit detection and interpretation of parameters of clinical relevance. Many parameters derived from the EHG signal have been considered, both in time (Garfield et al., 1998b; Marque et al., 1986; Verdenik et al., 2001) and in frequency domains (Doret et al., 2005; Garfield et al., 2005; Maner et al., 2003; Marque et al., 1986; Verdenik et al., 2001). This remains a considerable challenge. Extensive clinical studies are required for understanding the relation between the parameters derived from the EHG signal and the processes leading to labor.

The physiological phenomena underlying labor remain however badly understood. It is well known that uterine contractility depends on the excitability of uterine cells but also on the propagation of the electrical activity to the whole uterus (Devedeux et al., 1993).
These two aspects, excitability and propagation, both influence the spectral content of EHG, mainly composed of two frequency components traditionally referred to as FWL (Fast Wave Low) and FWH (Fast Wave High). These frequency components may be related to the propagation and to the excitability of the uterus respectively (Devedeux et al., 1993).
The majority of methods used in the literature for preterm labor prediction most often use only the analysis of the high frequency content of the EHG. A change in the characteristics of EHG signals has been observed at delivery (Buhimschi et al., 1998; Buhimschi and Garfield, 1996; Devedeux et al., 1993; Garfield et al., 1998a; Garfield et al., 1998b; Marque et al., 2007; Vinken et al., 2009). Bursts of electrical signals responsible for contractions have been reported to be more frequent and their duration more constant in labor (Buhimschi et al., 1997; Maner and Garfield, 2007). An increase in peak amplitude and frequency of EHG signals, assessed by powers spectrum analysis, has also been observed prior to labor (Maner et al., 2003; Marque et al., 1986).

 These methods are however not currently used in routine practice due to a high variance of the results obtained and an insufficient prediction rate. Taking into account both the excitability and propagation information may help to increase the prediction capability of the EHG for preterm labor threat identification.

Only the study by Lucovnik et al. (Lucovnik et al., 2011) has to our knowledge concentrated on characterizing the propagation of electrical activity in the labor detection and prediction of preterm labor. Their results are certainly important and very encouraging. But they are only

based on a rough evaluation of the speed of the propagation as far as they reveal in their paper. The aim of this work is the propagation analysis of uterine electrical activity in the view of clinical application.

Our contribution to this field is structured around four main themes:

1. **Monovariate Analysis**: Use of monovariate techniques to investigate the nonlinear characteristics in the EHG signals and then test the capacity of these methods to classify pregnancy and labor signals.

2. **Bivariate Analysis**: Study the methods detecting the relationships between signals recorded at different locations for a given contraction. Amplitude and phase relationships will be exploited in the time and time-frequency domain.

3. **Multivariate analysis**: Model the multichannel EHG recordings with multivariate autoregressive modeling to take into account all the possible connections between the available channels.

4. **Denoising Monopolar EHG signals**: A real challenge is the contamination of monopolar EHG signals by different noise sources. We aim to develop algorithm which can remove artifacts from monopolar EHG signals in order to get a signal/noise adequate to use these signals for propagation analysis.

Thesis objectives and organization of this monograph

The global aim of this thesis is to study the phenomenon of propagation of the uterine contractile activity of the uterus. The expected results will be used both to enrich scientific knowledge in this field and to try to improve the performance of the prediction of preterm birth in women.

In this aim, based on work done on the brain, we have explored the possibility of analyzing the synchronization of different parts of the uterus at different times during pregnancy and labor.

The number of available methods for analyzing signal relationships has greatly increased in the last few years. These methods can be divided into two types depending on the underlying suppositions of dependence between signals: (i) Linear methods include the linear cross-correlation and the coherence function (ii) Nonlinear methods include the nonlinear correlation coefficient, the phase synchronization and methods coming from physics and chaos theory.

There is a high probability that the relations between the uterine signals are non stationary, especially in the case of labor signals. For this reason, a part of our EHG relationships analysis will be devoted to time-frequency approach by using the wavelet transform in order to respect as much as possible the non stationarity of the signals.

The monograph is organized as follows:

- In Chapter 1 we present the state of the art of anatomical and physiological background of the uterine activity. Then we describe the different propagation studies that have been done in the past as well as the experimental protocol used to obtain the signals used throughout this work.

- In Chapter 2 we introduce the nonlinear characteristics of the uterine signals during pregnancy and labor. Three nonlinear methods, Time reversibility, approximate entropy and correntropy, are compared on synthetic signals. Then the method with the highest performances is applied to the real EHG signals.

- In chapter 3 we present the linear and nonlinear relationship methods. This chapter describes the results obtained from the application of these methods to investigate the difference in synchronization between pregnancy and labor. Moreover, we present the evolution of the synchronization with term, as well as the greater efficiency of multichannel recordings when analyzing this synchronization. Then we investigate the relationships between the uterine contractions in the Time-Frequency (TF) domain. We used methods estimated by the wavelet transform to compute separately or simultaneously the TF amplitude and/or phase relation. We also propose a method based on surrogates data to get the significance of the relationship detection.

- Chapter 4 is devoted to the multivariate analysis of the uterine multichannel signals. We tested the Multivariate Autoregressive Model (MVAR) on synthetic and real signals and we propose a preliminary adaptive version (AMVAR).

- In Chapter 5 we present a novel algorithm to denoise the EHG monopolar signals. All the work presented in the preceding chapters was done by using bipolar signals. They gave good results, but were not useful when investigating the localization or directivity of the uterine activity. A combination between Blind source Separation and Empirical Mode Decomposition for de-noising the EHG signal is proposed in this chapter and is quantitatively and qualitatively analyzed.

- Discussion and general conclusions of this thesis are given in Chapter 6 with propositions for possible future work.

The results obtained in this thesis have been published in several journal papers and conference proceedings.

Chapter 1 Uterine electrical activity propagation: An overview

1.1 Introduction

The aim of the thesis is the analysis of the propagation of the uterine electrical activity (EHG) during pregnancy and labor in the view of detecting labor and predicting preterm labor. The physiological phenomena underlying labor are however still not completely understood. It is well known that uterine contractility depends on the excitability of uterine cells but also on the propagation of the electrical activity to the whole uterus. Predicting preterm delivery is currently achieved mainly by analysis of parameters representative of uterine excitability. Very few studies have been interested in characterizing the propagation of electrical activity in the aim of detecting preterm labor.

One of the powerful ways to analyze signals propagation (such as propagation of electroencephalogram signals in the brain) is the analysis of the relationships between signals recorded at different locations. Before describing these methods and their applications, we introduce the physiological background of the uterus, the factors that influence the uterine contractility and especially the factors that regulate the uterine signal propagation. At the end of this chapter we present an overview of the different propagation analysis that have been done on EHG, the multichannel recordings used in prior work by others. Then we describe our own experimental protocol used to acquire the signals used throughout this thesis.

1.2 Anatomical and physiological background

1.2.1 Uterus

The uterus occupies an anterior and central position in the pelvis. In its non pregnant state, the uterus weighs between 30 and 80 g. The uterus lies midway between the urinary bladder and the rectum.

The uterus is a hollow, pyriform, muscular structure measuring 7 to 8 cm in length, 4 to 5 cm in width at its upper portion, and 2 to 3 cm in thickness. The uterus is divided into three portions: cervix, corpus, and fundus (Baggish et al., 2007). The narrowed area between the

cervix and body is called the isthmus and corresponds to the level of the internal os or the opening between the cervical canal and the uterine cavity (**Figure** 1.1).

In most species, the uterine wall is composed of three distinct layers: an inner layer, the endometrium that lines the lumen of the organ an intermediate layer, the myometrium, and an external layer, the perimetrium. The endometrium is the uterine innermost membrane which thickens in preparation for the implantation of a fertilized egg upon its arrival into the uterus. The myometrium is the middle and thickest layer of the uterus. It is composed of longitudinal and circular layers of smooth muscle. During pregnancy the myometrium increases both by hypertrophy of the existing cells and by multiplication of the cell number. When parturition takes place, coordinated contractions of the smooth muscle cells in the myometrium occur to expel the fetus out of the uterus. After delivery the myometrium contracts to expel the placenta. The serosa or peritoneum is the outermost layer of the uterus. This serosa is a multilayered membrane that lines the abdominal cavity and supports and covers the organs.
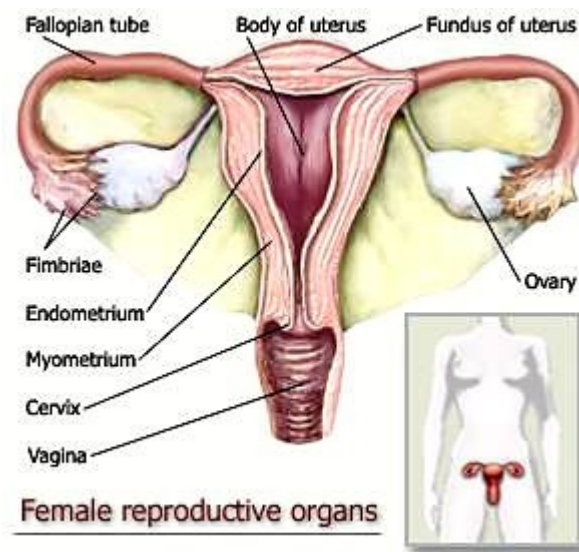
Figure 1.1: The three major subdivisions of the uterus are clearly identified: cervix, corpus, and fundus. The thickest musculature is seen in the corpus and fundus.

The smooth cells increase progressively in size during the last stage of gestation with a maximum length of 300 μm and a maximum width of 10 μm (Csapo, 1962). Contractions of smooth muscle cells happen during the interaction of myosin and actin filaments.

1.2.2   Uterine cell excitability

The electrical activity of the uterus can be described by means of two types of potential: the resting potential and the action potential. The resting potential is the difference between the negative inside and the positive outside of a cell. When recording the electrical activity of a membrane, the resting potential is unstable. It presents slow waves that are low amplitude and long duration variations, responsible for the electrical base lines. However, when the resting potential of a cell depolarizes, the potential difference across the cell membrane reverses. The resting potential becomes more and more positive and eventually reaches a certain threshold; when reaching this threshold, a burst of action potentials is generated. In this case, action potentials appear as fast waves superimposed on the slow waves. These action potentials are generated spontaneously. Their shape and characteristics vary during pregnancy, from a single spike, an irregular train of action potentials, to a regular train of action potentials observed at the end of term. The alternance between resting state and repetitive single spikes is denoted bursting behavior. This is especially observed at end of gestation(Sanborn, 1995).

During pregnancy, uterine cells are generally quiescent and characterized by a resting membrane potential varying slightly under hormonal influence. It passes throughout pregnancy from -60 mV at mid-term to -45 mV at term (Coleman and Parkington, 1990; Sanborn, 1995). In some uterine cells, the pacemaker cells, a spontaneous depolarization occurs, added to the resting membrane potential.

The frequency of the burst discharges and the number of spikes in each burst vary considerably, and are largely influenced by hormonal and gestational factors, as well as by pharmacological agents. Burst discharge frequency and spikes frequency within bursts present values for rat at term (1.2 bursts/min and 1.5 spikes/sec respectively) (Garfield, 1994; Miller et al., 1989) that are different from the ones at earlier stages of pregnancy (0.45 burst/min and 4 spikes/sec, respectively). The duration of bursts is shorter at delivery (21.5 sec), when compared to earlier stages of pregnancy (32 sec) (Garfield, 1994; Miller et al., 1989). On a single cell level, myometrial single action potential (AP) recorded after a short depolarizing pulse has a duration of approximately 133 msec (Kao and McCullough, 1975). In response to longer depolarizing pulse, a burst of action potential is observed and the AP duration is increased to approx. 200−250msec. The increase in the action potential amplitude due to the longer depolarizing pulse can be explained by the different time constants of each individual myometrial cells and the charges concentrated in the capacitance membrane of the

myometrial cell. The spiking activities present peak amplitude of 54.6 mV in depolarized cells (Kao and McCullough, 1975). The main myometrial ionic channels that regulate the cell excitability are the sodium voltage dependant channels, Calcium voltage dependant channels, potassium channels and chloride channels.

Another important factor that plays a main role in the generation of myometrial electrical activity is the intracellular calcium. Ca^{2+} may be seen as the main transporter of charges in a uterine cell. Ca^{2+} plays a major role in the modulation of the EHG throughout pregnancy. Like in other smooth muscles, the contractility of uterine muscle cells is largely dependent on the intracellular free calcium concentration. The rise in $[Ca^{2+}]_i$ (intracellular Ca^{2+} concentration) occurs when efficient stimulation is applied inducing a major entry of Ca^{2+} ions into the uterine cell through the L-type Ca^{2+} channels (Shmigol et al., 1998). The efflux or the decrease in the intracellular calcium concentration needed to membrane repolarisation is controlled by different mechanisms such as calcium pumps, Na^+/Ca^{2+} exchangers and calcium sequestration by the intracellular compartments.

1.2.3   **Propagation of the uterine electrical activity**

In skeletal muscles, the contraction is initiated by the nervous system. The motoneuron initiates an action potential that propagates through the neuromuscular junction to the muscle end plate, ultimately causing the muscle fiber to contract. Neuromuscular junctions of the highly structured type of skeletal muscle do not occur in smooth muscle.

At the opposite, control of uterine contractility is mainly myogenic, the muscle is solely responsible for its contraction, although intrinsic control (mechano-receptor ...) and extrinsic (sympathetic and parasympathetic system) are present. The organization of the uterine muscle is an important factor in its contractility.

All myocytes (uterine muscle cells) are collected close in a package or "bundle" (Ø 300 + / - 100 microns) with junctions between them. Packets are contiguous within a bundle or Fasciculus. Adjacent beams are connected by communicating bridge cells. A diagram of this structural organization is shown in **Figure** 1.2. These bridges are responsible for conducting the rapid communication of the action potential between different bundles (Young and Hession, 1999). The beams are arranged parallel to the surface of the uterus, transversely at the fundus and obliquely downward.

In the myometrium, action potentials are initiated in pacemaker cells, open ion channels and allow the entry into the cell of Ca^{2+} to induce contraction, and then propagates to surrounding nonpacemaker cells (Lammers et al., 2008). There is no evidence for a fixed pacemaker anatomic area in the uterine muscle: any muscle cell can act as pacemaker cell and pacemaker cells can change from one contraction to the other (Devedeux et al., 1993). It has been shown that non-pacemaker regions can become pacemakers by application of oxytocin or prostaglandin but not simply by depolarizing the membrane with high K^+ solution (Lodge and Sproat, 1981).

Many studies indicate that myometrial cells are electrically coupled by gap junctions (Garfield et al., 1998b; Garfield et al., 1977; Miller et al., 1989). A gap-junction is a structure composed of two symmetrical portions of the plasma membrane from two adjacent cells. Gap junction proteins within the opposed cell membranes are thought to align themselves and create channels (of about 1.5 nm) between the cytoplasm of the two cells. These channels are sites of electrical and metabolic coupling between cells. There is evidence that gap junctions form a pathway for the passage of action potentials by forming a low-resistance electrical contact between the cells (Garfield et al., 1977; Miller et al., 1989). Dedicated studies demonstrated that throughout most of pregnancy, the cell-to-cell gap junctions are absent or present in very low density, indicating poor coupling and limited electrical conductance (Garfield et al., 1977).

On the other hand, contractile uterine activity during term or pre-term labor is invariably associated with the presence of a large number of gap junctions between myometrial cells (Garfield et al., 1977). The presence of gap-junctions is controlled by changing oestrogen and progesterone concentration in the uterus. Progesterone downregulates and progesterone antagonist upregulates the myometrial gap-junction density (Garfield et al., 1998b). It is generally believed that the improved electrical communication among cells can facilitate synchronous excitation of a large number of myometrial fibers and permit the evolution of forceful, coordinated uterine activity, able of effectively terminate pregnancy by helping the fetus to descend into the birth canal (Miller et al., 1989).
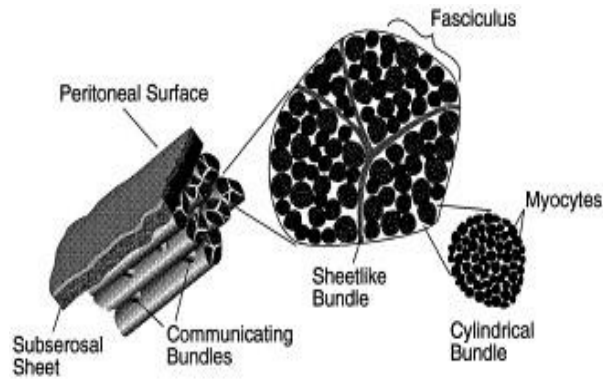
Figure 1.2 : Three-dimensional structure of the woman uterus. (Young and Hession, 1999)

Gap Junctions (GJ) realize the three-dimensional electrical coupling of myometrial cells.. They are thought to be necessary in order to achieve the coordinated contraction required for fetal expulsion during normal birth. Increased GJ number is therefore associated with improved propagation of electrical impulses, increased conduction velocity and coordinated contractility of the myometrium. As action potentials are conducted to neighboring myometrial cells through GJ, group of cells contract, leading to what is perceived by the woman as a uterine contraction (Devedeux et al., 1993; Rihana et al., 2009). The number of GJ grows almost exponentially until delivery. They disappear quickly after delivery (Garfield and Hayashi, 1981).

During pregnancy, uterine activity is weak and localized [36]. The propagation is limited due to the lack of GJ. This condition favors quiescence of the myometrium and the maintenance of the pregnancy. At term, however, before delivery, an abrupt increase in GJ is significantly observed, allowing a faster propagation of action potentials and increasing the coordination of contractility. The electrical activity increases due to the increase in the ability of the muscle cells to generate action potential (excitability) and the increase in their propagation (Devedeux et al., 1993; Rihana et al., 2009). Therefore, the contractions become more and more frequent and increase in strength.

Another mechanism for controlling the EHG is through calcium waves (Young, 1997). However, it is necessary to distinguish two types of wave: the intracellular calcium wave and the intercellular calcium wave.

The intracellular calcium wave is consistent with rapid changes in intracellular calcium concentration [Ca2 +] in a single cell. This wave is capable of crossing the cell membrane and becomes an intercellular calcium wave. The intercellular calcium wave propagates slowly (~

4 microns / sec) and to a maximum distance relatively low (~ 300 microns) corresponding to the size of a bundle (Young, 1997, 2000).

If, as we have seen, the structures or the regulation of processes involved in the propagation are well known (hormones ...), the initiation of electrical activity before it propagation is an important parameter whose origin remains uncertain. As with other smooth muscles (arteries, intestine ...), the initiation of electrical activity is performed by a cell or group of cells called pacemakers. Myometrial cells may be alternately pacefollower or pacemaker, that is to say capable of entering into contraction, driven by the activity of a neighboring cell, and in turn activate other cells nearby. Many hypotheses on the pacemaker cells have been issued including their number, position ... It seems that there is a one or more preferential pacemaker activities loci near the fundus as found by Caldeyro-Barcia et al. (Caldeyro-barcia and Poseiro, 1960). This activity is then propagated in all directions, but ultimately from the fundus to the cervix. Duchene et al. also show the existence of a constant chronogram during labor by studying the correlation of EHG envelopes recorded at several sites in the uterus of pregnant macaque (Duchêne et al., 1990).

The placenta seems to alter the direction of the activity propagation. Indeed, there is an inhibition of the propagation from the cells from the non-placental region to the placental ones, but not the reverse (Planque, 1990).

Details about the different methods used to analyze the EHG propagation in a clinical point of view will be presented in the next sections.

1.3 Clinical application

1.3.1 Uterine contraction monitoring

To date, different methods have been developed for labor monitoring with variable success. Intrauterine pressure (IUP) catheters provide the best information concerning uterine contractions, allowing the exact quantification of the mechanical effect of contractions, but the clinical usefulness of this technique is limited by its invasiveness, since it requires rupture of membranes in order to insert the pressure device into the uterus. This can increase the risk of infection or accidental induction of labor (Schlembach et al., 2009). Tocodynamometers (TOCO) are external force measurement devices which are used to detect changes in abdominal contour as an indirect indication of uterine contraction. Their non-invasiveness

allows the devices to be used for pregnancies without risk to the fetus or to the mother, and to be used in nearly all births in a medicalized setting. Nevertheless, TOCO monitoring is uncomfortable, often inaccurate and depends on the subjectivity of the examiner. In addition, the use of TOCO is limited to obtaining the frequency of appearance of contractions and does not permit any direct measurement of the properties that control both the function and state of the uterus. The many advantages of a non-invasive method for providing uterine contraction data has led to its widespread adoption, despite the limitations inherent to this method. While a few techniques currently used can identify some of the signs of oncoming labor, none of them offer objective data that accurately predicts labor over a broad range of patients (Garfield and Maner, 2007). The currently used techniques are :

- *Multiple preterm labor symptoms*: This technique includes cervical dilation and effacement, vaginal bleeding, or ruptured membranes. These signs are determined by a clinician. But they have had minimal success in reducing preterm labor rates over the past decade.

- *Maximal uterine contractions*: This technique measures highest observed number of contraction events seen in any 10-min period. This is assessed by a clinician based on tocodynamometer *(*TOCO*)*. However, TOCO has been shown to be unreliable as a predictor for preterm or even term labor (Dyson et al., 1998; Maul et al., 2004).

- *Bishop scoring system*: This score attempts to predict the success of induction by assessing five factors: position of the cervix in relation to the vagina, cervical consistency, dilatation, effacement and station of the presenting part. Bishop scoring has not lead to a reduction in preterm labor.

- *Cervix length via endovaginal ultrasonography*: It has been used to detect premature labor (Iams et al., 1996; Romero et al., 1992) with some limited degree of success. However, predictive values are obtained only after the onset of preterm labor symptoms. So its use is limited, as is the potential for treatment upon diagnosis using this method. Furthermore, the measurement of the cervical length by ultrasonography is made unreliable due to varying amounts of urine in the bladder (Iams, 2003a, b).

- *Cervical or vaginal fetal fibronectin (FFN)*: It has recently been suggested as a screening method for patients at risk for premature labor. Results from some studies show that FFN might be used to predict actual premature labor (Iams, 2003a; Lockwood, 2001) although with poor likelihood ratios [Garfield R.E. et al., Ann N Y Acad Sci, 2001, 943: 203-24].

- ***Light-induced auto fluorescence (LIF)***: This technique that attempts to measure cervical tissue changes during gestation and labor, was proposed for labor monitoring (Garfield et al., 1998b) Specifically this technique attempts to assess the concentration of collagen in cervical tissue in an optical, non-invasive manner, since collagen degradation and rearrangement plays a crucial role in the softening and ripening process of the uterine cervix during pregnancy and labor. The studies in animal model and also in humans have shown its capability for estimating the cervical status which could provide useful information for forecasting preterm labor. It is not already used in routine practice.

- ***Magnetomyography (MMG)***: it is a noninvasive technique that measures the magnetic fields associated with the uterine action potentials. First, MMG recordings of spontaneous uterine activity were reported by Eswaran and colleagues (Eswaran et al., 2002) using 151 magnetic sensor array. Then different applications have been done on the MMG signals such as uterine contractions segmentation using Hilbert transform (Furdea et al., 2009), synchronization analysis using the phase methods (Ramon et al., 2005). Eswaran et al. confirmed the power shift towards higher-frequencies associated with an increase in the synchrony in the higher-frequencies bands from 38 weeks to 48h before active labor (Eswaran et al., 2009). It remaisn presently as a research tools, due to the high price of the equipment.

- ***Uterine electromyography (uterine EMG) or Electrohysterogram (EHG))***: Uterine EMG is the result of electrical activity originating from the depolarization-repolarization of billions of smooth muscle myometrial cells. It has been proved that synchronous myometrial and abdominal activities occur, which are temporally correlated with the mechanical activity of the uterus during pregnancy and labor, whatever the species, including humans (Devedeux et al., 1993). Numerous studies have shown that EHG can be appraised accurately and reliably from non-invasive transabdominal surface measurement (Devedeux et al., 1993; Garfield and Maner, 2007; Schlembach et al., 2009). EHG-derived contraction pattern has been shown to correlate better with the intrauterine pressure catheter than tocodynamometry in obese women, in whom tocodynamometry could be inadequate (Euliano et al., 2007) . Unlike other methods, abdominal uterine electromyogram has been shown to provide some useful information for deducing contraction efficiency, since changes in uterine myoelectric activity have been associated with the progression of pregnancy and the onset of labor. Therefore this technique has emerged as a potentially powerful tool in characterizing the human parturition state thanks

to its high sensitivity and positive prediction value (Devedeux et al., 1993; Garfield and Maner, 2007).

1.3.2   Detection labor and prediction preterm labor using EHG

One of most promising biophysical markers of preterm labor is the electrical activity of the uterus, the EHG signal. Preterm labor is an important public health problem in Europe and other developed countries as it represents nearly 7% of all births. It is the main cause of morbidity and mortality of newborns.

The physiological phenomena underlying labor remain however badly understood. It is well known that uterine contractility depends on the excitability of uterine cells but also on the propagation of the electrical activity to the whole uterus (Devedeux et al., 1993).

These two aspects, excitability and propagation, both influence the spectral content of EHG mainly composed of two frequency components traditionally referred to as FWL (Fast Wave Low) and FWH (Fast Wave High). These frequency components may be related to the propagation and to the excitability of the uterus respectively (Devedeux et al., 1993). Thus labor detection or preterm prediction has been analyzed by extracting parameters from these two aspects. The main studies using excitability parameters as well as propagation parameters can be summarized as following:

1.3.2.1   Excitability parameters

The first EHG signal ever reported in the literature was measured in 1931 as the deflection of a galvanometric needle during a uterine contraction (Bode, 1931). Many studies have proved that the external recording of the electrical activity of the uterus during contractions can be an attractive alternative to traditional TOCO recordings for pregnancy monitoring. Furthermore, over the last years, EHG has become the object of many studies, and has been proved to be of interest in offering a better insight into the progression of pregnancy and the onset of labor (Devedeux et al., 1993; Garfield et al., 2002; Garfield et al., 1998b). This signal, detected as early as 18 weeks of gestation, may provide a non-invasive, more objective and highly accurate method for pregnancy monitoring and the prediction of labor (Devedeux et al., 1993). Thus, EHG may not only replace the invasive or inaccurate methods that are currently employed for contraction monitoring during labor, but could also be an alternative tool for predicting delivery.

All the studies have been focused on turning EHG measurements into a relevant clinical application, which remains a challenge. More precisely, the researches concentrate on the developing of dedicated signal analysis techniques that permit detection and interpretation of parameters of clinical relevance to the patients. Extensive clinical studies are required for understanding the relation between the parameters derived from the EHG signal and the processes leading to labor. For this reason, many parameters derived from the EHG signal have been considered, both in time (Garfield et al., 1998b; Marque et al., 1986; Verdenik et al., 2001) and in frequency domain (Doret et al., 2005; Garfield et al., 2005; Maner et al., 2003; Marque et al., 1986; Verdenik et al., 2001).

In terms of results, a change in the characteristics of EHG signals has been observed at delivery (Buhimschi et al., 1998; Buhimschi and Garfield, 1996; Devedeux et al., 1993; Garfield et al., 1998a; Garfield et al., 1998b; Marque et al., 2007; Vinken et al., 2009). Most studies agreed on the fact that bursts of electrical signals responsible for contractions have been reported to me more frequent and their duration more constant in labor (Buhimschi et al., 1997; Maner and Garfield, 2007). An increase in peak amplitude and frequency of EHG signals, assessed by powers spectrum analysis, has also been observed prior to labor (Maner et al., 2003; Marque et al., 1986).

1.3.2.2   **Propagation parameters**

The methods cited above from the literature for preterm labor prediction most often use only the analysis of the high frequency content of the EHG which is thought to be primarily related to excitability. These methods are however not currently used in routine practice due to a high variance of the results obtained and an insufficient prediction rate. Taking into account both the excitability and propagation information might help to increase the prediction capability of the EHG for preterm labor identification.

Only few studies have been done to understand the propagation of EHG signal. These studies can be summarized as following:

- Planes et al. used the delay of the cross-correlation function maximum to analyze the uterine propagation using signals for women during labor. The results indicated a 2.18cm/s conduction velocity with direction from up to down in 65% of the case (Planes et al., 1984).

- Propagation velocity (PV) of electrical signals in the myometrium has been shown in vitro to increase before delivery when gap junctions are increased (Miller et al., 1989; Miyoshi et al., 1998). As a result, it has been suggested that EHG could be used to assess the PV in vivo.

- Using the linear correlation coefficient, Marque et al. have observed more correlation in the low frequencies than high frequencies. This study was done on women during pregnancy and labor (Marque, 1987).

- Surface multichannel EHG recordings have been used to analyze the uterine activity propagation by estimating the inter-electrode delay (Rabotti et al., 2009). The results were focused on localizing pacemaker zones and localization on the upper part was been observed on 65% of case.

- Spatial analysis of EHG signals in arrested and normal labor, by using multichannel recordings, indicated a significant correlation between upward movement of the center of uterine activity (fundal dominance) and labor progress (Euliano et al., 2009).

All the studies show complex propagation patterns like re-entry or ascending front detected by mapping the electrical potentials over the uterine muscle. However, none of these studies have applied the results to the detection of labor or to predicting preterm labor.

Recently an interesting piece of work used the propagation as a tool to predict labor (Lucovnik et al., 2011). The authors used propagation velocity (PV) to classify term and preterm labor. The PV was compared with the classical amplitude and frequency parameters used in the literature such as median frequency, median amplitude, mean burst duration, mean inter burst duration, etc. The results of the study showed that the PV present highly significant difference between labor and non-labor signals but no significance between labor and preterm labor.

This study demonstrated clearly how the use of parameters related to the propagation phenomena can be more powerful than the classical parameters based on the excitability phenomena, which is the basic assumption of the work presented here.

Until now, the main methods used for EHG propagation analysis has been linear inter-correlation. In reported work, the inter correlation coefficients calculated on EHG envelope are usually good (~80%) but the coefficients calculated on temporal signals are much lower (Duchêne et al., 1990; Karlsson et al., 2007). This is however a low significance results, as

even the inter correlation of the envelope of uncorrelated noise gives very high correlation coefficients.

As we mentioned above, Marque et al showed, by using correlation coefficient that the strongest correlation between bursts is in the low frequency component (Marque and Duchene, 1989), i.e. FWL. Mansour et al. used the inter-correlation function to analyze the propagation of the EHG on four internal electrodes, in the uterus of a monkey in labor (Mansour et al., 1996). The signals were first filtered in the frequency bands of the two waves, FWL and FWH. Then the inter-correlation function was calculated for each wave between the two pairs of electrodes. The result indicated that the inter-correlation coefficient is always higher for FWL than for FWH.

Linear synchronization measures (cross correlation and coherence functions) have been recently used by Kitlas et al. (Kitlas et al., 2009; Oczeretko et al., 2006) to differentiate between non pregnant subjects with normal contractions, dysmenrrhea, fibromyomas in the follicular phase and patient with endometriosis.

On the other hand, it is well known that one of the powerful way to analyze the signal propagation is the detection of the relationship between the signals recorded at different locations during the same time (Pijn and Lopes Da Silva, 1993). Methods detecting relationships between signals such as amplitude correlation, phase synchronization, mutual information, etc, have been widely used to analyze propagation of the brain electrical activity at different situations. Nonlinear (amplitude) correlation coefficient has been proposed and used by Pijn et al. to analyze the propagation of brain electrical activity during epileptic seizure (Pijn and Lopes Da Silva, 1993). Mutual information has been also used to analyze the propagation of seizure activity in kindled dogs (Mars and Lopes da Silva, 1983). Recently, a new way to analyze relationships between multichannel signals was introduced and based on methods estimated from Multivariate Autoregressive model (MVAR). The different estimators computed from the MVAR model coefficients have been widely used to analyze propagation of EEG signals (Franaszczuk et al., 1994; Korzeniewska et al., 1997; Kus et al., 2004).

Although the importance of these methods to analyze biosignal propagation, they have still rarely been applied on the EHG signals. The aim of this work is therefore to test the power of these different methods to detect the evolution of uterine synchronization from pregnancy to labor. As the anatomical structure of the uterus and of the communication pathways between

uterine cells (gap junction) does not permit to expect a linear propagation of the uterine electrical activity, our main assumption is that these tools would be more efficient for uterine synchronization analysis that the classical linear tools used until now.

## 1.4   Our experimental protocol: Multichannel EHG recordings

Most of the recordings that can be found in the litterature have used two to five electrodes and have therefore concentrated on the local excitability of the uterus. But limited effort has been made to investigate the electrical activity concurrently at different locations and the organisation of the whole organ in preparation of birth. We can cite here the studies of Euliano and al. using 8 channels located on the woman's abdomen to explore the spatiotemporal characteristics of the EHG in order to differentiate between normal and arrested labor (Euliano et al., 2009). We can also cite the work of Rabotti et al., by using 8 electrodes, to estimate the internal uterine pressure (Rabotti et al., 2008) or analyze EHG propagation on large-scale (Rabotti et al., 2009).

Multichannel EHG signals is usually obtained by placing a grid of electrodes on the mother's abdomen. In order to obtain a precise mapping of uterine electrical field during contractions, a high spatial resolution is needed. The total number of electrodes is however limited by the abdominal surface, specially when the electrodes should be put along or as near a possible the vertical mean axis in order to get a better signal-noise ratio (SNR). In this sense, the use of monopolar recordings (potential measured compared to a remote and/or electrically inert patient ground) permits to improve spatial resolution.

In order to study the propagation of the uterine electrical activity in the view of prediction preterm labor, (Karlsson et al., 2007) we planed to map EHG by placing electrodes in a four by four grid on the woman's abdomen. This may help to better understand the underlying mechanism of uterine contractions as well as to improve the prediction values for preterm labor (PL).

This technique passed through two stages: at the beginning the electrodes were placed one by one which was a time-consuming task. Furthermore, the attachment of the electrodes with the desired washer overlap (to maintain the proper electrode spacing) required great operator 's attention and precision. Moreover, as the propagation analysis will need collecting data from many women and different countries, a more efficient electrode positionning method would be needed. For this reason a project has been done in Iceland to design a placement system

that decreases placement time and reduces the complexity of the electrode positionning method. The new design retained involves a guide with holes, guiding the placement, as well as adhesion of the electrodes by means of a double coated adhesive sheet. A simple frame ensures correct positioning of the guide onto the adhesive sheet, while positioning the electrodes. With about 2cm inter-electrode distance, the 16 electrodes arranged in a 4x4 matrix, this system permitted us to standardize the signals acquisition during this French-Icelandic EHG propagation analysis project. A typical example of the matrix placement is illustrated **Figure** 1.3.
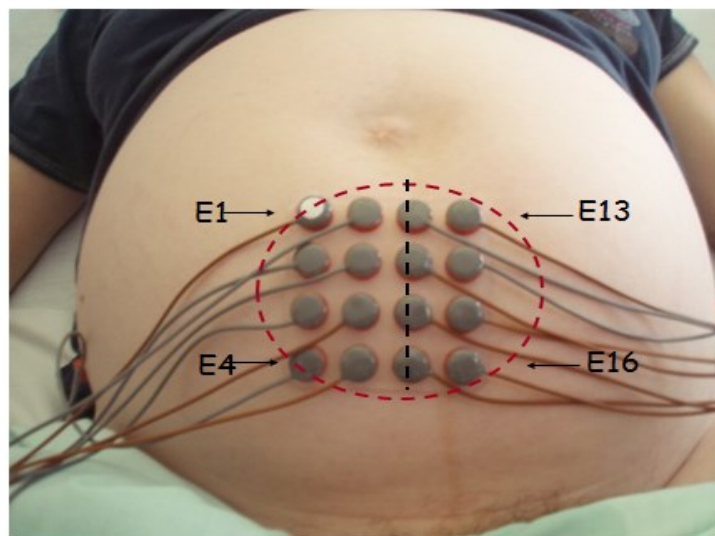
Figure 1.3: Typical example of the 4x4 electrodes matrix positioned on the woman's abdomen

The measurements were performed by using a 16-channel multi-purpose physiological signal recorder most commonly used for investigating sleep disorders (Embla A10). Reusable Ag/AgCl electrodes were used (8mm diameter). The measurements used in this work were performed at the Landspitali University hospital in Iceland following a protocol approved by the relevant ethical committee (VSN 02-0006-V2. The subjects were healthy women either in the first stages of labor having uneventful singleton pregnancies (Labor population), or healthy women having normal pregnancies at varying gestational age (Pregnancy population). After obtaining informed consent, the skin was carefully prepared using an abrasive paste and alcoholic solution. After that, the sixteen electrodes were placed on the abdominal wall according to **Figure** 1.3. The third electrode column was always put on the uterine median

axis and the 10-11th electrode pair on the middle of the uterus (half way between the fundus and the symphysis). Two reference electrodes were placed on each of the woman's hip.

The signal sampling rate was 200 Hz. The recording device has an anti-aliasing filter with a high cut-off frequency of 100 Hz. The tocodynamometer paper trace was digitalized in order to facilitate the segmentation of the uterine contractions.

However, the monopolar signals are very noisy and have low Signal to Noise Ratio (SNR). The monopolar electrohysterogram (EHG) signals were often corrupted by electronic and electromagnetic noise as well as movement artifacts, skeletal EMG and electrocardiogram from both the mother and the fetus, preventing their direct use for propagation analysis.

For this reason this thesis is devided in two parts:

- Use of bipolar signals to increase the SNR: vertical bipolar signals (BP1,... BP12) are computed as it is shown in **Figure** 1.4. These signals are used when analyzing nonlinear characteristics of the EHG signal (chapter 3) and EHG propagation (chapter 4 and 5).

- Find tool(s) to remove artifacts from the monopolar signals (objective of chapter 5).
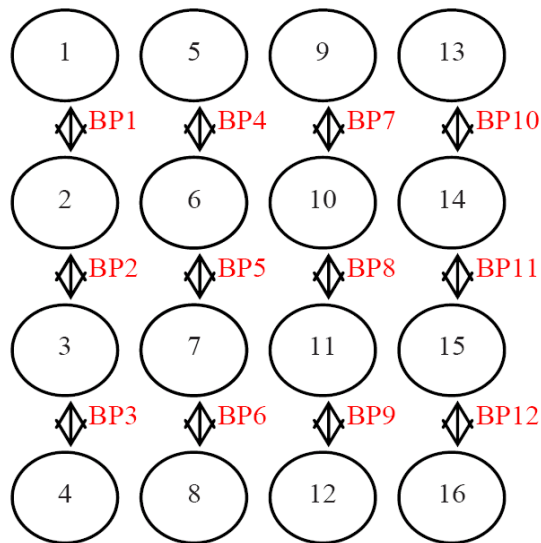
Figure 1.4: Electrode configuration on the woman's abdominal wall

An example of the signals obtained is illustrated in **Figure** 1.5. the **Figure** presents the digitilized TOCO trace, the monopolar signals and the vertical bipolar signals recorded on a woman during labor.
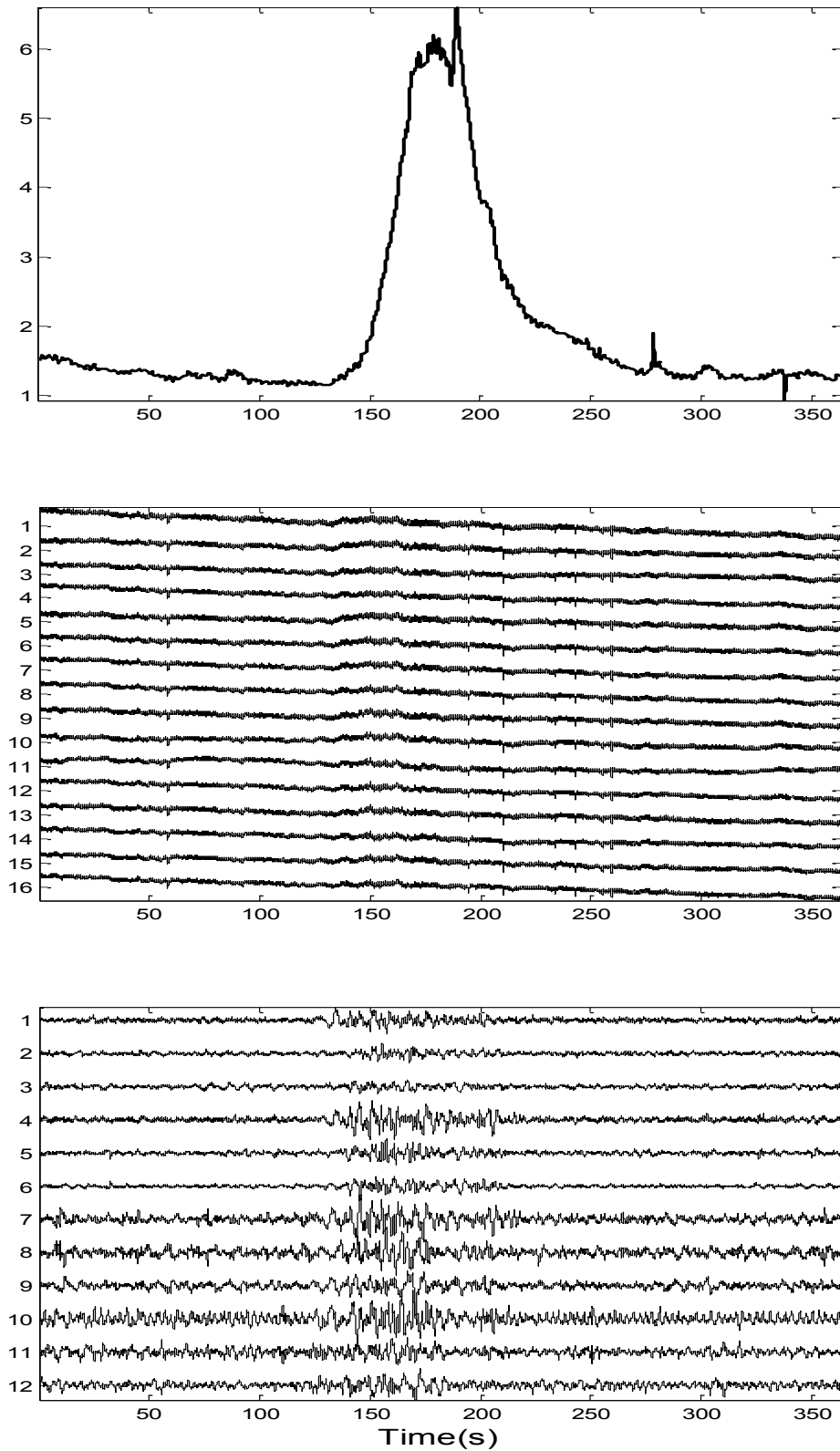
Figure 1.5: A) Digitalized TOCO trace B) Original monopolar signals C) Corresponding bipolar signals.

In the monopolar signals the uterine bursts is totally hidden by the artifacts. Even with the help of the TOCO signals, we cannot identify and segment the uterine bursts. While, by using the vertical bipolar signals it is easier to identify and then segment the uterine bursts.

This **Figure** permits to evidence the correlation between the mechanical (TOCO) and electrical (EHG) bipolar activities.

Due to the very low SNR of monopolar signals, before developing a suitable denoising tool to remove the different artifacts, we chose to use the bipolar signals for propagation analysis. The result of this analysis are presented in the next 2 chapters. The development of a novel denoising algortithm is presented in chapter 5.

Six women in spontaneous labor were recorded at 39 and 41 weeks of gestation. Recording sessions were also conducted on seven women during pregnancy, at 29 to 38 weeks of gestation. The recording duration was approximately 1 hour for each subject. All the EHG were manually segmented with the help of the tocodynamometer trace. Each segmented EHG has duration about 150 s and contains baseline segments before and after the contraction-associated burst. After the segmentation, were obtained 30 pregnancy EHG and 30 labor EHG to be used for propagation analysis.

1.5 Discussion and conclusion

In this chapter we briefly introduced the physiological origin of the uterine EHG. We have also explained the two phenomena that control the generation of uterine contraction: cells excitability and propagation of the uterine activity.

The different monitoring way of the uterine contractions were also described. The EHG was considered as the best way to monitor the uterine contractility for non-invasive pregnancy follow up. We then provided and overview of previous studies made on prediction normal and preterm labor, by using either excitability or propagation parameters. We noticed that only few studies have been proposed to use propagation analysis as a tool to detect or predict preterm labor. Recent studies confirmed that detection by propagation parameters is more powerful than detection by excitability parameters.

A novel multichannel EHG recordings using 4x4 matrix posed on the women abdomen was described in this chapter and has been used to obtain the signals processed for propagation analysis.

Chapter 2 Nonlinear characteristics of EHG signal

One of the most common ways of obtaining information about neurophysiologic systems is to study the features of the signal(s) by using time series analysis techniques. These techniques can be divided into three types: monovariate, bivariate and multivariate methods. In spite of their different aims and scopes, univariate and multivariate time series analysis present an important common feature: they traditionally rely on linear methods in both time and frequency domains (Bendat and Piersol, 2000).

Unfortunately, these methods cannot give any information about nonlinear features of the signal. Due to the intrinsic nonlinearity of most of biological systems, these nonlinear features may be present in physiological data. This has led researchers to develop other techniques that do not present the aforementioned limitations.

Univariate nonlinear time series analysis methods started to be applied to neurophysiological data about two decades ago (Babloyantz and Lourenco, 1996; Elbert et al., 1994; Faure and Korn, 2001; Lehnertz et al., 1999; Stam, 2005). Several methods have been applied to the EEG signals, such as the use of correlation dimension to characterize the nonlinear behavior of the EEG signals. This index has been used for sleep-wake research (Pereda et al., 1998), mental load research (Lamberts et al., 2000), monitoring the depth of anesthesia (Widman et al., 2000) and in epilepsy analysis (Pijn et al., 1990). Other parameters like Lempel–Ziv complexity (LZC) and different entropy based methods (approximate entropy…) have been also widely applied to EEG signals (Burioka et al., 2005; Stam, 2005). More recently, these methods have been used to quantify the degree of unconsciousness and to the possible prognosis of unconscious subjects (Wu et al.).

As to EHG signals, monovariate linear methods have been widely applied for different objectives such as calculation of the peak frequency of the bursts power spectrum (Garfield et al., 2005), calculation of burst energy levels (Maul et al., 2004), of duration and number of bursts, means and deviations of the frequency spectrum combined with neural networks (Maner and Garfield, 2007). Other approaches included calculating the root mean square value of the signals and the median frequency value of the power spectrum of the signals for whole 30-min records of uterine activity (Verdenik et al., 2001).

Based on the hypothesis that the underlying physiological mechanisms of most biological systems are at least partly nonlinear processes (Akay), nonlinear methods have recently been applied to EHG signals.

The comparison between linear parameters (root mean square value of the signal, peak and median frequencies of the power spectrum, autocorrelation zero-crossing) and nonlinear ones (the sample entropy, maximal Lyapunov exponent and correlation dimension) has demonstrated the clear superiority of the nonlinear methods (specially the sample entropy) to separate term and preterm delivery groups (Fele-Zorz et al., 2008).

In this chapter we focus on nonlinear univariate methods to investigate the capacity of these methods to characterize uterine activitiy and to correctly distinguish between pregnancy and labor signals. We will describe the different nonlinear methods proposed in the literature, their pros and cons. We will then compare the selected methods performance when applied to EHG signals.

2.1   State of the art

For any data analysis, the application of nonlinear time series methods has first to be justified by establishing the nonlinearity of the time series under investigation.

Several measures have been proposed to detect nonlinear characteristics in time series. The first category includes methods inspired from chaos theory such as: maximal Lyapunov exponents, correlation dimension (Grassberger and Procaccia, 1983) and transfer entropy (Nichols et al., 2005). The main disadvantage of these methods is that they depend on different parameters, like embedding dimension, which complicate the interpretations of the results. The second category of methods is based on the predictability of time series. These ones include delay-vector variance (Gautama et al., 2004) and approximate entropy (Ocak, 2009). They are more robust than the first ones but their interpretation is still not easy due to their sensitivity to the different parameter choices (Aysegul and Jose, 2009). The last category of methods is based on a statistical approach. This category includes methods such as: time reversibility (Schreiber and Schmitz, 2000) and higher dimensional autocorrelation functions (Schreiber, 1999). A new method called correntropy was recently proposed by Santamaria et al. It computes a similarity index that combines the signal time structure and the statistical distribution of signal amplitudes in a single function (Santamaria et al., 2006). This method is then proposed as a measure for nonlinearity test (Aysegul and Jose, 2009).

A well-known way to test the performance of nonlinearity detection methods is to use the surrogate technique. The method of surrogate data (Schreiber and Schmitz, 2000) provides a rigorous framework for nonlinearity tests which main elements are the null hypothesis and a nonlinearity measure. The most commonly used null hypothesis states that the examined time series is generated by a linear Gaussian stochastic process collected through a static nonlinear measurement function. Thus, properly designed surrogate data should have the same linear properties (autocorrelation and amplitude distribution) as the original signal, and be otherwise random. The generated surrogate data are compared to the original data under a discriminating nonlinear measure. We test if the value of the measure for the original time series is likely to be drawn from the distribution of values of the surrogates within a confidence level. If the measure gives comparatively different values than for the original series, the null hypothesis is rejected and the original series is considered to be nonlinear.

Recently, much attention has been paid to the use of nonlinear analysis techniques for the characterization of biological signal (i.e. EEG data (Elger et al., 2000; Hornero et al., 2008; Lehnertz et al., 2001)). Few nonlinear analysis methods have been applied to uterine electromyogram (EMG), also called electrohysterogram (EHG). Most of them are only descriptive and aim to demonstrate the presence of nonlinear characteristics in EHG signal, not to classify pregnancy vs. labor signals for labor prediction. We can cite here the use of approximate entropy (Oczeretko et al., 2005) to detect nonlinearity in uterine activity signals, the use of fractal dimension to analyze uterine contractions (Oczeretko et al., 2004) and the comparison between linear (peak and median frequency,…) and nonlinear methods (Lyapunov exponent, sample entropy and correlation dimension) to separate EHG records of term and pre-term delivery groups (Fele-Zorz et al., 2008). The question that arises here is what is the most appropriate method? And which one could best respect the different signals characteristics for example non-stationarity?

In this chapter we present a comparison between three methods largely used for nonlinearity detection: (i) time reversibility (Tr) (ii) approximate entropy (ApEn) and (iii) correntropy (CorrEn). We computed the false alarm rate (FAR) with the number of surrogates on different types of signals (linear, nonlinear stationary and nonlinear nonstationary), in order to evaluate the efficiency of each method in the detection of nonlinearity characteristics. The two best methods, in terms of low FAR, were then applied on real EHG signals during labor and pregnancy, in order to evaluate their possible use for labor prediction in women.

2.2   **Materials and Methods**

2.2.1   **Data**

- *Synthetic signals*

To compare approximate entropy, correntropy and time reversibility, we used different types of synthetic signals:

1. Linear (AR: autoregressive).
2. Nonlinear stationary (Rössler, Henon, logistic and TAR: Threshold Autoregressive).
3. Nonlinear nonstationnary (ARCH: Autoregressive Conditionally Heteroscedastic).

Table 2.1 summarizes the signals equations and the parameters used for each signal. **Figure** 2.1 presents an example for each signal. The number of point is fixed at 1000 for all the signals.

- *Real signals*

Signals recorded by the experimental protocol described in Chapter 1 are used in this chapter. In total 30 pregnancy bursts and 30 labor bursts are used from 7 women during pregnancy and 5 women in normal labor.
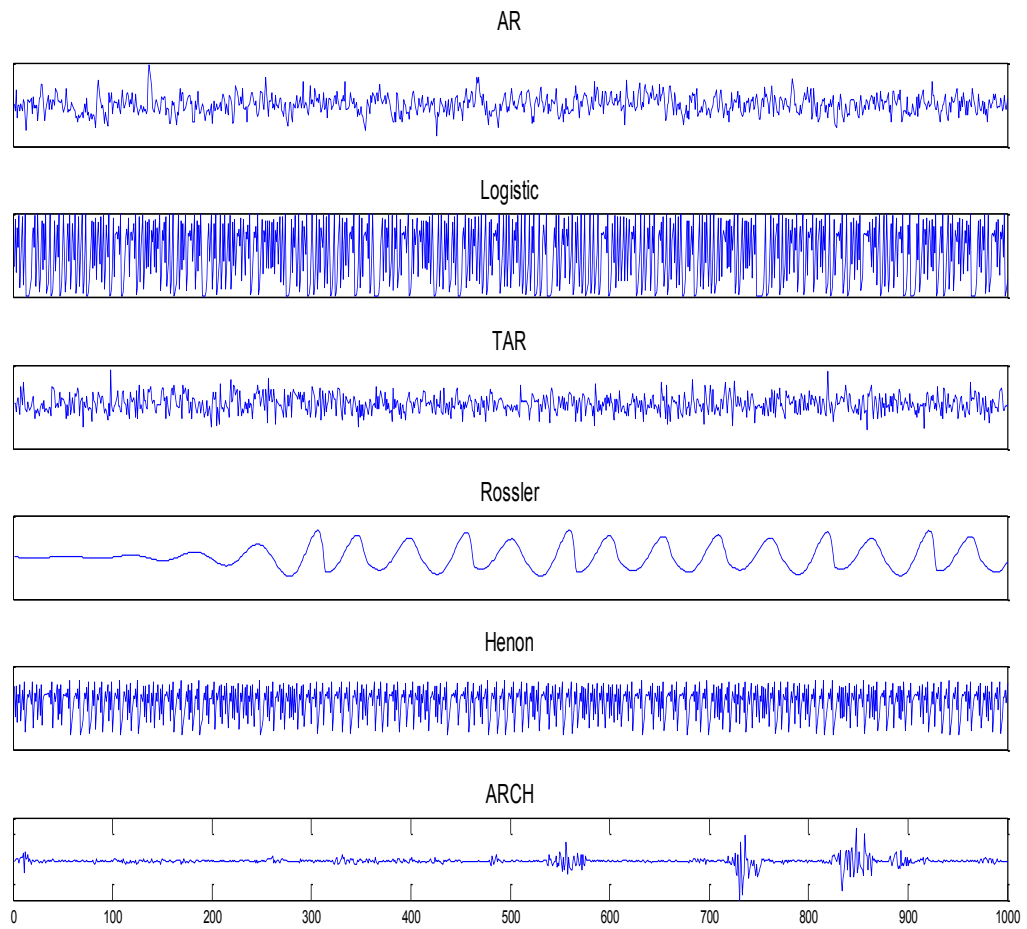
Figure 2.1: Examples of the synthetics signals used. From top to bottom: Autoregressive (AR), Logistic map, Threshold Autoregressive (TAR), Rössler, Henon, and ARCH.

Label	Model	Type
AR(0.4,1)	$X_t = 0.4X_{t-1} + \varepsilon_t$	LS
TAR(2;1,1)	$X_t = \begin{cases} -0.5X_{t-1} + \varepsilon_t, & X_{t-1} < 0.5 \\ 0.4X_{t-1} + \varepsilon_t, & otherwise \end{cases}$	NLS
Logistic	$x_{n+1} = 4x_n - 0.8x_n(1-x_n)$	NLS
Rössler	$\dfrac{dx_1}{dt} = -w_x x_2 - x_3$ $\dfrac{dx2}{dt} = w_x x1 + 0.15x_3$ $\dfrac{dx3}{dt} = 0.2 + x_3(x_1 - 10)$ where $w_x = 0.95$	NLS
Henon	$x(n+1) = 1.4 - x^2(n) + b_x x(n-1)$ Where b_x=0.3	NLS
ARCH	$X_t = \varepsilon_t \sqrt{h_t}$ with $h_t = 0.000019 + 0.846\{X_{t-1}^2 + 0.3X_{t-2}^2 + 0.2X_{t-3}^2 + 0.1X_{t-4}^2\}$	NLNS

Table 2.1 Linear Gaussian, Linear non Gaussian and Nonlinear processes used to generate the synthetic signals

AR: Autoregressive, TAR: Threshold Autoregressive, Rössler: Rössler dynamic systems, Henon: Henon dynamic systems, ARCH: Autoregressive Conditionally Heteroscedastic, LS: linear stationary, NLS: nonlinear stationary, NLNS: nonlinear nonstationary.

2.2.2 **Nonlinearity detection methods**

2.2.1.1 **Time reversibility**

A time series is said to be reversible if and only if its probabilistic properties are invariant with respect to time reversal. In (Diks et al., 1995), the authors proposed a test for the null hypothesis to indicate that a time series is reversible. Rejection of the null hypothesis implies that the time series cannot be described by a linear Gaussian random process, so time irreversibility can be taken as a strong signature of nonlinearity (Schreiber and Schmitz, 2000). One of the simplest ways to measure time asymmetry is by taking the first differences

of the series to some power. In this work we used the simple way to compute time reversibility for a signal *S*, described in (Schreiber and Schmitz, 2000), as:

$$Tr(\tau) = \frac{1}{N-\tau} \sum_{n=\tau+1}^{N} (S_n - S_{n-\tau})^3$$

where *N* is the signal length. In this paper we used $\tau = 1$ which is a common choice for τ.

Time irreversibility implies that observed time series look 'different' when viewed in forward and reverse time (imagine playing an audio tape backwards). Reversible time series 'look similar' (e.g. have similar dynamic flows) when viewed both in forward (natural) time and in reverse time. Linear Gaussian random processes (LGRP) are reversible. The verification of irreversibility for the observed data excludes these types of process as possible models for the data. Irreversibility is one of the 'symptom' of nonlinearity (Cox, 1981). Time reversibility has been applied on different physiological signals such as for the investigation of nonlinear characteristics of the EEG signals during epilepsy (van der Heyden et al., 1996) and during sleep in children(Berryman et al., 2005).

2.2.1.2   Correntropy

Correntropy is a similarity measure of signals, nonlinearly mapped into a feature space (Santamaria et al., 2006). In essence, correntropy generalizes the autocorrelation function to nonlinear spaces: if $\{x_t, t \in T\}$ is a strict stationary stochastic process within an index set *T*, then the autocorrelation and correntropy functions are defined respectively as:

$$R(s,t) = E\{\langle x_s, x_t \rangle\}$$
$$V(s,t) = E\{\langle \phi(x_s), \phi(x_t) \rangle\}$$

where ϕ is a nonlinear mapping from the input space to the feature space (Santamaria et al., 2006). Correntropy makes use of the ''kernel trick'' which defines the inner product of the nonlinear mappings as a positive-definite Mercer kernel (Scho¨lkopf and A., 2002):

$$k(x_s, x_t) = \langle \phi(x_s), \phi(x_t) \rangle$$

A widely used Mercer kernel is the Gaussian kernel given by:

$$k(x_s, x_t) = \frac{1}{\sqrt{2\pi\sigma^2}} \exp(\frac{-\|x_s, x_t\|^2}{2\sigma^2})$$

where σ is the size of the kernel. Using a Taylor series expansion for the Gaussian kernel, it can be shown that the information provided by the autocorrelation is included within the correntropy by setting n = 1 in the expansion (Santamaria et al., 2006) :

$$V(s,t) = \sum_{n=0}^{\infty} \frac{(-1)^n}{2^n \sigma^{2n} n!} E\|x_s - x_t\|^{2n}$$

The two functions have many properties in common: both are symmetric with respect to the origin, and take on their maximum value at zero lag. Moreover, it can be observed that for $n>1$, correntropy involves higher order even moments of the term $\|x_s - x_t\|$ and exhibits other important properties autocorrelation function does not possess.

. In Principe et al. (Santamaria et al., 2006) the Fourier transform of correntropy was introduced as the generalized power spectral density and named correntropy spectral density (CSD). Its expression is given as follows:

$$P_v[w] = \sum_{m=-\infty}^{\infty} V[m] e^{-jwm}$$

It retains many properties of the conventional power spectral density.

The Kolmogorov–Smirnoff goodness-of-fit test is a powerful tool which examines whether two signals are random samples from the same distribution. Authors in [26] compare the empirical cumulative distribution functions (ecdfs) calculated from the CSDs of the original and surrogate series. The maximum difference between the ecdfs of the two series, denoted by F, across all frequencies in range, denoted by f, is the test statistic

$$D = \max_f \left| F_{org}(f) - F_{surr}(f) \right|$$

This D-value is compared to a critical value given by

$$D_\alpha = c(\alpha)\sqrt{2/N}$$

where N is the common sample size of the two series and the coefficient $c(\alpha)$ depends on the significance level. For a $\alpha = 0.05$, this value equals 1.36.

The Kolmogorov–Smirnoff test states that if the empirical D-value is greater than the critical value, then the hypothesis that the two series were generated from the same distribution should be rejected.

In this study, the bandwidth of the kernel is selected according to Silverman's rule of thumb (Sheather, 2004) defined as:

$$\sigma = 0.9AN^{-1/5}$$

where N is the data length and A stands for the minimum of the empirical standard deviation of data, in the one hand, and the data interquartile range scaled by 1.34, in the other hand, as defined in Silverman's rule.

2.2.1.3   Approximate entropy

Approximate entropy (ApEn) first proposed by Pincus (Pincus, 1991) is a measure that quantifies the regularity and predictability of signals. ApEn value is low for regular time series and high for complex, irregular ones. The first step in computing ApEn for a given time series, y_i, i = 1. . . N is to construct the state vectors in the embedding space, R^m, by using the method of delays:

$$x_i = \left\{ y_i, y_{i+\tau}, y_{i+2\tau}, ..., y_{i+(m-1)\tau} \right\}$$
$$1 \le i \le N-(m-1)\tau$$

where m and τ are the embedding dimension and time delay, respectively. Then we define the correlation sum $C_i^m(r)$ by:

$$C_i^m(r) = \frac{1}{N-(m-1)\tau} \sum_{j=1} \theta(r - d(x(i), x(j)))$$

where $\theta(x) = 1 \, for \, x > 0$, $\theta(x) = 0$ for $x<0$, also known as the standard Heaviside function, r is the vector comparison distance and $d(x(i),x(j))$ is a distance measure defined by:

$$d(x(i), x(j)) = \max_{k=1,2,...,m} \left(\left| y(i+(k-1)\tau) - y(j+(k-1)\tau) \right| \right)$$

ApEn is given by the formula:

$$\text{ApEn}(m, r, \tau, N) = \Phi^m(r) - \Phi^{m+1}(r)$$

where

$$\Phi^m(r) = \frac{1}{N-(m-1)\tau} \sum_{i=1}^{N-(m-1)\tau} \log C_i^m(r)$$

In this paper, we used the "differential entropy based method" (Gautama et al., 2003) to compute the optimal m and τ values. We define the filter parameter r as r=0.2*SD which is a common choice of r, where SD is the standard deviation of the signal. For the real signals, we obtain m=2 and τ=6 as optimal values computed on set of uterine bursts.

2.2.3   **Surrogate data**

To test a particular hypothesis on a time series, surrogate data are classically used. They are built directly from the initial time series in order to fulfill the conditions of a particular null hypothesis.

Surrogate data are time series which are generated in order to keep particular statistical characteristics of an original time series while destroying all others. They have been used to test for nonlinearity (Schreiber and Schmitz, 2000) or nonstationarity (Borgnat and Flandrin, 2009) of time series for instance. The classical approaches to construct such time series are phase randomization in the Fourier domain and simulated annealing (Schreiber and Schmitz, 2000). Depending on the method used to construct the surrogates, a particular null hypothesis is assumed. The simulated annealing approach is very powerful since nearly any null hypothesis might be chosen according to the definition of an associated cost function. As a first step, we chose the Fourier based phase randomizing approach.

The Fourier based approach consists mainly in computing the Fourier transform, F, of the original time series $x(t)$:

$$X(f) = F\{x(t)\} = A(f) e^{i\Phi(f)}$$

where $A(f)$ is the amplitude and $\Phi(f)$ the phase. The surrogate time series is obtained by rotating the phase Φ at each frequency f by an independent random variable φ taking values in the range $[0, 2\pi)$ and going back to the temporal domain by inverse Fourier transform F^{-1}, that is:

$$x(t) = F^{-1}\{X(f)\} = F^{-1}\{A(f) e^{i[\Phi(f)+j(f)]}\}$$

By construction, the surrogate has the same power spectrum and autocorrelation function as the original time series but not the same amplitude distribution. This basic construction method has been refined to assume different null hypothesis. Several method to generate surrogates time series have been proposed and an important overview about these methods can be founded in (Schreiber and Schmitz, 2000). We used the iterative amplitude adjusted Fourier transform method to produce the surrogates (Schreiber and Schmitz, 2000). This iterative algorithm starts with an initial random shuffle of the original time series. Then, two distinct steps will be repeated until a stopping criterion is met, i.e. mean absolute error between the original and surrogate amplitude spectrum. The first step consists in a spectral

adaptation of the surrogate spectrum and the second step in an amplitude adaptation of the surrogate. At convergence, the surrogate has the same spectrum and amplitude distribution of the original time series, but all nonlinear structures present in the original time series are destroyed.

2.2.4   IAAFT algorithm

Let $\{x_i\}$, $i=1,...N$ is the observed time series. According to the null hypothesis, $x_i=H(s_i)$ where $\{s_i\}$ is a Linear Gaussian Stochastic Process and H is a statistic function, possibly nonlinear. To generate the surrogate data $\{z\}$ (of length N) we should respect two conditions:

- $R_z(\tau) = R_x(\tau)$ for $\tau=1,...,\tau`$
- $A_z(z)=A_x(x)$,

where R is the autocorrelation, A is the amplitude distribution and $\tau`$ the maximum time lag.

We start by a random permutation $\{z^{(0)}\}$ of the data $\{x\}$, the idea is to repeat two steps: i) Approach Rx by adapting the power spectrum of $\{z^{(i)}\}$ to be identical to that of $\{x\}$called $\{y^{(i)}\}$ note that at each iteration the Fourier transform of the iterated time series is calculated and its squared coefficients are replaced by those of the original time series. ii) Regain the identical Ax by reordering $\{x\}$ to have the same rank structure as $\{y^{(i)}\}$ called $\{z^{(i+1)}\}$. The desired power spectrum gained in i) is changed in ii) and therefore several iterations are required to achieve convergence of the power spectrum. The algorithm terminates when the exact reordering is repeated in two consecutive iterations, indicating that the power spectrum of the surrogate cannot be brought closer to the original.

2.2.5   Comparison between the three measures of non-linearity

Here, the statistical significance of the results of the three methods: approximate entropy (ApEn), correntropy (CorrEn) and time reversibility (Tr) was tested by using surrogates.
In the case of CorrEn the original and surrogate values are compared to a reference value to reject or accept the hypothesis. We use the nonlinearity test for CorrEn with surrogate data described in (Aysegul and Jose, 2009). For ApEn and Tr the acceptance and the rejection of the hypothesis is based on the difference between original and surrogates values. The nonlinearity test for time reversibility for example is defined as follow:

51

When a time series has significant nonlinearity, the value of Tr for the surrogate data (Tr_{surr}) will be different than the one of the original time series (Tr_{org}). Thus, nonlinearity can be tested by comparing the Tr_{org} and Tr_{surr}. The underlying null hypothesis is that, like the surrogate data, the original data was also created by a Gaussian linear stochastic process. The null hypothesis is tested by comparing the Tr_{surr} and Tr_{org} by using a statistical test. If the null hypothesis is rejected, it is concluded that the original data has nonlinear properties; whereas if the null hypothesis is accepted, it is concluded that the original data comes from a Gaussian linear stochastic process.

The "Rank test" is used to reject or accept the null hypothesis. Basically, [Tr_{org}; Tr_{surr}] is sorted in increasing order and the rank index for Tr_{org} is returned. With a number of surrogates (n_surr =100 for example), if this rank is > 95 and < 5 (significance level at 95%), this means that it lies in the tail of the distribution, and that the null hypothesis can be rejected (two-tailed test) with a significance of p=2*(1/ (n_surr+1)) =0.019.
The test used for ApEn is essentially the same.

2.2.6   **Statistical parameters**

To evaluate the possible use of the proposed parameters for the classification of contractions, we used the classic Receiver Operating Characteristic (ROC) curves. A ROC curve is a graphical tool permitting the evaluation of a binary, i.e. two classes, classifier. A ROC curve is the curve corresponding to TPR (True Positive Rate or sensitivity) vs. FPR (False Positive Rate or 1-Specificity) obtained for different parameter thresholds. ROC curves are classically compared by five different parameters:

1. Area Under the Curve (AUC). The AUC was estimated by the trapezoidal integration method.
2. Accuracy (ACC) :

$$ACC = \frac{(TP+FN)(TP+TN)(FP+TN)}{TP(FP+TN)+FP(TP+FN)}$$

3. Matthew's Correlation Coefficient (MCC) :

$$MCC = \frac{TP*TN-FP*FN}{\sqrt{(TN+FN)(TN+FP)(TP+FN)(TP+FP)}}$$

4. Specificity:

$$Specificity = \frac{TN}{FP+TN}$$

5. Sensitivity

$$Sensitivity = \frac{TP}{TP+FN}$$

where TP, TN, FP and FN stand respectively for True Positive, True Negative, False Positive and False Negative values.

In order to measure quantitatively the difference between the original data and the surrogates, we compute the z score value defined as:

$$z = \frac{\left| S_{org} - <S_{surr}> \right|}{\sigma_{surr}}$$

where S_{org} denotes the value of the discriminating statistics for the original data set. If S_{surr} denotes the values of S for the realizations of the surrogate time series, $<S_{surr}>$ is the S_{surr} mean and σ_{surr} is the S_{surr} standard deviation.

It is important to notice here that z score is so used for two aims: the first one is to test the significance of the nonlinearity of the signals, and the second aim is to use z score as a parameter to differentiate between pregnancy and labor contractions when computing the ROC curves. For statistical comparison, we used the two tailed sign test.

2.3 **Results**

2.3.1 **On synthetic signals**

We computed the false alarm rate (FAR) of approximate entropy, correntropy and time reversibility with different surrogate numbers on different signals types: linear, nonlinear stationary and nonlinear nonstationary signals. Our first objective was to choose the optimal number of surrogates. Our second objective was to choose the method with the lowest FAR to apply it to real EHG signals for labor prediction purposes. In **Figure** 2.2 we show the evolution of FAR with the number of surrogates on AR (Autoregressive), TAR (Threshold Autoregressive), Rössler, Henon dynamic systems and ARCH (Autoregressive Conditionally Heteroscedastic) signals. **Figure** 2.2A indicates that ApEn correctly detects nonlinearity in

53

Rössler, Henon, logistic and ARCH signals. ApEn totally failed in the nonlinearity detection of TAR signal (FAR = 70% with surrogates number =100) and has high FAR with the linear signal AR (25%). **Figure** 2.2B indicates that the correntropy method provides good performance with the linear signal (AR), whereas it is less efficient with nonlinear signals, as it totally failed with the TAR signal (100% FAR) and gave 30 % FAR with Rössler signals. **Figure** 2.2C shows that all the linear and nonlinear signals are very well classified by using Tr with all our synthetic signals and whatever the number of surrogates.

2.3.2   **On real EHG signals**

The results presented above permitted us to choose the time reversibility method to be used on the EHG signals, due to its power to detect linearity and nonlinearity characteristics for different signals type. For a significance requirement of 95%, we need at least 39 surrogate time series for the two-sided tests. As the results of **Figure** 2.2 show low FAR for all the surrogate numbers, we decided to use 100 surrogates time series to boost the confidence, with an average uterine bursts length used about 24000 samples. The aim then is to test the ability of time reversibility to differentiate between signals recorded during pregnancy and signals recorded during labor.

Figure 2.3 presents an example of a surrogate signal generated from labor burst by using the IAAFT method.

As the signals are segmented manually as explained in the previous chapter, most segmented EHG contain baseline (noise). In order to investigate the influence of the baseline content on the results, we computed the distribution of Tr_{surr} and Tr_{org} on labor signals with baseline (**Figure** 2.4 left) and on the same bursts but without baseline (**Figure** 2.5 left). The results indicated that the labor burst plus baseline signal provide significant difference (null hypothesis rejected) between original and surrogates data. The same labor burst with no baseline signal also presents a significant difference. Furthermore the results of the same test performed on pregnancy contractions (**Figure** 2.4 right) indicates that the difference between original and surrogates data is not significant (null hypothesis accepted). The same conclusion was obtained on the signal without baseline (**Figure** 2.5 right). These results clearly demonstrate that the linearity observed for pregnancy bursts and the nonlinearity for labor ones are related to the uterine activity bursts and not to the presence or the influence of baseline (noise). It permitted us to conclude that a very precise segmentation is not essential when applying time reversibility to these signals.
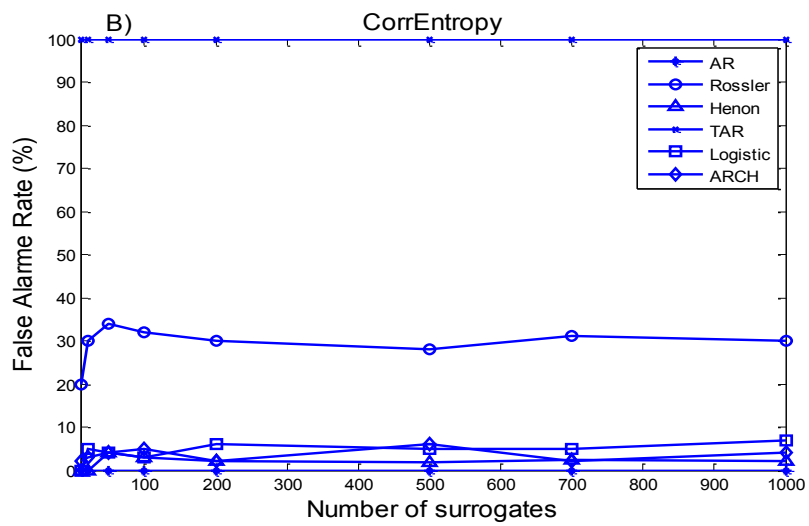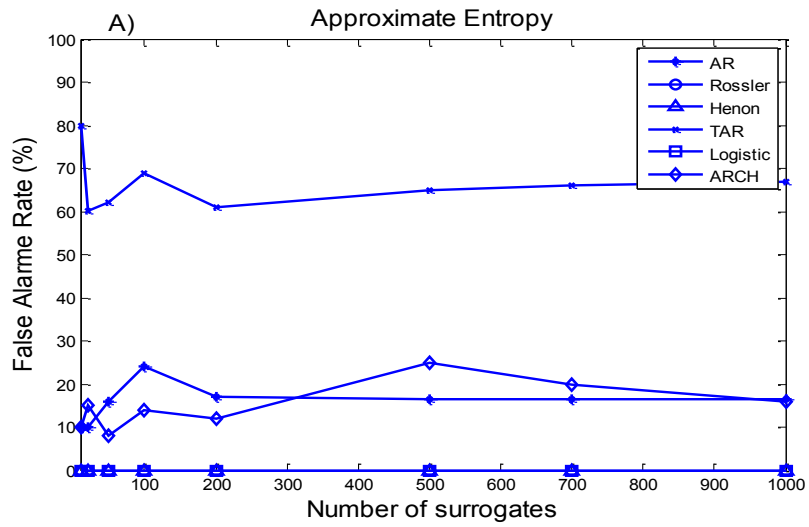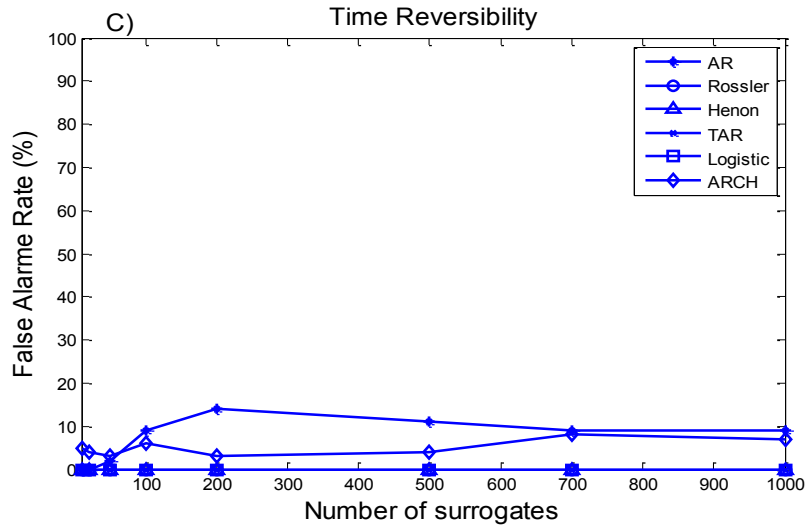
Figure 2.2: Evolution of FAR with the number of surrogates for ApEn (A), CorrEn (B) and Tr (C).
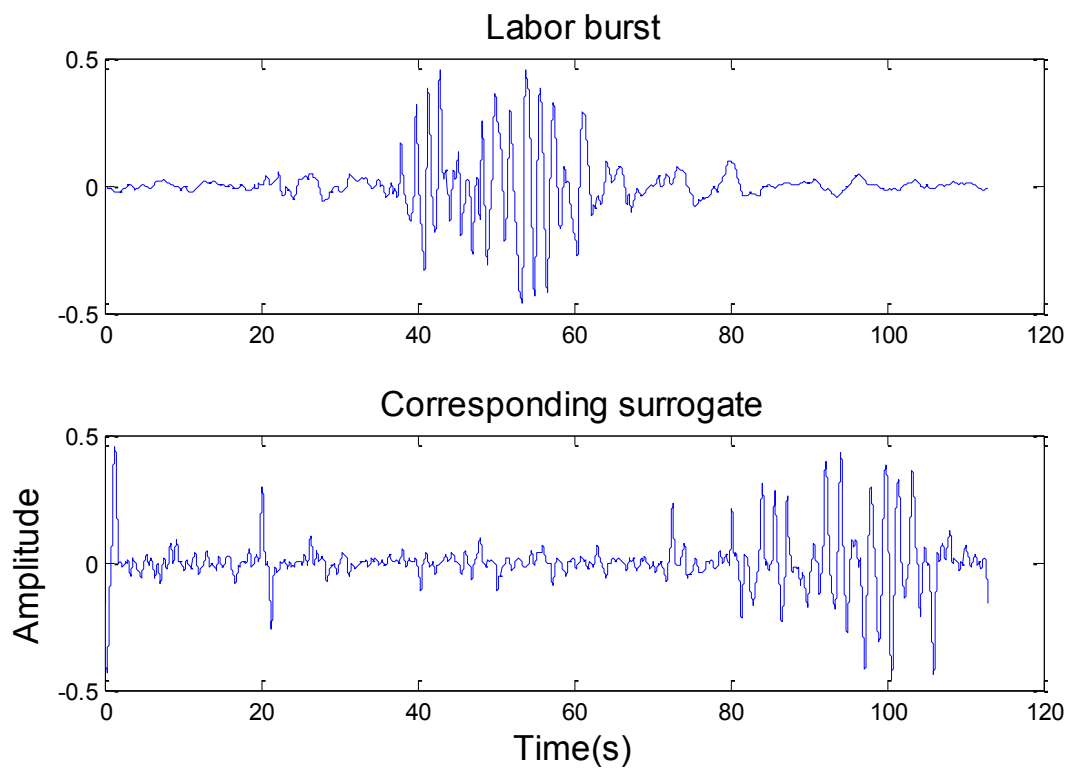
Figure 2.3: The original labor EHG burst (Top); Corresponding surrogate (Bottom).
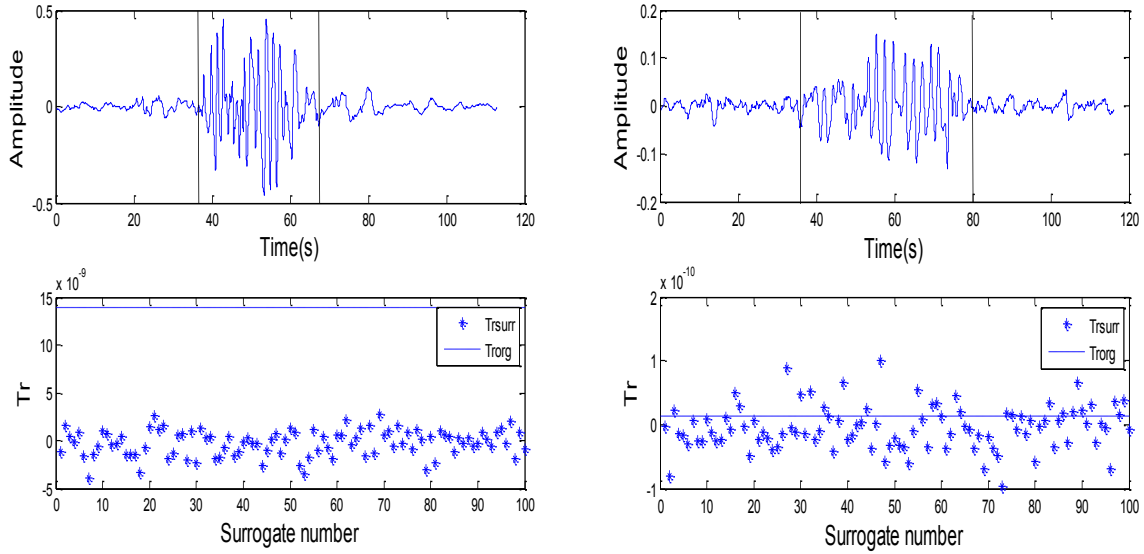
Figure 2.4: (Top): uterine burst + baseline. (Bottom): the distribution of Tr_{surr} and Tr_{org} during pregnancy (right) and labor (Left). The vertical lines present the start and the end of the uterine segmented bursts without baseline as presented in **Figure** 2.5. The * are the Tr_{surr} values and the dashed lines represent the Tr_{org}.
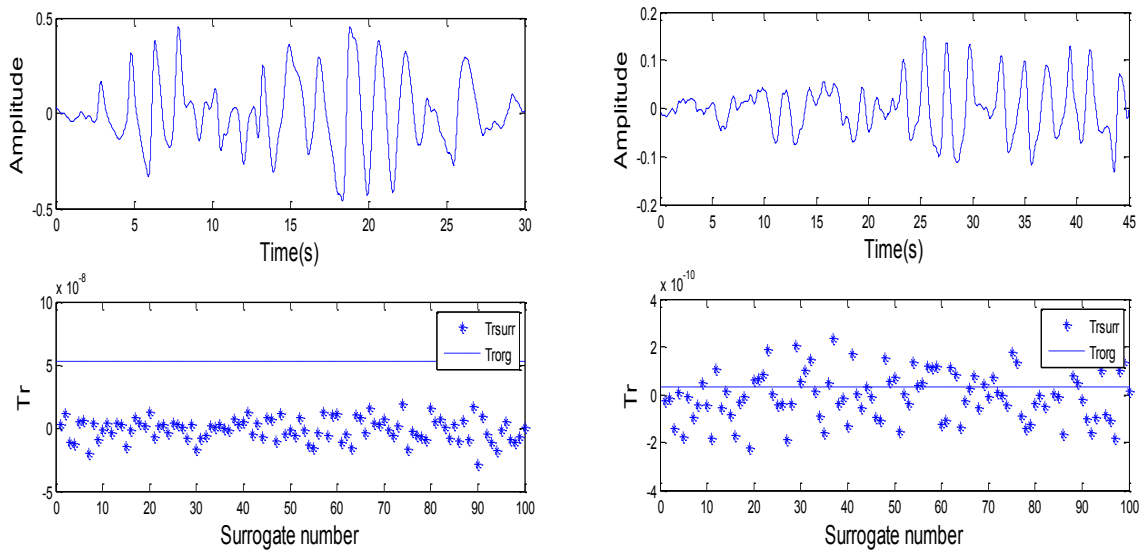
Figure 2.5: Top: Same bursts as used in **Figure** 2.4 but segmented with no baseline. Bottom: distribution of Tr_{surr} and Tr_{org} during pregnancy (right) and labor (Left). The * represent the Tr_{surr} values and the dashed lines represent the Tr_{org}.

2.3.3   **Clinical Application**

Investigating nonlinear behavior in the EHG signals is an important objective. It will allow us to better understand how the uterus works at different situation and different stages

(pregnancy, labor). The results mentioned above indicated a strong nonlinearity present in the EHG signals especially during labor.

The principle aim of applying the different linear/nonlinear methods (here: time reversibility) is to test their performance in view of a possible clinical application. This clinical application can be defined as: the classification of pregnancy and labor signals, labor prediction and, the ultimate goal, the prediction of preterm labor.

2.3.3.1 Classification pregnancy/labor

Figure 2.6 presents the results of the z score computed by time reversibility in order to classify pregnancy and labor signals.
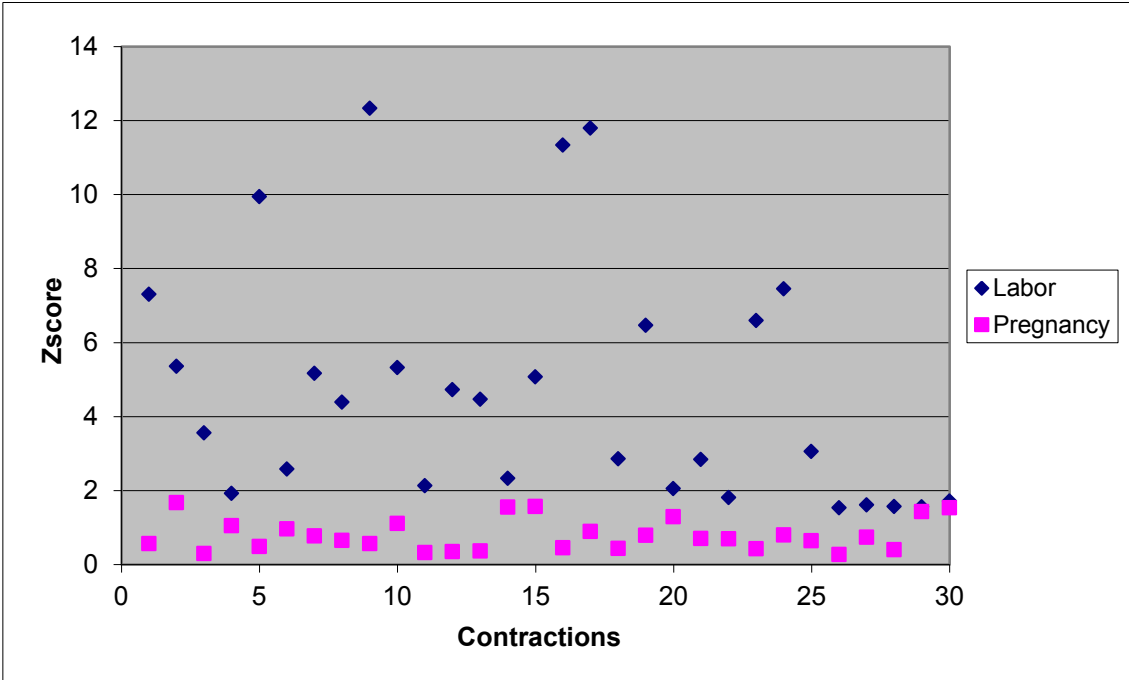
Figure 2.6: Classification of pregnancy and labor signals using the z scores computed from time reversibility method

The associated null hypothesis will be rejected with 95% level for z score>1.96. That is to say, the original time series is nonlinear with a probability of 95%. The null hypothesis cannot be rejected when z score <1.96.

The results presented in **Figure** 2.7 show that the median value of z score for labor signals is > 1.96 and the median value of z score for pregnancy signals is <1.96. This indicates that generally the signals recorded during pregnancy are reversible and the signals recorded during labor are irreversible. There is a significant (p=0.0001) difference between median values of z scores for the pregnancy bursts (median=0.702) and for the labor bursts (median=3.97).
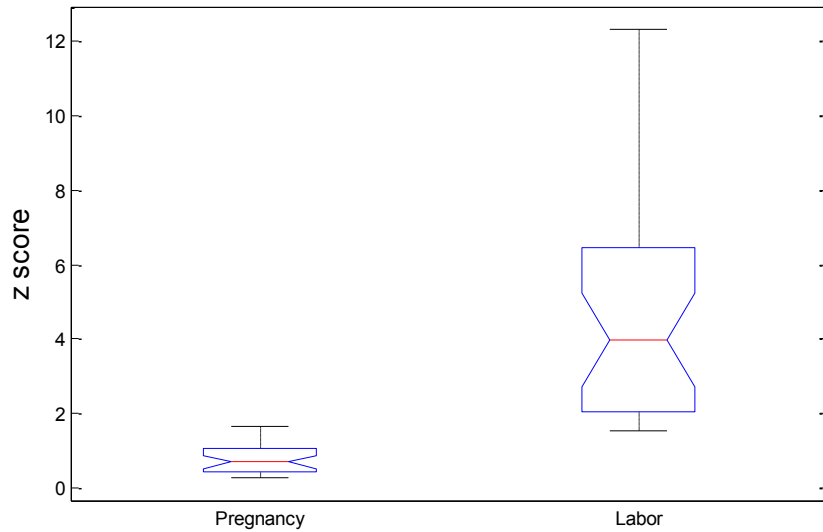
Figure 2.7: Median z scores for the 30 pregnancy bursts and the 30 labor bursts. The difference between the two distributions is significant (p<0.01).

2.3.3.2   Labor prediction

Figure 2.8 presents the ROC curve obtained by using 3 methods for labor vs. pregnancy classification: a well-known linear method classically used in the literature (Mean Power Frequency (MPF)), and 2 non-linear ones, ApEn and Tr. As we can see also from the ROC curve, time reversibility permits us to distinguish clearly between signals recorded during pregnancy and labor. **Table** 2.2 presents the ROC curve parameter comparison between MPF, ApEn and Tr. We observed that MPF has a high sensitivity (0.8) and low specificity (0.5) while it is the opposite for ApEn with low sensitivity (0.52) and high specificity (0.8). Time reversibility has a high sensitivity (0.93) and high specificity (0.96). The probability of correctly classifying labor increases markedly from 0.63 AUC with Mean power frequency to 0.99 with time reversibility.
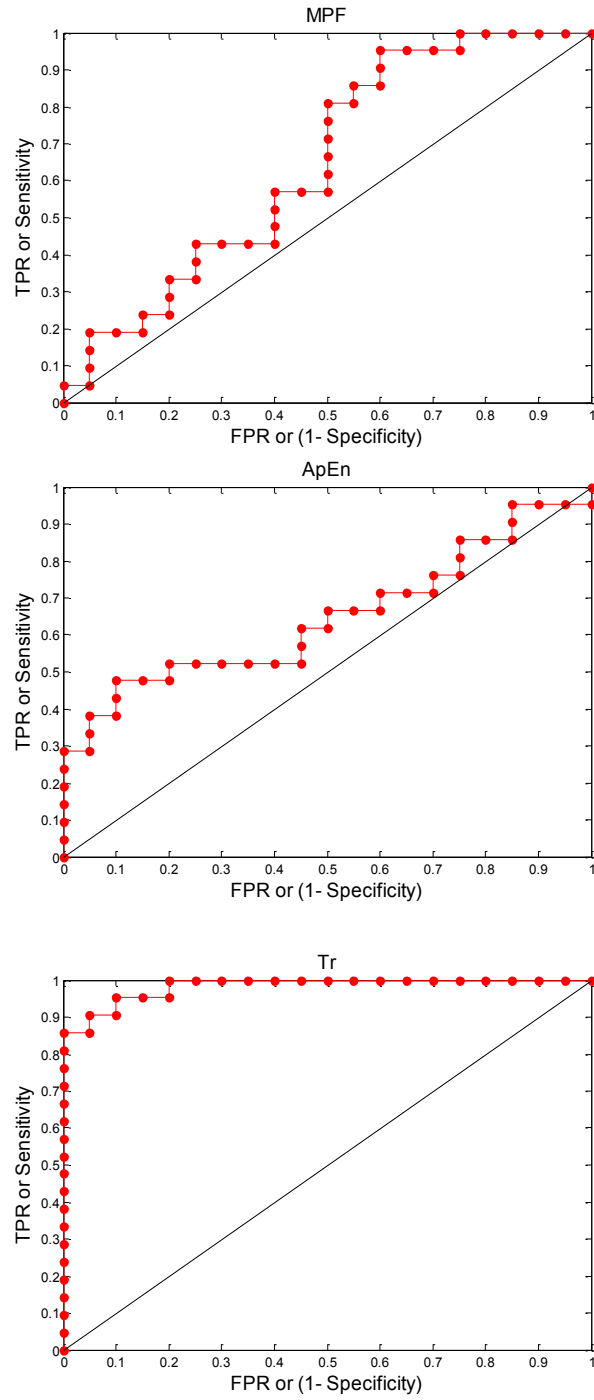
Figure 2.8: ROC curves obtained from the three methods (MPF, ApEn and Tr) for labor vs. pregnancy classification.

	Specificity	Sensitivity	MCC	AUC	ACC (%)
MPF	0.5	0.8	0.32	0.63	65.66
ApEn	0.8	0.52	0.33	0.64	65.8
Tr	0.96	0.93	0.9	0.99	95

Table 2.2 Parameter of the ROC curves obtained with the 3 different methods

MPF: Mean Power Frequency; ApEn: Approximate Entropy; Tr: Time reversibility

2.4   **Discussion**

In this chapter a comparison between three nonlinear methods (approximate entropy, correntropy and time reversibility) was done on linear, nonlinear stationary and nonlinear nonstationary signals in order to choose the best method to apply to real EHG signals. Indeed EHG signals are thought to exhibit non linear as well as non stationary characteristics. The evolution of FAR of each method was computed with different surrogate numbers. The comparison demonstrated the superiority of time reversibility in the detection of linearity and nonlinearity of the different signals, whatever the surrogate number.

We then tested EHG signals for their time reversibility property by using time reversibility. The results indicate that uterine contractions during pregnancy are reversible, whereas labor contractions are temporally irreversible. We have shown how the time reversibility could become a powerful tool to differentiate between pregnancy and labor contractions.

2.5   **Global Conclusion about Chapter 2**

The main conclusions can be taken from this chapter:

- Time reversibility is better than the other tested nonlinear methods in detecting nonlinearity on the synthetic signals.
- An increase of the nonlinearity characteristics of EHG signals from pregnancy to labor is noticed by using Time reversibility and Z score.
- During pregnancy the EHG signals are reversible while during labor the EHG are irreversible.
- Better performance of the nonlinear methods compared to linear methods is obtained for the classification of pregnancy and labor signals.

- Uterine contractile system contains strong nonlinear characteristics, especially during labor.

The direct consequence of these conclusions is that the best choice is to use nonlinear bivariate methods to look into the linear/nonlinear associations between different EHG signals, in order to analyze the propagation of the uterine activity. This is the subject of chapter 3.

Chapter 3 Analysis of EHG propagation

Evaluation of synchronization between signals can give new insights into the functioning of the systems under investigation. We are interested here in the analysis of the relationships between uterine EMG signals acquired on different sites of the pregnant abdomen in order to investigate the propagation of the uterine electrical activity. We introduce in this chapter the theoretical background of several methods used to study the relationships between signals in the time (nonlinear methods) and time-frequency domain. Then we present the results of the application of each method on the EHG signals.

3.1 Methods for measuring statistical coupling between signals

The methods proposed so far can be divided into two types depending on the supposed underlying dependence between signals. Linear methods include essentially the linear cross-correlation (Brazier and Casby, 1952) or the coherence function (Brazier, 1968). These methods are efficient but rely on the assumption of linear dependence between the investigated signals. In most real biological cases however, the relationship between two signals has non linear characteristics.

The development of non linear methods is more recent (Pikovsky A. , 2001). Mars et al. were the first who applied methods based on mutual information on the EEG signals, to determinate relationships and time delays between simultaneously recorded EEG signals during an epileptic paroxysm (Mars and Lopes da Silva, 1983). Pijn et al. also used non linear regression in EEG analysis (Pijn and Lopes Da Silva, 1993). Finally, methods coming from non linear physics (non linear dynamical systems) and chaos theory have been applied to investigate non linear interdependence between biological signals (Lehnertz et al., 1999).

We used in our study the three main families of methods detecting relationships between signals:

- Nonlinear correlation coefficient (h^2): we exclude the classical linear correlation coefficient from this study as it has been demonstrated that h^2 can detect linear as well as nonlinear correlations between signals.

- Phase synchronization methods

- General synchronization methods

All these methods have been widely applied on the EEG signals (Arnhold et al., 1999; Bhattacharya, 2001; Lachaux et al., 1999; Meeren et al., 2002; Mormann et al., 2003; Pijn and Lopes Da Silva, 1993; Quian Quiroga et al., 2002; Wendling et al., 2001).

3.1.1 Nonlinear correlation coefficient

Non linear correlation analysis is a non-parametric method used for evaluating the dependency of a random process (a time-series Y recorded from G_Y, for instance) on another process (signal X recorded from G_X, for instance), independently of the type of relationship between the two processes. Pijn and al. showed that this method performed better than methods based on linear regression for analyzing the interdependences between intracerebral EEG signals (Pijn et al., 1992). Wendling and al. showed that this method can be applied to human intracerebral EEG data for characterizing seizure patterns (Wendling et al., 2001).

Kalitzin et al. confirmed the usefulness of the h^2 parameter in the quantification of the statistical relationships between random signals (Kalitzin et al., 2007). More recently, a robustness study has shown the evolution of h^2 from: pre-ictal period→seizure onset→seizure termination on EEG signals (Wendling et al., 2009).

Non linear regression analysis is a bivariate method that estimates the degree of dependence between two variables. The non linear correlation coefficient h^2 is computed from the signals $X(t)$ and $Y(t)$, by considering that the value of X is seen as a function of the value of Y. The value of Y, given X, can be predicted according to a non linear regression curve. The variance of Y according to this regression curve is termed as the explained variance, since it is explained or predicted by the knowledge of X. The unexplained variance is estimated by subtracting the explained variance from the original one. The correlation ratio, h^2, describes the reduction of variance of Y that can be obtained by predicting the Y values from those of X, according to the regression curve, as h^2 = (total variance - unexplained variance)/total variance.

In practice, to estimate the non linear correlation coefficient h^2, a scatter plot of Y versus X is studied. The values of X are subdivided into bins; for each bin we calculate the X value of the

midpoint (p_i) and the average value of Y (q_i), computed from the same bin interval. The regression curve is approximated by connecting the resulting points (p_i, q_i) by straight line segments (Pereda et al., 2005). Then, the non linear correlation coefficient between the two signals X and Y is calculated as follows:

$$ h^2_{Y/X} = \frac{\sum_{k=1}^{N} X(k)^2 - \sum_{k=1}^{N} (Y(k) - f(X_i))^2}{\sum_{k=1}^{N} Y(k)^2} $$

where $f(X_i)$ is the linear piecewise approximation of the non linear regression curve. The values of h^2 evolve between 0 (X and Y are independent) and 1 (Y is determined by X). One of the advantages of the non linear regression is that it can be applied to signals independently of whether their relationship is linear or not. Another interesting property of the non linear correlation coefficient h^2 is that it is asymmetrical: the h^2 value, from signal X to signal Y, differs from the value from signal Y to X. Wendling et al. used this property and proposed a new parameter named "direction index" to show the direction of the dependency between X and Y (Wendling et al., 2001).

***Illustrating example 1****:*

To better understand the computation of h^2 and its evolution with the degree of coupling between the signals, we present here the different steps to compute h^2 as well as its behavior when analyzing correlation between synthetic signals generated by a Rössler system.

The used Rössler system is a dynamical system of two coupled chaotic oscillators, x et y, defined as:

$$\frac{dx_1}{dt} = -\omega_x x_2 - x_3$$

$$\frac{dx_2}{dt} = \omega_x x_1 + a x_2$$

$$\frac{dx_3}{dt} = b + x_3(x_1 - 10)$$

$$\frac{dy_1}{dt} = -\omega_y y_2 - y_3 + C(x_1 - y_1)$$

$$\frac{dy_2}{dt} = \omega_y y_1 + 0.15 y_2$$

$$\frac{dy_3}{dt} = 0.2 + y_3(y_1 - c)$$

where a=0.15, b=0.2 and c=10. The factor C permits us to control the coupling strength between the two oscillators. C varies from 0 (independence) to 1 (total coupling). The two signals that we use to evaluate the relation are x_1 and y_1. We used ω_x=0.95 and ω_y=1.05 which are the values used in (Rosenblum et al., 1996). **Figure** 3.1 presents typical examples of the h^2 computation steps with different coupling values. The behavior of h^2 with the different coupling values indicate that when C=0 the h^2 value is ~0 while when C=1 the h^2 value is 0.89. This indicates that h^2 is a good indicator of the relationships between signals.
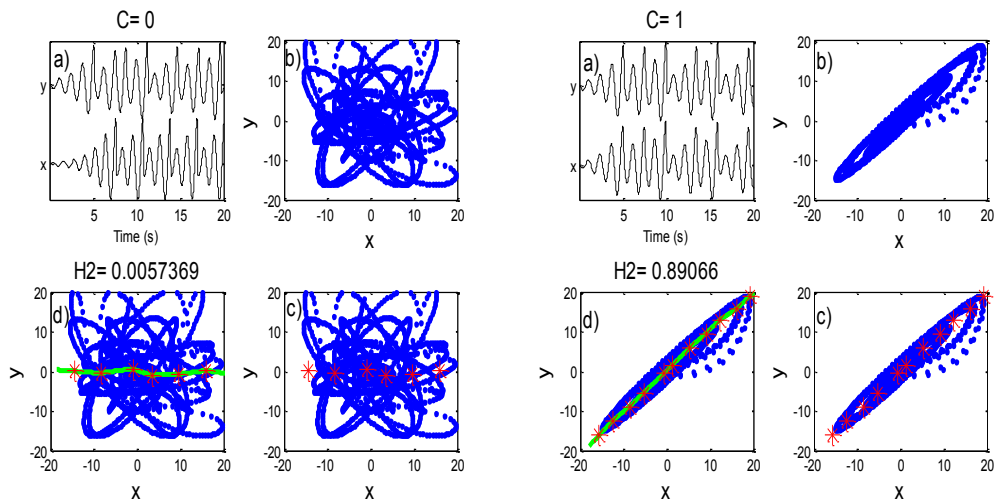
Figure 3.1 a) Two signals generated by Rössler system (Left C=0: independence signals; Right C=1: signals totally correlated). b) Scattergrams: the amplitude values of *y* plotted as a function of the corresponding amplitude values of *x*. c) The ordinate is split into equal-sized interval. Within each interval, the average of *y* values is calculated. The red star is the point

with coordinate (average y, midpoint of each interval). d) h^2 is then computed as the difference between the total variance of all the y-values minus the unexplained variance (the sum of the square of the deviations of each sample from the curve -green line-), all divided by the total variance.

3.1.2 Phase synchronization

It is well known that the phases of two coupled nonlinear (noisy or chaotic) oscillators may synchronize even if their amplitudes remain uncorrelated, a state referred to as phase synchronization (PS).

The principle of PS corresponds to a phase locking between two systems defined as:

$$\varphi_{n,m}(t) = \left| n\Phi_x(t) - m\Phi_y(t) \right| \leq C$$

where $\Phi_x(t)$, $\Phi_y(t)$ are the unwrapped phases of the signals (x and y) representative of the two systems, and C a constant. However, real signals are often noisy, and exhibit random phase slips of 2π. Therefore the $\varphi_{n,m}(t)$ is normally analyzed from the so-called *cyclic relative phase:* $\varphi'_{n,m}(t) = \varphi_{n,m}(t) \bmod 2\pi$ (i.e., the relative phase difference wrapped to the interval [0, 2π]).

In order to study the existence of PS synchronization between experimental signals, it is first necessary to obtain their phases.

3.1.2.1   Extracting the phase

Two closely related approaches are mainly used to obtain the phases of a time series. In both cases, the original real-valued signal $x(t)$ is transformed, with the help of an auxiliary function, into a complex-valued signal, from which an instantaneous value of the phase is easily obtained.

The first approach is the use of the Hilbert transform (HT). Classically, the analytical signal $h(t)$ for a temporal series $x(t)$ is defined as:

$$h_x(t) = x(t) + i\, \tilde{x}(t) = A_x^H(t) e^{i\phi_x^H(t)}$$

where $A_x^H(t)$ and $e^{i\phi_x^H(t)}$ are the amplitude and the phase of the signal $x(t)$ respectively, and $x_H(t)$ is the HT of $x(t)$ and defined as:

$$x_H(t) = \frac{1}{\pi}(CPV)\int_{-\infty}^{\infty}\frac{x(t')}{t-t'}dt'$$

with CPV denoting the Cauchy principal value defined as:

$$CPV\int_{-\infty}^{+\infty}. = \lim_{\substack{\varepsilon\to 0 \\ A\to\infty}}(\int_{-A}^{-\varepsilon}. + \int_{-\varepsilon}^{+A}.)$$

In the frequency domain, the analytical signal can be written as (Marple and S, 1999):

$$Z_x(f) = \begin{cases} 2X(f) & for\ f \succ \\ X(0) & for\ f = 0 \\ 0 & for\ f \prec \end{cases}$$

where *X(f)* is the Fourier transform of *x(t)*. The analytic signal contain only the frequency component of the signal *x(t)*. For real signal *x(t)*, the Fourier transform is symmetric hermitien so $X(-f)=X^*(f)$, where * represents the complex conjugate.

The instantaneous phase of signal *x(t)* is then given by:

$$\phi_x(t) = \tan^{-1}\frac{x_H(t)}{x(t)}$$

The second approach makes use of the wavelet transform and was recently introduced for EEG signal analysis (Lachaux et al., 1999). Complex Morlet wavelet is used in this approach given by:

$$\psi_0(t) = \pi^{-1/4}e^{i\omega_0 t}e^{-\frac{1}{2}t^2}$$

where ω_0 is the wavelet central pulsation

Wavelet coefficients $W_x(a,\tau)$ are produced through the convolution of a mother wavelet function $\Psi(t)$ with the analyzed signal *x(t)* or:

$$W_x(a,\tau) = \frac{1}{\sqrt{a}}\int x(t)\Psi^*(\frac{t-\tau}{a})dt$$

where *a* and τ denote the scale and translation parameters respectively; * denotes complex conjugation.

The phase of *x(t)* is then defined as:

$$\phi_x = \tan^{-1} \frac{\operatorname{Im} W_x(a,\tau)}{\operatorname{Re} W_x(a,\tau)}$$

The same way is used to compute ϕ_y from the signal *y(t)*.

It has recently been shown that the application of both approaches (i.e., HT and wavelet transform) produces essentially the same result (Quian Quiroga et al., 2002). For this reason we used the HT to extract the phase of the EHG signals as it is simpler to compute.ρ

3.1.2.2   Indexes of phase synchronization

The probability distribution of the relative phase modulo 2π ($\varphi = \varphi_x - \varphi_y[2\pi]$) for a random independent process is supposed to be uniform. Coupling between the processes may modify this distribution. Thus the intensity of the interaction between systems can be estimated by means of indices that quantify the deviation of this distribution from a uniform distribution having the same support.

Two different indexes of phase synchronization are often computed based on the distribution of the two phases ϕ_x and ϕ_y extracted in the first step. The first one is based on the Shannon entropy (Tass et al., 1998) and the second one is based on the characteristic function of the distribution of the phase difference between the two signals (Mormann et al., 2000).

A) Phase Entropy

The first phase synchronization measure uses the Shannon entropy, I_φ, of the distribution of $\varphi_{n,m}(t)$. The entropy is normalized according to the maximal entropy I_{max} obtained in the case of a uniform distribution of the phase difference, corresponding to no preferential value of $\varphi_{n,m}(t)$ (Pereda et al., 2005).

$$\rho_{n,m} = \frac{I_{\max} - I_\varphi}{I_{\max}}$$

where *n, m* are integers indicating the ratios of possible frequency locking. In this work, we assume *n=m=1* for simplicity.

B) Mean Phase Coherence

The second phase synchronization index is called *mean phase coherence* and is defined as:

$$\gamma_{n,m} = \sqrt{\left\langle \cos \varphi_{n,m}(t) \right\rangle^2 + \left\langle \sin \varphi_{n,m}(t) \right\rangle^2}$$

where ‹.› denotes average over time.

ρ and γ values evolve between 0 (no phase synchronization) and 1 (perfect synchronization). They increase monotonically with the degree of phase synchronization (Bhattacharya, 2001).

The two indexes presented above have the same range of variation [0: no phase synchronization – 1: perfect phase synchronization]. However, they do present some differences. Comprehensive comparative studies of their performances have been carried out in computer simulated as well as in EEG data (Kreuz et al., 2004; Tass et al., 1998). The authors indicated that by using $n=m=1$, ρ and γ present the greatest sensibility to the transition from weak coupling to PS state.

In most phase synchronization application to biosignals, authors used $n=m=1$ to simplify the analysis (Bhattacharya, 2001; Lachaux et al., 1999; Mormann et al., 2000; Quian Quiroga et al., 2002). We used the same values in this work.

Illustrating example 2:

We present here an example to study the performance of ρ and γ when analyzing phase synchronization between signal x and y. In this example $m=n=1$.

x and y are two sinusoidal signals with the same frequency $f_1=f_2=10$Hz (**Figure** 3.2 right) or y is a sinusoidal signal and x is a white noise (**Figure** 3.2 left).
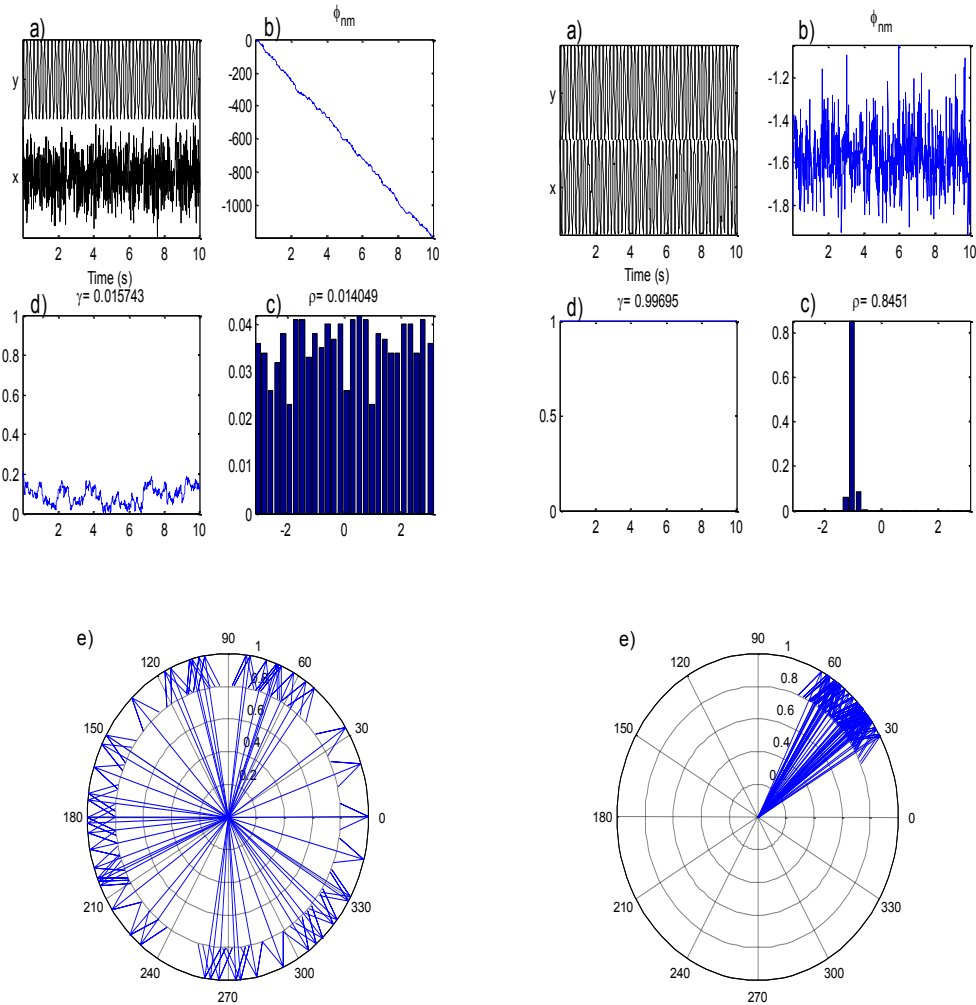
Figure 3.2: a) Right: x and y are two sinusoidal signals with $f1=f2=10$Hz and SNR=10dB; Left: y is sinusoidal signal and x is a white noise. b) Phase difference $\varphi_{n,m}(t)$ c) $\varphi_{n,m}(t)$ distribution with the value of the phase entropy d) Evolution of the mean phase coherence with time window and the final value of γ . e) The values of $\varphi_{n,m}(t)$ are shown as solid line arrows in the unit circle.

Figure 3.2 shows how phase entropy and mean phase coherence can reflect the phase synchronization between two signals in two extreme cases. In **Figure** 3.2b-right, the phase

difference is quasi constant and gives a uniform distribution in **Figure** 3.2c-right, with a strong value for phase entropy, ρ=0.84. The **Figure** 3.2d-right represents the values of γ with a temporal window (1s). We can notice a constant high values for the temporal mean phase coherence with γ equal to 1. The values of φ$_{n,m}$(t) are shown as solid line arrows in the unit circle in **Figure** 3.2e-right. The relative phase is concentrated in one sector of the circle (γ~1). This is obtained for a strong phase correlation between the 2 signals.

Figure 3.2-left contrasts with the right part. It shows the case when no correlation exists between *x* and *y*. **Figure** 3.2b-left shows the decreasing (not constant) of phase difference, with a random distribution in **Figure** 3.2c-left. It gives a low value of ρ=0.01 and a random low values for the windowing γ, with a mean value equal to 0.01. The relative phase is randomly scattered over the circle (γ~0) (**Figure** 3.2e-left).

3.1.3 General synchronization

This type of methods were introduced after chaotic structure was discovered in EEG signals (Babloyantz et al., 1985). The study of synchronization between chaotic systems has been a topic of increasing interest since the beginnings of the 1990's. In brief, these measures quantify how well one can predict the trajectory in phase space of one of the systems, knowing the trajectory of the other. On the following pages we will describe in detail the robust set of measures proposed by (Arnhold et al., 1999; Quian Quiroga et al., 2002) to quantify how neighborhoods (i.e., recurrences) in one attractor maps into the other. This has turned out to be the most reliable way of assessing the extent of general synchronization (GS) in time series.

First, a state space trajectory is reconstructed from each scalar time series by using a time delay embedding method (Takens, 1981). This technique makes it possible to investigate the interaction between two nonlinear dynamical systems without any knowledge about the governing equations. First, for each discrete time *n,* a delay vector corresponding to a point in the state space reconstructed from *x,* is defined as:

$$x_n = (x_n, x_{n+\tau}, ..., x_{n+(m-1)\tau}), \quad n = 1, ..., N$$

where *m* is the embedding dimension and τ denotes time lag. Let $r_{n,j}$ and $s_{n,j}$, *j=1,....k,* denote respectively the time indices of the *k* nearest neighbors of x_n and y_n.

For each x_n , the mean squared Euclidean distance to its *k* neighbors is defined as

$$R_n^{(k)}(X) = \frac{1}{k}\sum_{j=1}^{k}(x_n - x_{r_{n,j}})^2$$

and Y-conditioned mean squared Euclidean distance is defined by replacing the nearest neighbors by the equal time partners of the closest neighbors of y_n,

$$R_n^{(k)}(X/Y) = \frac{1}{k}\sum_{j=1}^{k}(x_n - x_{s_{n,j}})^2$$

If $R(X) = (1/N)\sum_{n=1}^{N} R_n^{N-1}(X)$ then $R_n^{(k)}(X/Y) \approx R_n^{(k)}(X) \ll$ if the systems are strongly correlated, while $R_n^{(k)}(X/Y) \approx R(X) \gg$) if they are independent. Accordingly, we can define an interdependence measure $S^{(k)}(X/Y)$ (Arnhold et al., 1999) as:

$$S^{(k)}(X/Y) = \frac{1}{N}\sum_{n=1}^{N}\frac{R_n^{(k)}(X)}{R_n^{(k)}(X/Y)}$$

Since $R_n^{(k)}(X/Y) \geq R_n^{(k)}$ by construction, we have:

$$0 < S^{(k)}(X/Y) \leq 1.$$

with 0 means independence between x and y, while 1 indicates synchronization.

Another measure was proposed by Arnhold et al. called $H^{(k)}(X/Y)$ defined as:

$$H^{(k)}(X/Y) = \frac{1}{N}\sum_{n=1}^{N}\log\frac{R_n(X)}{R_n^k(X/Y)}$$

This is zero if X and Y are completely independent, while it is positive if nearness in Y implies also nearness in X for equal time partners.

Then a normalized version of H has been proposed by (Quian Quiroga et al., 2002) called $N^{(k)}(X/Y)$ and defined as:

$$N^{(k)}(X/Y) = \frac{1}{N}\sum_{n=1}^{N}\frac{R_n(X) - R_n^{(k)}(X/Y)}{R_n(X)}$$

The asymmetry of *S*, *H* and *N* is the main advantage over other nonlinear measures such as the phase synchronization described above. It means that S(X/Y), H(X/Y) and N(X/Y) are not equal to S(Y/X), H(Y/X) and N(Y/X) respectively. These measures can thus give an information about the direction of the relationship as well as the related driver-response relationships (Arnhold et al., 1999; Quian Quiroga et al., 2002; Schmitz, 2000).

To choose the optimal embedding dimension *m*, we use Cao's method described in (Cao, 1997). The optimal time lag, *τ*, is computed using the auto mutual information method described in the OpenTSTOOL toolbox (Merkwirth et al., 2002).

Illustrating example 3:

Figure 3.3 shows the results obtained by using the 3 nonlinear interdependence measures. Two cases are presented: in the case when there is no coupling between the two systems (top), the three measures indicates low values with S=0.001, H=0.05 and N=0.003. While with a strong coupling between the two nonlinear systems (Rössler and Lorenz, bottom), the three measures indicate strong values with S=0.275, H=3.6 and N=0.93.
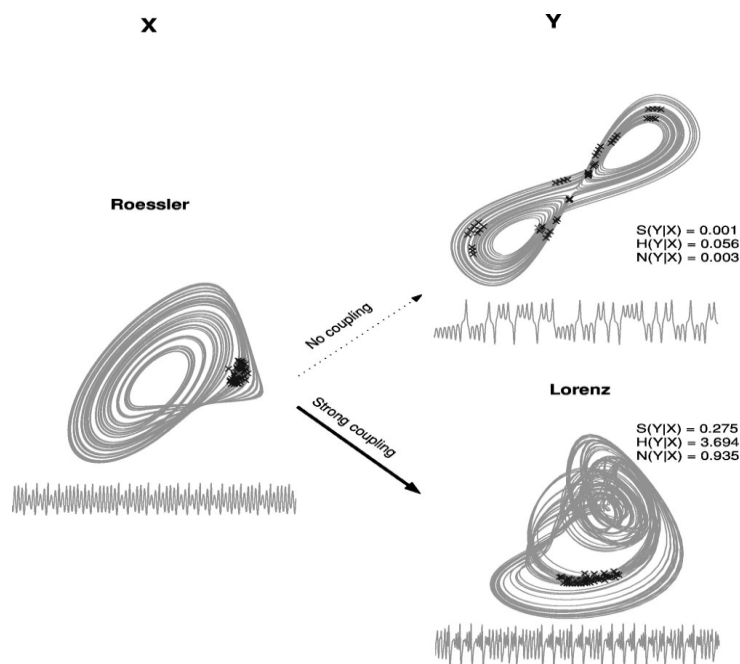
Figure 3.3: Example of nonlinear interdependence measures. The example shows a Lorenz system driven by a Rössler with zero coupling (upper) and with strong coupling (lower). Below each attractor, the corresponding time series is shown. The (*X/Y*) interdependences are calculated in the same way, starting with a neighborhood in *Y*. Each * represent a temporal point in the trajectory. **Figure** edited from (Quian Quiroga et al., 2002).

3.2 Results

3.2.1 Two channels vs multichannel

We have two main aims when analyzing the relationship between EHG signals:

- Classification of pregnancy and labor signals
- Monitoring of pregnancy i.e. the analysis of the evolution of uterine synchronization of the same woman at different times of gestation.

For these purposes, we first decided to compare the use of multichannel uterine EMG recordings vs. only two channel recordings, for the analysis of the different synchronization methods summarized in **Table** 3.1. We use ROC curves in the two cases (one channel vs multi channel analysis), to quantify the performances of the different methods for the classification of signals measured on women, either during normal pregnancy or during labor.

Methods group	Method name	Abbreviation
Regression	Nonlinear correlation coefficient	h^2
Phase synchronization (PS)	Mean phase coherence	γ
	Phase entropy	ρ
General synchronization (GS)	Similarity index 1	S
	Similarity index 2	H
	Similarity index 3	N

Table 3.1: The different methods used in this chapter classified by groups

The different index values, h^2, γ, ρ, S, H and N, were computed in two ways: (i) Between two bipolar channels (Vb7-Vb8 mentioned in chapter 1) (ii) Mean values over the entire possible pairs (144-12=132 possible pairs for correlation analysis between the 12 bipolar signals). As our aim is to compare these indexes for two classes of contraction (pregnancy, labor), the six parameters are computed from 30 EHG bursts recorded on women during pregnancy and 30 EHG bursts recorded on women during labor. ROC tests are used to identify the most pertinent method for the differentiation between EHG recorded during pregnancy and EHG recorded during labor (**Figure** 3.4, 3.5 and 3.6).
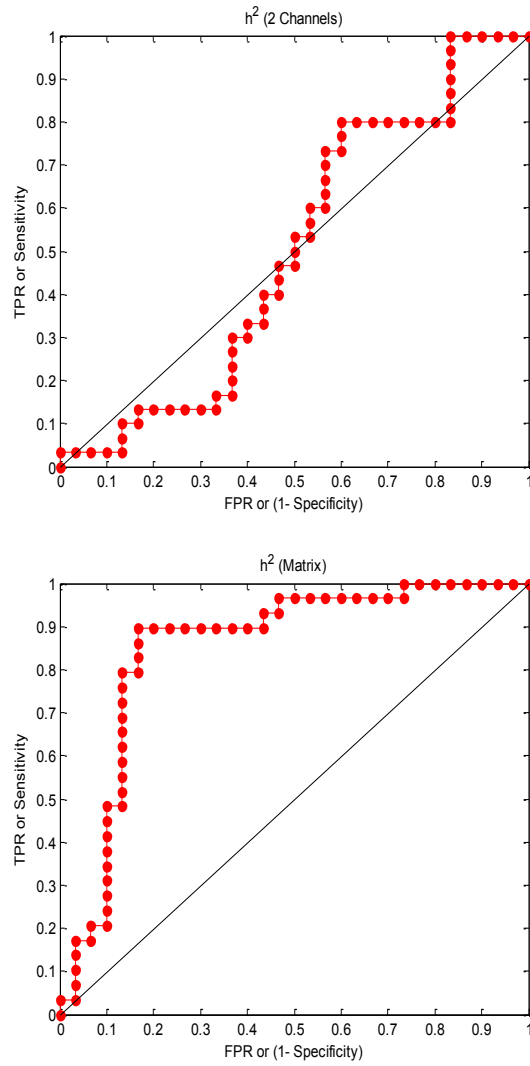
Figure 3.4**:** ROC curves obtained from the regression method with two channels (Up) and with the whole pairs (Bottom) for the prediction of labor.
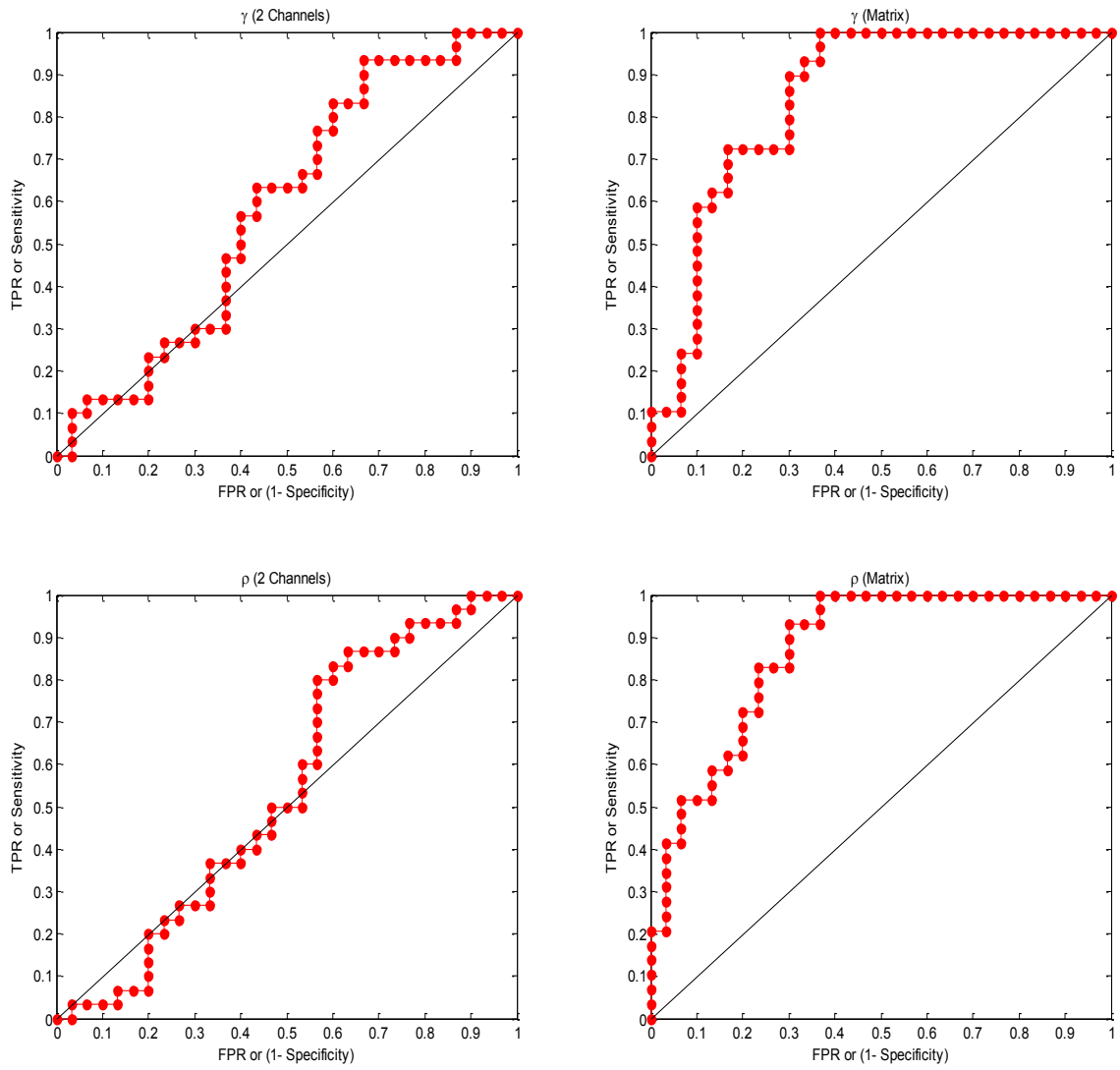
Figure 3.5: ROC curves obtained from the phase synchronization methods with two channels (left) and with the whole pairs (right) for the prediction of labor.
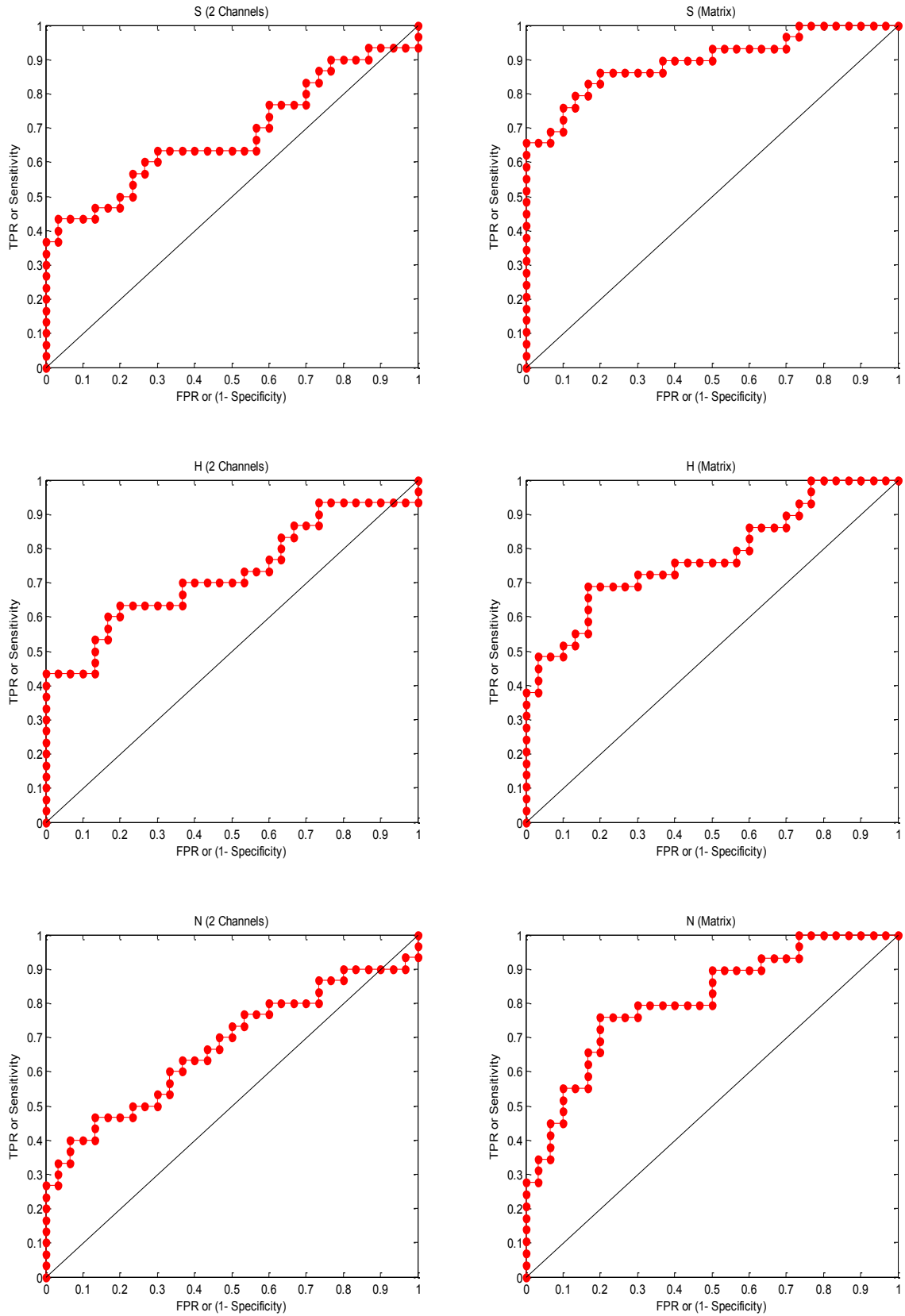
Figure 3.6: ROC curves obtained from the general synchronization methods with two channels (left) and with the whole pairs (right) for the prediction of labor.

All the curves clearly indicate that the use of the whole pair mean markedly increases the performance of correct signal classification (**Figure** 3.4, 3.5 and 3.6 right), when compared to the use of only two bipolar channels, to evidence the difference between pregnancy and labor contractions (**Figure** 3.4, 3.5 and 3.6 left).

In **Table** 3.2 we can see the different parameters computed for the ROC curves. As an example, the *mean phase coherence* presents a very low specificity (0.43), a high sensitivity (0.8) and a very low area under the curve (AUC=0.54) when using only two channels. These values increase dramatically when computed from the whole pairs, with a high specificity (0.72), a slightly better sensitivity (0.82) and a high area under the curve (AUC=0.87). Similar results are obtained with the *phase entropy*. In general **Table** 3.2 demonstrates a strong increase in the classification parameters for all the methods used when using the whole pair mean.

We must notice here that all the methods have been applied on the uterine bursts without any special pretreatment: no subband filters were applied, and we do not take into account the effect of the noise.

An important result of this study is that the use of data computed from the 12 bipolar signals gives clearly better information than when only two bipolar channels are processed. In the light of these results, we will use the whole pairs data for further analysis.

Another important result is that the regression and the general synchronization methods indicated higher correlation during labor than pregnancy while the phase synchronization method evidenced the opposite. Some different phenomenon may exist that produce an increase in amplitude correlation and a decrease in phase coherence all along pregnancy.

		Specificity	Sensitivity	MCC	ACC (%)	AUC
2 Channels	h^2	0,4333	0,7333	0,1747	58,3333	0,5011
	ρ	0,4333	0,8000	0,2508	61,6667	0,5422
	γ	0,5667	0,6333	0,2004	60,0000	0,5878
	S	0,8333	0,6423	0,4763	73,3333	0,7011
	H	0,8000	0,6 33	0,4395	71,6667	0,7356
	N	0,6333	0,6333	0,2667	63,3333	0,6733
Multichannel	h^2	0,8333	0,8966	0,7307	86,4407	0,8506
	ρ	0,7667	0,8276	0,5949	79,6610	0,8701
	γ	0,7000	0,8966	0,6071	79,6610	0,8460
	S	0,8333	0,8276	0,6609	83,0508	0,8943
	H	0,8333	0,6897	0,5291	76,2712	0,7782
	N	0,8000	0,7586	0,5593	77,9661	0,8080

Table 3.2: Comparison of ROC parameters for the different methods for labor vs. pregnancy contraction classification.

3.2.2   Correlation analysis during the contraction

In this part we explore the correlation evolution within the uterine bursts and the difference in correlation between base line (before and after burst) and during the burst of uterine activity. **Figure** 3.7 presents the set of 12 bipolar contraction bursts from a woman in labor.

We compute the h^2 values before, during and after the uterine activity, with a sliding window equal to 30 s corresponding to a typical duration of the uterine burst. The results are presented as a 12x12 matrix. Each value (i,j) of the matrix represent the parameter computed to study the correlation between EHGi and EHGj. The values on the diagonal, representing the autocorrelation, are not used when computing the mean value of the matrix.

Figure 3.7 illustrates the evolution of h^2 matrices along the uterine burst for a labor contraction. The **Figure** indicates that before the burst, there is no noticeable correlation between the different channels, while with the start of the burst, the correlations between the different channels clearly increase, to then decrease when the burst is finished.

Figure 3.8 represents the evolution of h^2 matrices for a pregnancy contraction. The **Figure** confirms the results of the labor contraction: absence of correlation before the uterine burst then an increase in the correlation, followed by a decrease at the end of the burst.

The results indicate that high correlation is related to uterine activity and not a random effect or noise correlation. Consequently, the results show that manual segmentation has no big effect on the correlation analysis as the difference in correlation between the non-contractile parts of the signal (baseline) and during the uterine activity is obvious.

We should note here that the precision of the start of the uterine burst is visual and based on the corresponding TOCO signal.
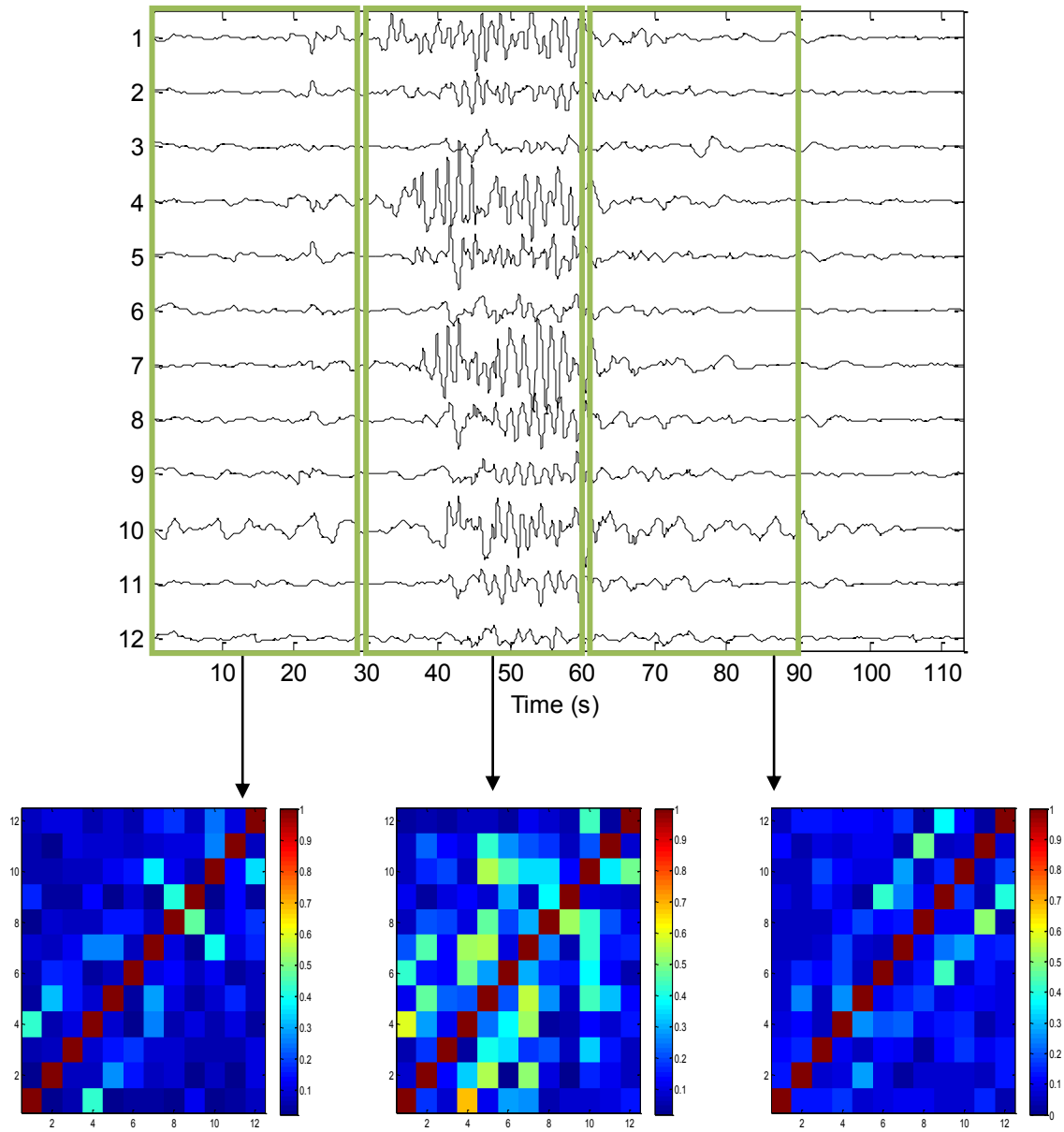
Figure 3.7**:** Evolution of h^2 matrices before, during and after the burst for a labor contraction
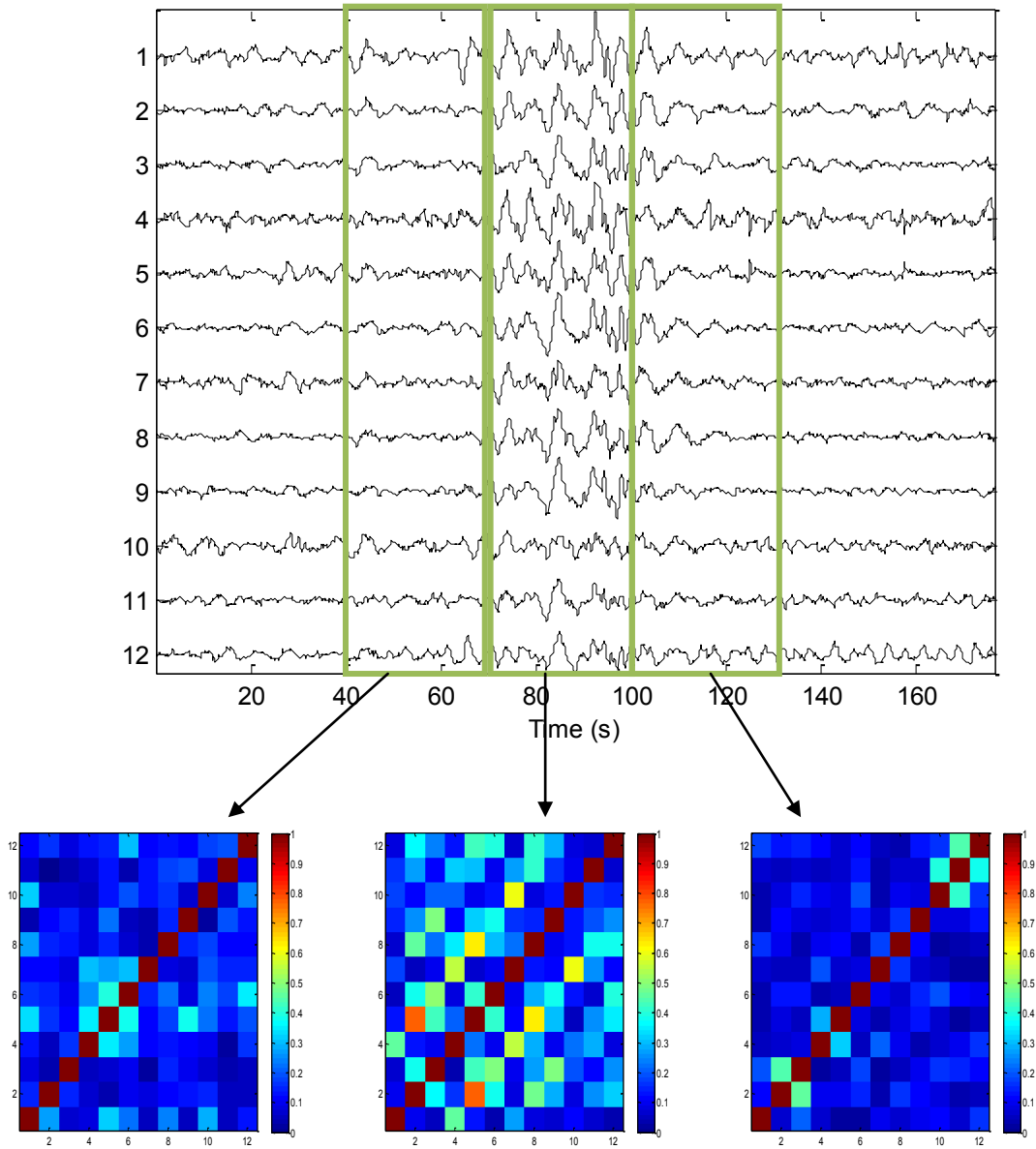
Figure 3.8: Evolution of h^2 matrices before, during and after the burst for a pregnancy contraction

3.2.3   Pregnancy monitoring

If we are able to find a method to distinguish between pregnancy and labor contractions in general, this will help us to develop a method to separate true preterm labor from painful physiological pregnancy contractions. In addition to collecting and comparing recordings from different women in different situations, we are also interested in knowing how contractions are likely to evolve along pregnancy for the same woman. We expect by this analysis to better understand the EHG propagation phenomena and then used them as tool for clinical application. For this reason a special set of recordings has been collected, called 'longitudinal recordings'. We have thus recorded signals from the same woman at different times of gestation.

We chose h^2, the nonlinear correlation coefficient, to evidence a longitudinal evolution along gestation, due to its fast computation, its capacity to detect linear and nonlinear amplitude correlation. Furthermore, it has demonstrated capacity to detect propagation phenomena when applied to EEG analysis (Pijn and Lopes Da Silva, 1993).

The h^2 values were computed pair wise and to represent them in color-coded non linear correlation matrices. One correlation matrix represents therefore all the information concerning the h^2 values for the relevant contraction. We first computed the h^2 matrix for each contraction studied, and then we computed the mean matrix over all the contractions obtained for each week of gestation (WG) for a given recording. We thus obtain one matrix for each WG.

Table 3.3 summarizes the main information for the 5 women used in the longitudinal analysis. Only for one woman we have signals during pregnancy and labor. For the others 4 we got only pregnancy signals. Here we don't take into account the effect of the placenta position. All the signals are from women with normal labor i.e. no preterm deliveries. Signals from 7 others women have at this time been recorded 'longitudinally' but unfortunately without any uterine contractions occurring during the recordings.

Woman		Term	Mode of delivery	Term of delivery	Contractions number
W1	G1	33	Normal	40+6	4
	G2	35	Normal	40+6	2
	G3	37	Normal	40+6	3
W2	G2	29+5	Normal	41+4	2
	G2	31+5	Normal	41+4	2
W3	G1	39+2	Normal	40+2	5
	G2	40+1	Normal	40+2	6
W4	G1	33+6	Normal	37	3
	G2	35+6	Normal	37	4
	G3	36+6	Normal	37	3
	Labor	37	Normal	37	3
W5	G1	34+1	Normal	38	4
	G2	36+1	Normal	38	4
	G3	37+1	Normal	38	4

Table 3.3: Information about the women used in the longitudinal analysis.

Figure 3.9 presents the evolution of h^2 computed from data recorded at different increasing pregnancy terms for W1. As an example, for W1 we compute h^2 and then the average over all the contractions observed during these three recording sessions: 4 contractions at 33 WG (G1), 2 contractions at 35 WG (G2) and 3 contractions at 37 WG (G3). **Figure** 3.9 evidences noticeable modifications of h^2 values (interpreted as correlation between channels) occurring along term (**Figure 3.**7a: 33WG 3b:35WG 3c: 37WG). The mean values evolve from 0.27 (at 33 WG) to 0.44 (at 37 WG).
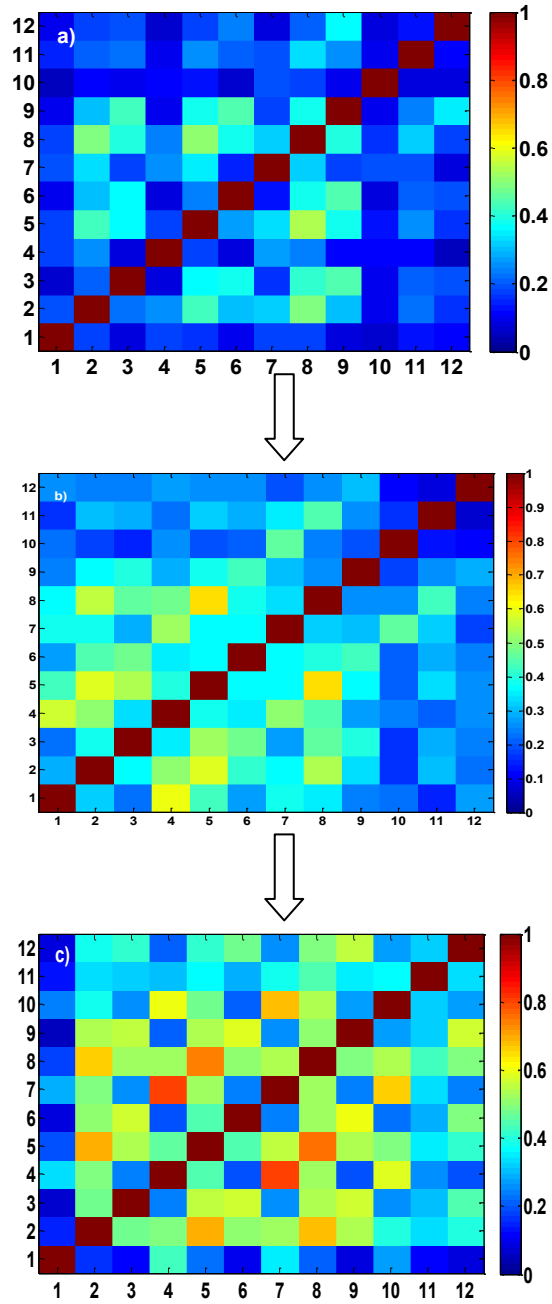
Figure 3.9: Evolution of the h^2 matrix along term for W1 a) G1: 33WG b) G2: 35WG c) G3: 37WG.
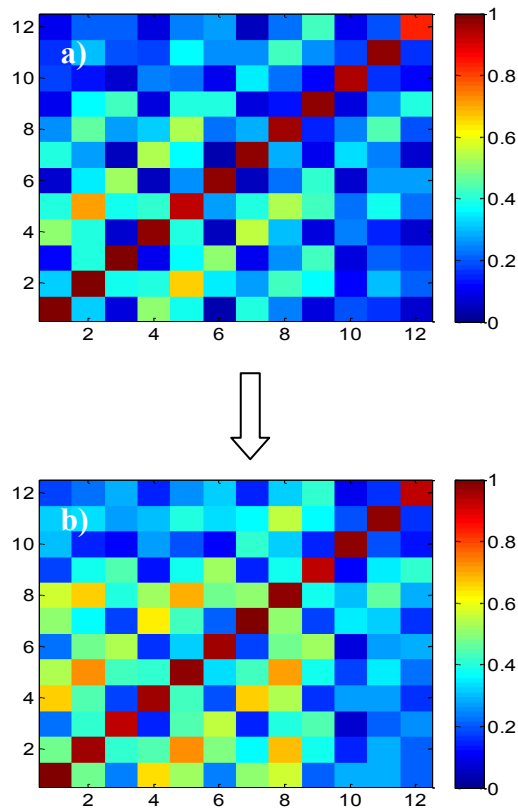
Figure 3.10: Evolution of the h^2 matrix along term for W2 a) G1: 30WG b) G2: 32WG.

Figure 3.10 presents the evolution of h^2 on W2 at two different terms: G1 at 30WG and G2 at 32 WG. The results confirm the observation of **Figure** 3.7, i.e. an increase in the correlation with the term.

Also we present in **Figure** 3.11 the evolution of h^2 matrix on W4 at three different WG and labor. The results confirm the observations on W1 and W2 with an increase in the correlation with term (especially from G2 to G3) then an increase of the correlation from G3 (pregnancy) to labor.
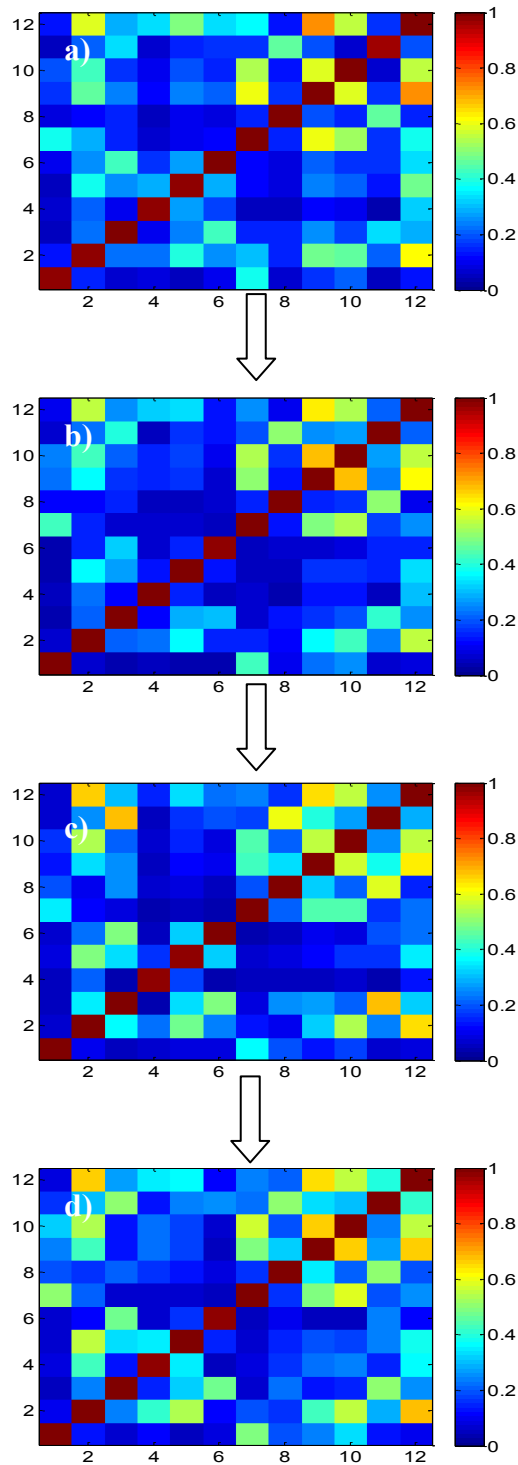
Figure 3.11: Evolution of the h^2 matrix along term for W4 a) G1: 33(+6) WG b) G2: 35 (+6) WG c) G3: 36 (+6) WG and d) Labor at 37 WG

3.3   Conclusion and discussion

Our study of the relation between two EHG signals indicates that a difference exists between the values of the non linear correlation coefficient in pregnancy and labor, associated with a general increase in h^2 with term and a decrease in phase synchronization. The ultimate goal of this work is to find a method that can be used for pregnancy monitoring and then prediction of premature labor.

Until now, we only have longitudinal data for five women. And for two of these women, we only get two term points. The evidences provided by this scanty dataset are far from being conclusive of the evolution of h^2 along term. It does not neither permit us to give a quantitative value for this increase. However the results obtained for available signals recorded from these 5 women (**Figure** 3.12) indicate an increase in h^2 with term, when term is computed in weeks before labor. The absolute value of h^2 is however very different for every different woman. We need therefore to increase our data set, and to study different tools that will permit to quantify with some 'absolute' value the physiological evolution along term, in order to be able to detect a pathological situation (i.e. preterm labor).
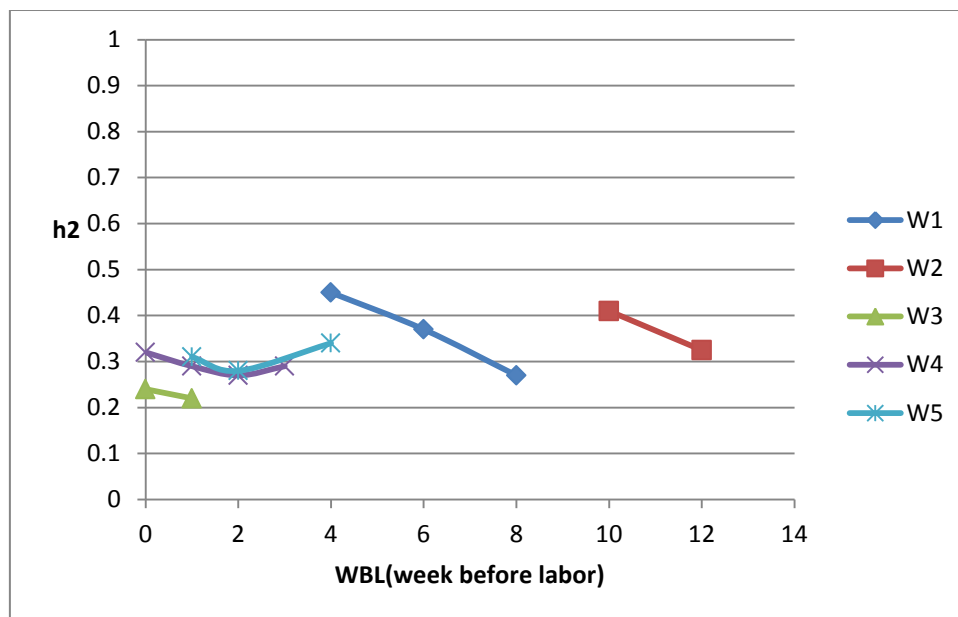
Figure 3.12: The evolution of h^2 with week before labor for the 5 women.

3.4 Time-frequency Approach to analyze the statistical relationships between signals

Inter-correlation is a purely temporal method; it cannot be used to analyze the interplay of various frequency components independently.

Furthermore, classical interrelation measures such as Fourier-based coherence and correlation rely on the stationarity of the measured signals, which is a condition that is rarely fulfilled with real biological signals.

Time frequency distributions (TFD's) were introduced as means of representing signals whose frequency content varies with time, and for which either one or both time domain representations or frequency domain representations are inadequate to appropriately describe the signal. Many different TFDs of a signal exist, including, but not limited to, the Wigner-Ville distribution (WVD), the spectrogram using a Short Time Fourier Transform (STFT), the wavelet transform (WT), the Hilbert Huang transform (HHT) and other methods that evaluate several parameters with TFD, such as the relationship between the instantaneous frequency (IF) and the TFD's (Boashash, 1992).

Recently, alternative tools to investigate coherence between signals, based on wavelet analysis have been developed and successfully applied to biological signals like EEG/MEG signals (Lachaux et al., 2002). They allow tracking the time-course of coherence in non-stationary neuronal signals with good temporal and frequency resolution.

Several approaches have been taken to study the relationship between nonstationary signals in the time-frequency domain. The three main approaches are:

1. Multiple window time frequency analysis (MW-TFA) (Xu et al., 1999).

2. Frequency-dependant correlation coefficient (Ansari-Asl et al., 2006).

3. Time varying causal coherence function (TVCCF) based on the multivariate autoregressive model (Zhao et al., 2007).

As the comparison between these different methods is not the aim of our analysis. We will not describe all these methods in detail. We chose to use the complex-wavelet analysis. Indeed, its variable window length, depending on the analyzed frequency band, does not suppose a particular model of the data. Furthermore, another advantage is the possibility it offers to extract phase information. In addition, wavelet analysis has been used with success on many

types of signals such as EEG signals (Li et al., 2007) as well as geophysical time series (Grinsted A. et al., 2004).

3.4.1 **The continuous wavelet transform**

The wavelet transform can be used to analyze time series that contain nonstationary power for many different frequencies (Daubechies, 1990).

The continuous wavelet transform (CWT) can decompose a signal into a set of finite basis functions. Wavelet coefficients $W_X(a, \tau)$ are produced through the convolution of a mother wavelet function $\Psi(t)$ with the analyzed signal $X(t)$ or:

$$W_X(a, \tau) = \frac{1}{\sqrt{a}} \int X(t) \Psi^* (\frac{t-\tau}{a}) dt$$

where a and τ denote the scale and translation parameters respectively; * denotes complex conjugation. By adjusting the scale a, different frequency components in the signal can be extracted. The factor $\sqrt{a}$ is for energy normalization across the different scales. The wavelet transforms thus projects the information of the time series $X(t)$ on the two dimension space (scale a and translation τ).

In this study, we used the complex Morlet wavelet, given by:

$$\psi_0(t) = \pi^{-1/4} e^{j\omega_0 t} e^{-\frac{1}{2}t^2}$$

where ω_0 is the wavelet central pulsation. In this paper we used $\omega_0 = 2\pi$. Morlet wavelet is a Gaussian–windowed complex sinusoid. The Gaussian's second order exponential decay of the Morlet function gives a good time localization in the

time domain (Torrence and Compo, 1998). We chose this wavelet (the fact that it is complex) as it provides simultaneously the signal amplitude and phase. This property allows us to use the complex Morlet Wavelet transform (cMWT) to investigate the coherence/synchronization between two signals recorded at two different sites simultaneously.

Based on cMWT, the wavelet power of a time series $X(t)$ at the time scale space is called the scalogram. It is simply defined as the squared modulus of $W_X(a, \tau)$.

3.4.2 The cross wavelet transform

Given two time series X and Y, their cMWT are $W_X(a,\tau)$ and $W_Y(a,\tau)$ respectively. Their cross-cMWT is defined as

$$W_{XY}(a,\tau) = W_X(a,\tau)W_Y^*(a,\tau),$$

where * denotes the complex conjugate. The plot of $|W_{XY}(a,\tau)|^2$ is called cross-scalogram (Li et al., 2007). It provides the mean to indicate the coincident events over frequency, for each time in the signals X and Y.

3.4.3 Wavelet coherence

The cross-scalogram is a measure of the similarity of power, at different frequency bands, for two separate uterine signals. It gives a 'direct' estimation of the correlation of two uterine activities in the time–frequency domain. So the estimated values contain bias and noise information. To solve this problem we use the wavelet coherence defined as:

$$(C(a,\tau))^2 = \frac{\left| W_{XY}(a,\tau) \right|^2}{W_{XX}(a,\tau)W_{YY}(a,\tau)}$$

with the cross-scalogram defined as:

$$W_{XY}(a,\tau) = 1/a \int_{-\Delta t}^{+\Delta t} W_X(a,\tau+t)W_Y^*(a,\tau+t)dt$$

Note that the hermitian product defined above is replaced by an estimation given by an averaging over time ($\tau\pm\Delta t$).

The Auto-spectra $W_{XX}(a,\tau)$ and $W_{YY}(a,\tau)$ can be calculated by using the above equation. When using these definitions, the coherence is bounded between $0 \le ((C(a,\tau))^2 \le 1$.

3.4.4 Amplitude and phase correlation

The wavelet coherence computes the relation in phase and amplitude simultaneously. It does not permit to describe separately the relations of amplitude and phase between uterine electrical activities from two separates location on the abdomen. As we are interested in identifying the nature of the relation between EHG signals, we choose to use two different methods that focus on separate aspects of the relationship between the signals, namely the phase and the amplitude:

- The first method is the Wavelet local correlation coefficient (WLCC), proposed by (Buresti G., 1999) and defined as:

$$WLCC(a,\tau) = \frac{\mathrm{Re}\left[\left|W_{XY(a,\tau)}\right|\right]}{\left|W_X(a,\tau)\right|\left|W_Y(a,\tau)\right|}$$

where Re is the real part of W_{XY}.

WLCC is a tool that describes the phase correlation between two time series in the time-frequency domain.

- The second method is the cross wavelet coherence function (CWCF) which computes the amplitude (intensity) relation between two signals in the time-frequency domain (Sello S and J, 2000). It is defined as:

$$CWCF(a,\tau) = \frac{2\left|W_{XY(a,\tau)}\right|^2}{\left|W_X(a,\tau)\right|^4 + \left|W_Y(a,\tau)\right|^4}$$

The values of CWCF range from 0 (no amplitude correlation between X and Y) and 1 (X and Y are totally correlated in amplitude).

The application of these 2 methods on EEG signals has indicated that phase correlation decreases and amplitude correlation increases during the transition from interictal to ictal stages (Li et al., 2007).

Simultaneously, with CWCF and WLCC, we computed the phase difference between X and Y in the time-frequency plane, defined as:

$$\phi(s,\tau) = \tan^{-1}\left(\frac{\mathrm{Re}(W_{XY}(s,\tau))}{\mathrm{Im}(W_{XY}(s,\tau))}\right)$$

Re is the real part of the cross-cMWT and Im is its imaginary part.

In our results, the phase difference is represented by arrows. Phase arrows indicate the phase difference of the two bursts being compared. This can also be interpreted as a lead/lag: if the arrows are oriented to the right it means that the two signals are in phase and if they are oriented to the left it means that the signals are in anti-phase.

The statistical significance of the results of the two methods WLCC and CWCF was tested by using surrogates. We can thus be sure that the results obtained are not due to chance and that they correspond to real features present in the signals. We used the iterative amplitude

adjusted Fourier transform (IAAFT) method to produce the surrogates in the case of WLCC and bootstraps in the case of CWCF (cf previous chapter). The choice of the type of surrogates depends on the way the surrogate is resampled in the particular method. We used the bootstraps in the case of CWCF (linear relation) because its resampling is linear, whereas when studying the phase correlation (nonlinear relation) nonlinear resampling is needed. IAAFT is appropriate in this case. In IAAFT, surrogates have the same power spectrum and autocorrelation function as the original time series, but their phases are totally different.

The method we propose to use in this work can be described with the following steps, for WLCC for ex:

1. Compute WLCC between the two original signals X and Y, we obtain WLCCorg.

2. Generate N surrogates from signal Y, so we obtained: Y_s(s=1... N).

3. For each surrogate, calculate WLCC between X and Y_s then: WLCCsurr =WLCC(X, Y_s)

4. The confidence limits for WLCC are obtained from the tails of the WLCCsurr distribution.

5. The generated surrogates have the same amplitude information as Y but their phases are randomized. The null hypothesis is that the results related to amplitude information obtained on Y are the same as those obtained on the surrogates. By rejecting this hypothesis we can be sure (to within 1-p) that the phase information obtained is significant and not due to chance.

6. "Rank test" is used to reject or accept the hypothesis:

In a rank test, [WLCCorg; WLCCsurr (:)] is sorted in increasing order, and the rank index for WLCCorg returned. With a number of surrogates (n_surr =25 for example), if the rank of WLCCorg is unity or 25, this means that it lies in the tail of the distribution, and the null can be rejected (two-tailed test) with a significance of p=2*(1/ (n_surr+1)). In this paper the n_surr used was 100. Ranks <5 and > 95 were considered significant and the hypothesis thus rejected (p=0.05). The significant values were contoured by thick black lines and arrows are only plotted inside the contoured regions. Phase difference values that did not test as significant were not plotted on the graphs.

3.4.5 **Phase synchronization**

The parameter used for measuring phase synchronization is the relative phase angle between two oscillatory systems. The Morlet wavelet transform acts as a bandpass filter and, at the

same time, yields separate values for the instantaneous amplitude *A(t)* and the phase Φ *(t)* of a time-series signal at a specific frequency. Thus, the wavelet phases of two signals *X* and *Y* can be used to determine their instantaneous phase difference in a given frequency band, and to establish a synchronization measure (Wavelet Phase Synchronization: WPS) which quantifies the coupling of phases independently from amplitude effects.

In order to evidence the variation of the strength of phase synchronization between two EHG bursts, we used the intensity of the first Fourier mode of the distribution (mean phase coherence) described above.

Illustrating example 4

Suppose X and Y are two sinusoidal signals generated with three temporal stages:

$$\begin{cases} 0 \leq t \leq 12 \ \text{Phase and amplitude coupling} \\ 13 \leq t \leq 25 \ \text{Only phase coupling} \\ 26 \leq t \leq 40 \ \text{No coupling} \end{cases}$$

Figure 3.13 describes the behavior of the different method on two signals X and Y. The Co-scalogram W_{XY} between the two scalograms W_X and W_Y indicate a high common power between the two signals. The wavelet coherence (WC) evidences the coherence between the two signals, whatever the nature of the relationships. WLCC illustrates the phase correlation between X and Y, while CWCF shows high amplitude correlation in the first stage and no correlation when only phase relationship is present. It indicates that CWCF can detect only the amplitude relationship between the two signals. It is important to notice here that WLCC and CWCF indicate high values in region where we don't have any relationship. These observations justify the need of a statistical test to test the significance of the correlations detected. Wavelet phase synchronization (WPS) is then computed to detect the phase synchronization between X and Y. WPS shows a phase synchronization in stage one.

3.5 Results

The results will be divided in two sections: the first one contains the application of the wavelet coherence (WC) to investigate the relationships between the uterine bursts for the different frequency components (FWH and FWL) of the EHG signal, and to detect the zone with the higher/lower coherence. The purpose of the second part is the separation of amplitude and phase information to look into the type of relationship between the uterine

bursts, and lastly the quantification of the performances of the TF method in classifying pregnancy and labor signals.

3.5.1 FWL vs FWH

In this part, we applied the wavelet coherence method to signals recorded on women during labor. The first step was the manual segmentation of the bursts of contractile activity. The segmentation was used to isolate the burst from the non-contractile parts of the signal (baseline). Then we first applied the method on the segmented bursts to detect their coupling or synchronization.

The scalogram (**Figure** 3.14c, 3.14d) permits to identify the frequency components of the bursts X and Y. It clearly shows the two frequency components FWL and FWH. **Figure** 3.14e presents the wavelet coherence between the same two bursts recorded during the same contraction, from separate locations on a woman during labor. We can notice that the strongest correlation concentrates in the [0.1-0.3] frequency band, corresponding to FWL.

The second step of the study was to test the method on signals with no previous segmentation of the bursts. This was done in order to test the robustness of this method relatively to the baseline noise. In the results shown on **Figure** 3.15, we used two EHG signals, each one containing four bursts of activity. On the scalograms (**Figure** 3.15b, 3.15d), we can observe the two frequency components (FWL and FWH) of each segmented burst.
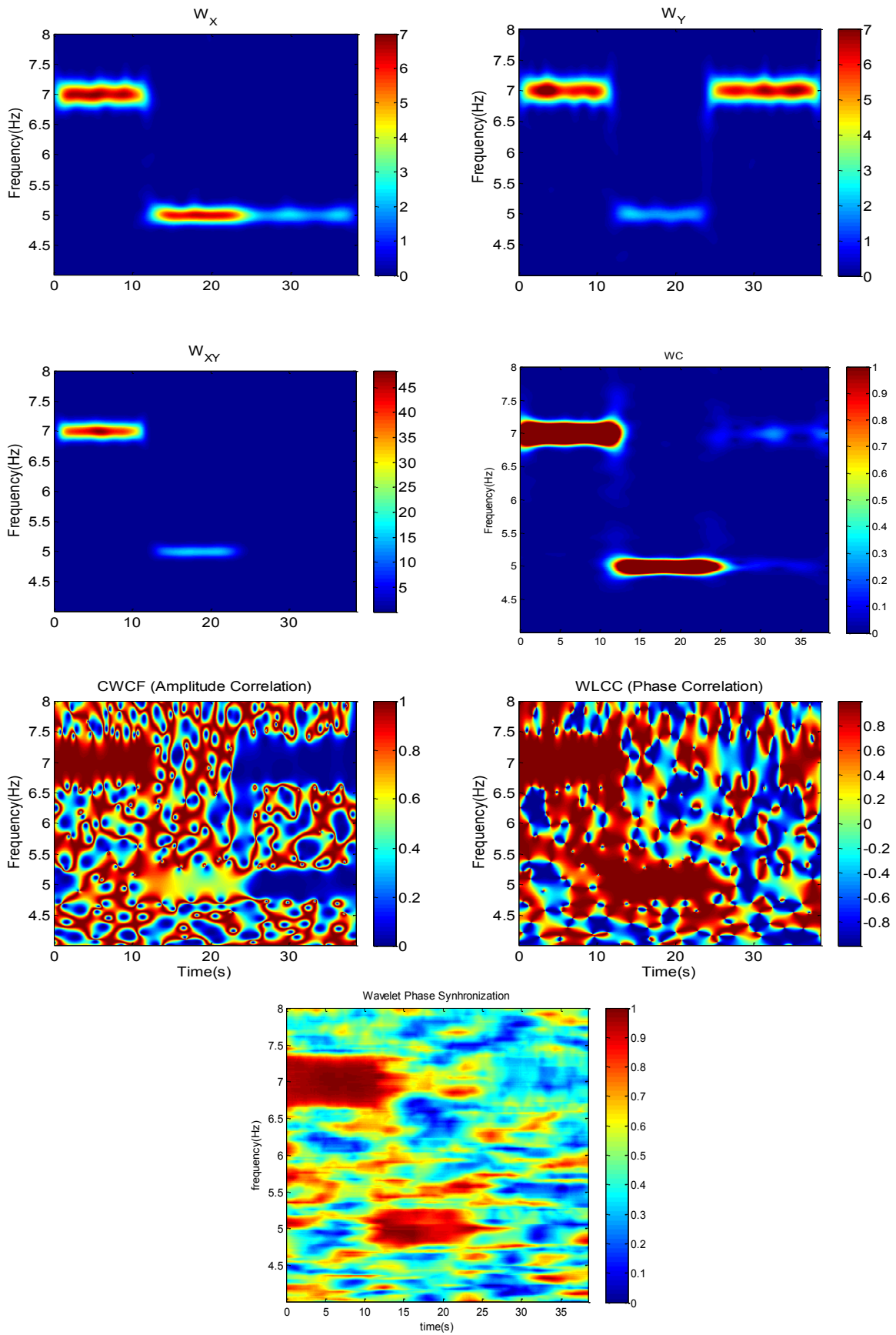
Figure 3.13: Synthetic demonstration of the different TF methods described above.

Figure 3.15e presents the result of the wavelet coherence between the two signals. We can observe strong coherence values during the activity bursts, and very small ones between the bursts (baseline).

This **Figure** also confirmed that the strongest coherence is related to FWL. We can conclude from this observation that it is not necessary to segment the contractions before analysis. The wavelet coherence can successfully be used directly on the signal containing many bursts, as the baseline is completely uncorrelated, unlike the part containing the uterine activity burst. This result could be of great importance and could ease the processing for clinical use.

We then add the phase information on the WC graph. Phase arrows show the relative phasing of the two bursts in question. This can also be interpreted as a lead/lag, if the arrows are ordered in a range means that they are some kind of phase synchronization between the two signals at this range.

In **Figure** 3.16 we see the wavelet coherence with the phase arrows between the two signals (different contraction than in **Figure** 3.14). On the one hand it confirmed the presence of strong coherence at FWL. On the other hand, we can notice that the arrows are more ordered in the frequency band where we have the higher coherence. This observation means that we have a strong coherence with constant phase shift between the two uterine activity bursts for FWL.
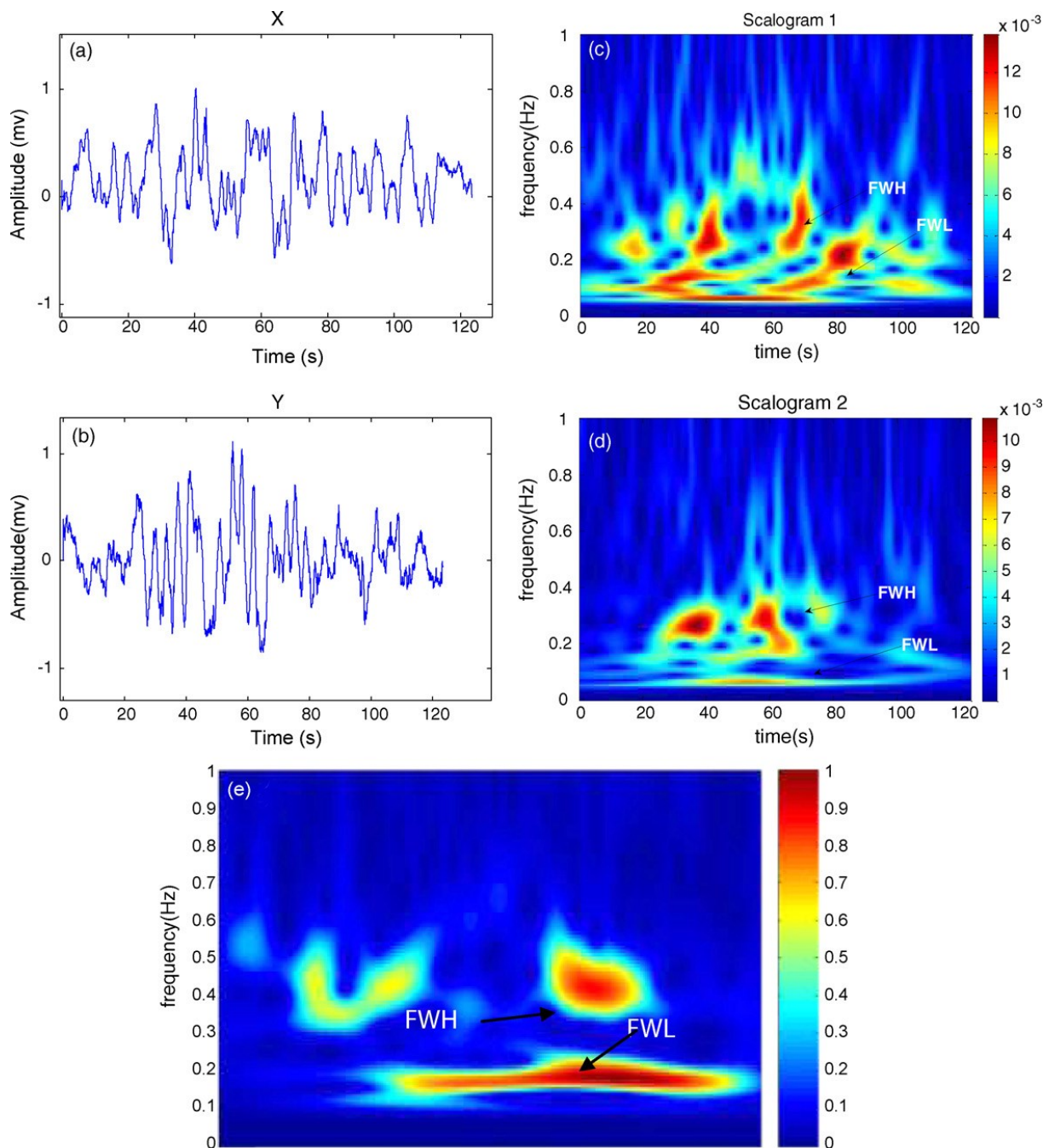
Figure 3.14: Two electrohysterograms (EHG) bursts in labor (a, b) and their respective scalograms (c, d), with the two frequency components, Fast Wave Low (FWL) and Fast Wave High (FWH), (e) wavelet coherence between the two segmented bursts showing the difference in coherence between FWL and FWH.
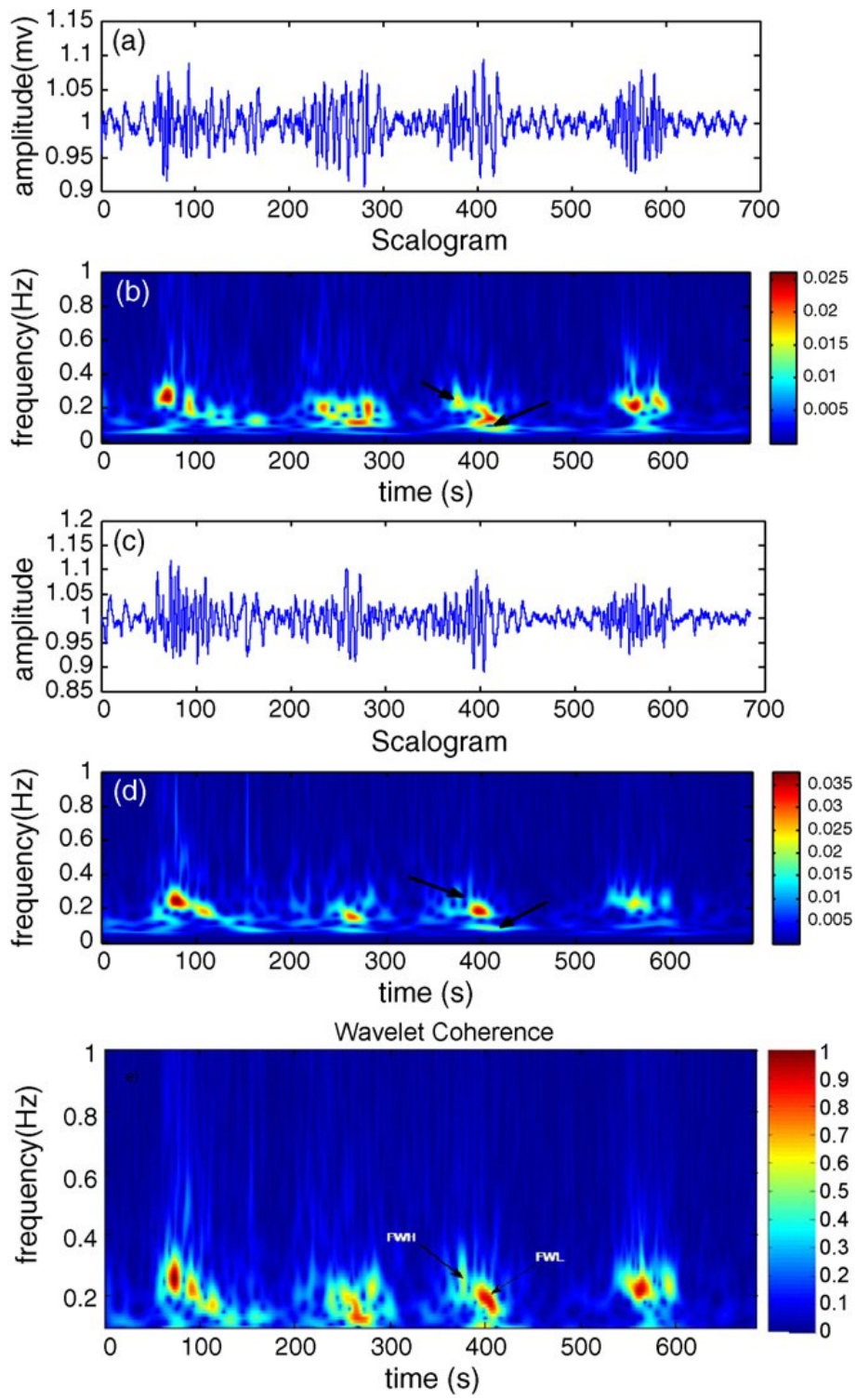
Figure 3.15: Two electrohysterograms (EHG) signals containing 4 bursts of activity (a, c) and their scalograms respectively (b, d); (e) wavelet coherence between the two non-segmented EHG signals.
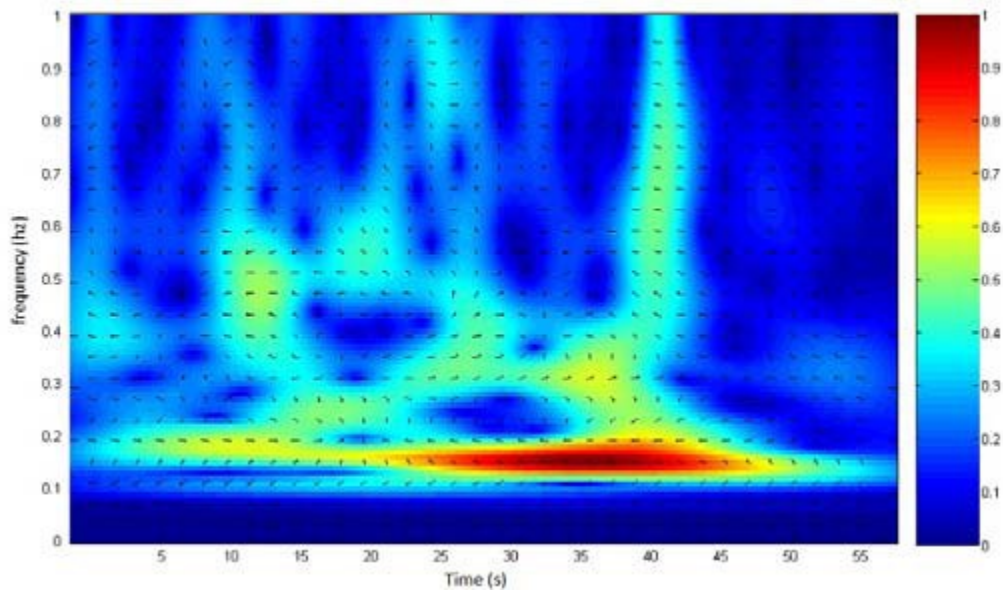
Figure 3.16: Wavelet coherence between two uterine bursts with the arrows phase representing the relative phasing.

3.5.2 Phase vs amplitude relationships and pregnancy/labor classification

As stated before, wavelet transform is a powerful tool to analyze non-stationary signals (Li et al., 2007). In this section we present the results of applying this powerful tool to analyze the relationship between uterine signals recorded at different locations during the same contractions and in two different situations: pregnancy and labor (**Figure** 3.17).

The scalogram displays the frequency content of the EHG signal over time. The difference in its aspect between pregnancy and labor bursts is clear as shown in **Figure** 3.18: in labor (**Figure** 3.18 A, B right) there are more high frequency components than during pregnancy (**Figure** 3.18 A, B left).
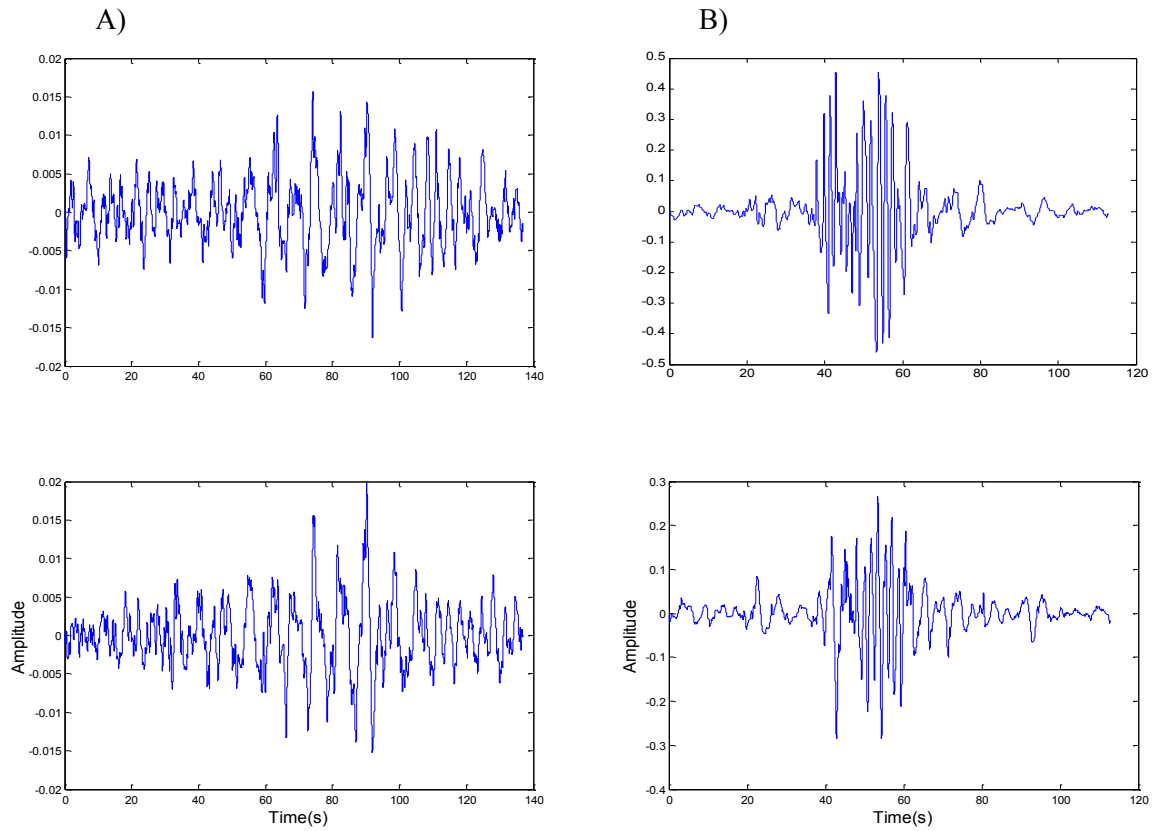
Figure 3.17: A) Two uterine bursts for the same contractions during pregnancy. B) Two uterine bursts for the same contractions in labor. Both A) and B) represent Vb7 (top) and Vb8 (bottom) bipolar signals.
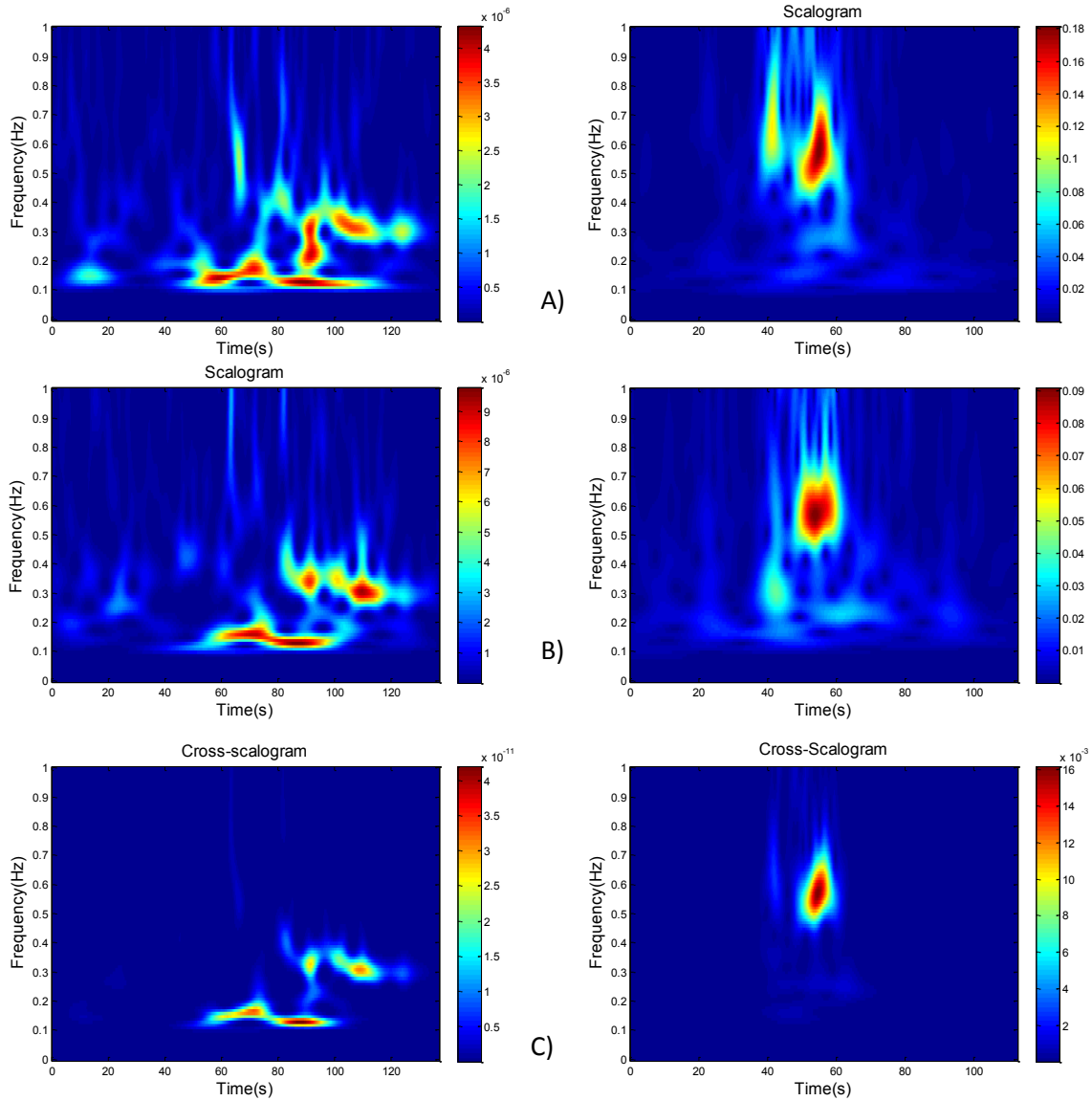
Figure 3.18: A) and B) Scalograms for the two bursts and C) Cross-scalogram between the two bursts. (Left): pregnancy, (Right): labor.

In **Figure** 3.17 and **Figure** 3.18, two EHG data sets are used: Vb7 (denoted by X) and Vb8 (denoted by Y); their MWT are $W_X(a,\tau)$ and $W_Y(a,\tau)$, respectively. The plot of $|W_{XY}(a,\tau)|^2$ displays the coincident events in the time-frequency domain for the two EHG signals: **Figure** 3.18C (left) shows the cross-scalogram of the two bursts measured during pregnancy; **Figure** 3.18C (right) shows the cross-scalogram of the two bursts measured during labor.

The cross-scalogram shows that the highest levels of common power are located during the uterine activity i.e. 50s-100s for the pregnancy bursts and 40s-80s for the labor bursts. This common power is therefore clearly due to and related to the contractile activity of the uterus.

On **Figure** 3.19, the uterine electrical activities, segmented from the Tocographic trace, are indicated between 50-100s for the pregnancy bursts and 40-80s for the labor bursts (vertical

lines). The values presented are CWCF indicating the amplitude correlation (**Figure** 3.19 A and B) and WLCC representing the phase correlation (**Figure** 3.19 C and D).
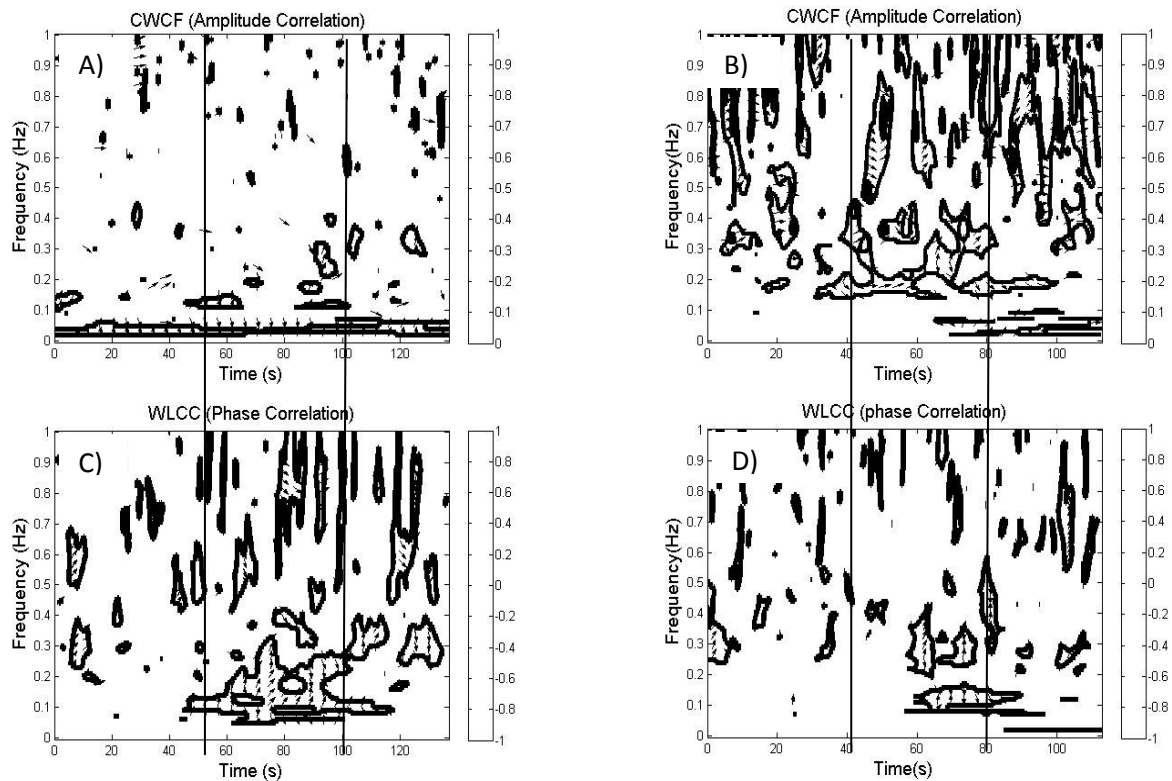
Figure 3.19: A)-B) Cross wavelet coherence function (CWCF): amplitude correlation between two bursts; C)-D) Wavelet local correlation (WLCC): phase correlation between two bursts. (Left): pregnancy, (right): labor. The vertical lines indicate the start and the end of the uterine activity extracted from the Topography trace. Inside the thick black line there is significant level of 95% with re-sampling of Bootstraps (CWCF) and IAFFT (WLCC). The phase difference of cross spectrum is shown by arrow direction (in-phase: arrow pointing right, means Vb7 leads Vb8; anti-phase: arrow pointing left, means Vb8 leads Vb7) only for the significant correlations.

The statistical rank test with surrogates is applied to the CWCF and WLCC methods. When the statistical test indicates that the values obtained are significant, the area where these values are located are contoured by a thick black line and any values obtained outside these regions (non significant) are shown as blank. The arrows indicating the phase difference are plotted only inside the regions where the values are found to be significant.

In the case of signals recorded during pregnancy, we notice a small area between 40s and 100s where the method shows significant values in the case of CWCF (**Figure** 3.19A) and

much larger area in the case of WLCC -phase correlation- (**Figure** 3.19C). For labor contraction we notice the opposite (between 40s and 80s): large areas of significance with CWCF and smaller ones with WLCC. These results indicate that during pregnancy, there is more phase correlation than during labor. At the opposite, there is more amplitude correlation during labor than during pregnancy. Some regions of significance can be seen outside the burst ranges that are probably due to noise. This is one of the disadvantages of both methods. The use of wavelet coherence has great advantages with respect to this problem, because it can be applied to the whole signal without segmentation.

The results of CWCF and WLCC confirm our previous observations: increase in the nonlinear correlation coefficient from pregnancy to labor and decrease in the phase coherence.

Concerning the results of wavelet phase synchronization, **Figure** 3.20 indicates that, for both labor and pregnancy, the highest phase synchronization is located in the lower frequencies of the signal. The phase synchronization is higher during pregnancy than during labor, which confirms the results of WLCC presented **Figure** 3.18.
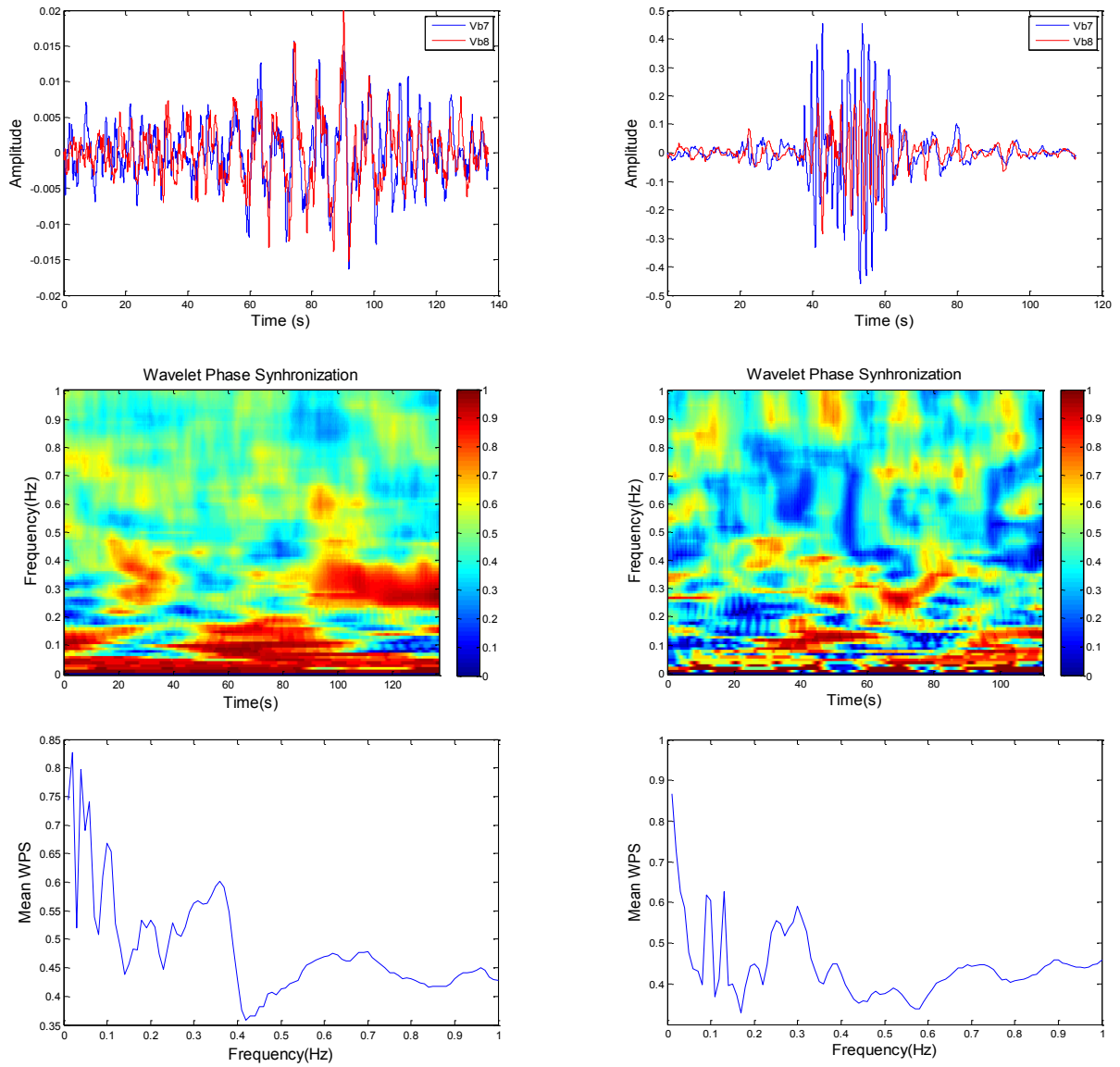
Figure 3.20: The phase synchronization between the two uterine bursts: pregnancy (left) and labor (right)

In order to quantitatively compare pregnancy and labor, the signals were numerically filtered in three frequency bands (0-0.25Hz; 0.25-0.5Hz; >0.5Hz). Then the mean of WPS was computed for each band. By doing this, we aim to evidence in which frequency bands the highest phase synchronization is located. The second aim of this analysis is to investigate the difference in phase synchronization (WPS) between pregnancy and labor bursts, in order to find if this method can potentially be used as a tool to classify pregnancy vs. labor EHG bursts.

The results in **Table** 3.4 correspond to the mean of WPS at different frequency bands calculated on 30 contractions (CTs) for 5 women during pregnancy (30 to 36 WG) and 30 contractions from 5 women during labor (delivery time of 39 to 42 WG). These results indicate that the highest phase synchronization during both pregnancy and during labor is present in the low frequency band (0-0.25Hz).

	Pregnancy	Labor
0< f(Hz) <=0.25	0.59 ± 0.05	0.57 ± 0.06
0.25< f(Hz) <=0.5	0.53 ± 0.07	0.48 ± 0.06
f(Hz) >0.5	0.49 ± 0.05	0.46 ± 0.02

Table 3.4: Comparison between mean (± standard deviation) of WPS at different frequency bands for 30pregnancy bursts and 30 labor bursts.

The values indicate also that during labor, the location of the high synchronization becomes clearer and that there is more difference between values at the low frequencies and higher ones, while this difference is less clear during pregnancy.

3.5.3 Possible interpretation of phase desynchronization

As we can see from the results presented above, the PS methods in time and time-frequency domain have indicated a higher PS during pregnancy than during labor and a decrease of PS with term (in contrast with all other relationships method).

We try here to explain the origin of a possible relationship between the increase in the nonlinearity (reversibility and complexity), evidenced in the previous chapter, and this phase desynchronization. For this reason, we use Henon nonlinear dynamical system. Indeed, this system eprmits to control the degree of the complexity of the generated signals. We evaluate the evolution of the values obtained from nonlinear methods (Time reversibility and approximate entropy) and relationships methods (phase synchronization) with the degree of complexity of the Henon system.
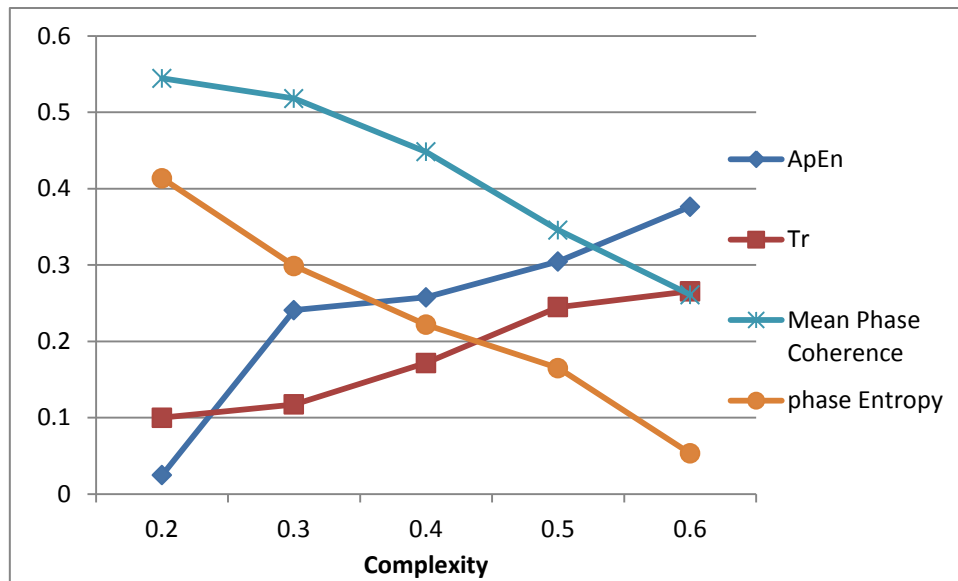
Figure 3.21: Evolution of nonlinear monovariate methods and phase synchronization methods with the degree of complexity in the signals.

Figure 3.21 shows that the nonlinear methods (Tr and ApEn) demonstrate an increasing with the degree of complexity of the system, while the phase synchronization between signals (Mean Phase Coherence and Phase entropy) decreases with the signal complexity. These preliminary results indicate a possible relationship between the increase in the nonlinearity showed in the chapter 2 and the decrease in phase synchronization evidenced in this chapter.

3.6   Conclusion and discussion

In this section, a study based on the Morlet wavelet transform has been done to analyze the difference between uterine electrical activity bursts recorded from woman during pregnancy and others from women during labor. The wavelet transform, cross wavelet transform, phase correlation, amplitude correlation, and phase synchronization of the two types of uterine signals were described.

The scalogram exhibited the previously observed observation: the presence of higher frequency components during labor than during pregnancy.

The cross-scalogram was used to detect which one of the two well-known components of the EHG (FWL and FWH) presents the highest common power. The highest common powers were found to be located in the lower frequencies (FWL) and were smaller during pregnancy than during labor.

WLCC and CWCF are two tools used to separate the phase and amplitude correlation. We used them in order to detect the nature of the relation between signals, during pregnancy and

labor. The results indicate that there is more significant amplitude correlation in labor than during pregnancy and more significant phase correlation during pregnancy than in labor.

Phase synchronization index in the time frequency domain, is then used to describe the phase synchronization between signals. The pregnancy signals again show more phase synchronization than the labor signals.

We noticed that the results of WLCC and CWCF are similar to the results obtained in EEG during the transition from preictal to ictal stages, a phase desynchronization and amplitude synchronization (Li et al., 2007). The question can be raised if some similarities exist in the physiological interpretation of the underlying phenomena.

Then we tried to correlate the observations made from the monovariate analysis (increase in signal complexity from pregnancy to labor) to the bivariate phase analysis (decrease in phase coherence from pregnancy to labor). It appears, on synthetic signals, that an increase in signal complexity induces a decrease in phase correlation. These preliminary observations have to be confirmed in further studies.

3.7   Global conclusions of the chapter 3

An overview of the main statistical and time frequency coupling methods that we have applied to uterine EMG signals has been presented in this chapter. These methods include linear (stationary/nonstationary) and nonlinear approach. In general, these methods can be grouped in 4 classes: *(i)* Regression methods; *(ii)* Phase synchronization; *(iii)* General synchronization; *(IV)* Time frequency methods.

The essential conclusions of this chapter are:

- The use of multichannel recordings is more efficient in classifying pregnancy and labor contractions than the simple use with two bipolar signals when the above methods are used.
- More amplitude correlation between uterine signals on different locations on the abdomen is observed during labor than during pregnancy, which may reflect more propagation during labor than in physiological pregnancy contractions.
- An increase in amplitude correlation with the term.
- More coherence in the low frequencies than the high frequencies of the uterine bursts, supporting the hypothesis that FWL has a stronger relation to propagation than FWH

- Increased amplitude correlation and decreased phase synchronization from pregnancy to labor.

- The synchronization methods can be powerful tools to classify pregnancy and labor signals.

Even if the methods discussed so far are defined for two signals only, a functional relationship is obtained by pair-wise analysis of bivariate signals. However, as discussed earlier, a bivariate method for each pair of signals from a multichannel set of signals does not account for all the covariance structure information from the full data set. For this reason, the multivariate analysis using Multivariate Autoregressive method (MVAR) will be the subject of the next chapter.

Chapter 4 Multivariate Autoregressive Model (MVAR): Application for labor detection

All the methods used in the previous chapter are bivariate i.e. compute the relationships directly between two channels. The '*matrix illustrations*' presented in chapter 3 is a multichannel 'representation' of bivariate method and does not take into account all the interrelation between channels. Amplitude correlation, phase synchronization and generalized synchronization all are bivariate methods. The results obtained by these methods are encouraging but still not ready for clinical application.

We think that taking into account the relationships between the whole matrix (all the channels) may lead to an improvement and can increase the classification rate between pregnancy and labor. This is based on the hypothesis that during pregnancy contractions are local and low propagated, while during labor the contractions propagate along the whole uterus in a short time (about 20s) and could therefore induce more channels interrelationships.

In this chapter we introduce the use of the Multivariate Autoregressive (MVAR) method which takes into consideration the simultaneous connectivities between all the channels. Firstly, we describe the classical stationary MVAR, and then we propose an adaptive version. Finally we will compare both models on synthetic and real signals.

4.1 State of the art

Multichannel recordings are necessary to investigate physiological phenomena that have an extended range over an organ, or an organ system, such as the brain, skeletal muscles or the uterus. Recently most of the actors in the field of uterine EMG or electrohysterogram (EHG) have adopted multi electrode configuration for the measurement and concentrate on the study of how the uterus synchronizes and starts to operate as a whole as labor progresses. The methods most often used in the literature for preterm labor prediction use only the analysis of the high frequency content of the EHG (Garfield et al., 1998a; Garfield et al., 2005; Garfield et al., 2001; Maner and Garfield, 2007; Vinken et al., 2009) which is thought to be primarily

related to uterine cell excitability (Devedeux et al., 1993). These methods are however not currently used in routine practice as far as we know. Recently, studies using propagation analysis for labor detection and preterm labor prediction have started to appear. They have shown better behavior of propagation parameters over the excitability parameters to detect labor.

For example, Lucovnik et al. indicated the superiority of the propagation analysis (using propagation velocity (PV)) over the excitability parameters to classify labor and non labor signals (Lucovnik et al., 2011). But this method is based on linear bivariate analysis tools. A new way to analyze relationships between multichannel signals, based on estimated coefficients from Multivariate Autoregressive model (MVAR) of the signals, has recently been presented. The main advantage of MVAR method is to take into account the connectivity between all the signals and not between only two signals at a time. The main connectivity estimators based on the MVAR model are the Granger causality index (GCI), the directed transfer function (DTF) and the Partial Directed Coherence (PDC). These methods have essentially been applied in various fields of brain research (Baccala and Sameshima, 2001a, b; Franaszczuk et al., 1994; Kaminski and Blinowska, 1991; Korzeniewska et al., 1997; Kus et al., 2004; Pereda et al., 2005; Winterhalder et al., 2005). They have not yet been applied on the EHG signals. A drawback of the MVAR method is that it assumes that the signals are stationary which is not the case of the majority of biosignals, and especially for EHG.

In this chapter we propose a windowing (time-varying) version of MVAR, called W-MVAR, that aim to respect the non-stationary characteristics of EHG signals. We compare W-MVAR with the classical MVAR on synthetic signals as well as on real EHG signals, in view of distinguishing between non labor and labor signals.

4.2   Materials and methods

4.2.1   The autoregressive model: an overview

An AR model is quite simple and useful to describe the stochastic behavior of a time series. It can be described by the following equation

$$x_k = a_1 x_{k-1} + \ldots + a_p x_{k-p} + \varepsilon_k$$

with

$$\varepsilon_k = N\{0, \sigma_x^2\}$$

x_k is a zero-mean-Gaussian-noise process with variance σ_x^2. The index k is an integer number and describes discrete, equidistant time points. The time t in seconds is $t = k / f_0 = k\Delta T$ with the sampling rate f_0 and the sampling interval $\Delta T = 1 / f_0$. X_{k-1} with $i=1..p$ are the p previous sample values; p is the order of the AR model and a_i are the AR model parameters. For simplicity, the vector notation is introduced for the AR parameters. The vector X_{k-1} consists of the past p samples, and A represents the parameter vector:

$$A = [a_1, ..., a_p]^T$$
$$X_{k-1} = [x_{k-1}, ..., x_{k-p}]^T$$

The AR model can thus be written as:

$$x_k = A^T X_{k-1} + \varepsilon_k$$

And the transfer function in the Z-domain is:

$$\frac{X(z)}{\varepsilon(z)} = \frac{1}{(1 - a_1 z^{-1} - ... - a_p z^{-p})}$$

The AR model can also be seen as a linear filter with random noise input. The output process is stationary if all poles (i.e. roots of the denominator) of the transfer function are inside the unit circle. While random noise has a flat spectrum, the spectrum of the model output (i.e. the observed EHG) is determined completely by the AR parameters. AR model also explains the spectral composition of a signal (shortly the AR spectrum):

$$S(f) = X(z, z = e^{j2\pi f \Delta T})$$
$$S(f) = \frac{\sigma_x}{(1 - \sum_i a_i e^{j2\pi f \Delta T})} \quad i = 1..p$$

with the sampling interval $\Delta T = 1/f_0$. Once the AR parameters are identified, they can be applied inversely to the observed process.

4.2.2   Model order

An important issue in AR modeling is the selection of the model order. Many different criteria are defined; twelve methods for model selection are proposed in the literature. The most common criteria are Final Prediction Error (FPE) (Akaike, 1969), Akaike Information Criterion (AIC) (Akaike, 1974), Bayesian AIC (BIC) (Akaike, 1979), Minimum Description

Length (MDL) (Rissanen, 1983), Schwartz Bayesian Criterion (SBC) (Schwarz, 1978) and the Phi-Criterion (Hannan and Quinn, 1979).

In this work we use FPE and SBC criterion to choose the optimal order model which are the most used methods to compute the order of autoregressive model and have previously been shown to possess a high degree of accuracy (Lutkepohl, 1985) .

4.2.3   MVAR

For multichannel signals X with m dimensions, the multivariate autoregressive (MVAR) process can be defined as:

$$\begin{pmatrix} x_1(k) \\ x_2(k) \\ . \\ . \\ . \\ x_m(k) \end{pmatrix} = \sum_{r=1}^{p} A_r \begin{pmatrix} x_1(k-r) \\ x_2(k-r) \\ . \\ . \\ . \\ x_m(k-r) \end{pmatrix} + \begin{pmatrix} \varepsilon_1(k) \\ \varepsilon_2(k) \\ . \\ . \\ . \\ \varepsilon_m(k) \end{pmatrix}$$

Where $\varepsilon_i(k)$ represents independent Gaussian white noise and $A_1,...A_p$ are the coefficient matrix (m x m).

This time domain representation can be translated to the frequency domain by computing the power spectral density matrix:

$$S(f) = H(f) \sum H^h(f)$$

Where h is the Hermitian transpose, $\sum$ is the variance matrix of the noise $\varepsilon(f)$ and H is the transfer function defined as:

$$H(f) = \overline{A}^{-1}(f) = [I - A(f)]^{-1}$$

Where $A(f)$ is the Fourier transform of the coefficients. Let $\overline{A}(f) = [\overline{a_1}(f)\overline{a_2}(f)...\overline{a_m}(f)]$ and $\overline{a_{ij}}(f)$ is the i, j^{th} element of $\overline{A}(f)$.

Several estimators have been proposed to analyze connectivity between signals by using the MVAR coefficients. The most popular methods are:

4.2.3.1   Granger causality index (GCI)

114

By definition, *an observed time series $X_j(n)$ Granger-causes another series $X_i(n)$, if knowledge of $X_j(n)$ past significantly improves prediction of $X_i(n)$.*

Granger causality is a well-defined idea originating in econometrics where it processes several statistical testing procedures. Its key notion is the exclusive consideration of past samples in prediction improvement.

To introduce a GCI in the time-domain, and to investigate directed influences from a component X_j to a component X_i of a *n*-dimensional system, *n*- and (*n-1*)-dimensional MVAR-models for X_i are considered. First, the entire n-dimensional MVAR model is fitted to the n-dimensional system. Second, a (*n-1*)-dimensional MVAR-model is fitted to (*n-1*)-dimensional subsystem $\{X_k; k = 1; \ldots ; n \text{ and } k \neq j\}$ of the *n* dimensional system.

A time-varying GCI quantifying linear Granger causality is proposed by Hesse et al. (Hesse et al., 2003) and defined by:

$$GCI_{ij}(t) = \ln\left(\frac{VAR(\varepsilon_{i,n-1}(t))}{VAR(\varepsilon_{i,n}(t))}\right)$$

where *VAR* is the residual variance.

Since the residual variance of the *n*-dimensional model is expected to be smaller than the residual variance of the smaller (*n-1*) dimensional model, GCI vary between zero (no connectivity) or larger than zero (presence of connectivity between channels). For a time resolved extension of the GCI, a time-variant MVAR-parameter estimation technique is used here by a windowing approach. In the present study, the time-varying GCI is the only analysis technique under investigation reflecting information about multivariate systems in the time-domain.

4.2.3.2 Partial directed coherence (PDC)

As a parametric approach in the frequency domain, PDC has been introduced to detect causal relationships between processes in multivariate dynamic systems. PDC accounts for the entire multivariate system and renders a differentiation between direct and indirect possible influences. It was initially proposed by Baccala et al. (Baccala and Sameshima, 2001b) and defined as

$$PDC_{ij}(f) = \frac{\overline{a}_{ij}(f)}{\sqrt{\overline{a}_j^h(f)\overline{a}_i(f)}}$$

where $\overline{a_{ij}}(f)$ is the i, j^{th} element of $\overline{A}(f)$ already described above.

The PDC from j to i represents the relative coupling strength of the interaction of a given source, signal j, with regard to some signal i, as compared to all of j's connections to other signals. Thus, PDC ranks the relative strength of interaction with respect to a given signal source while fulfilling the following properties:

$$0 \leq \left| PDC_{ij}(f) \right|^2 \leq 1$$

and

$$\sum_{i=1}^{m} \left| PDC_{ij}(f) \right|^2 = 1$$

For $i=j$, the PDC represents how much of X_i's own past is not explained by other signals.

4.2.3.3   Directed transfer function (DTF)

The DTF is a frequency-domain analysis technique to detect directions of interactions. It was proposed by Kaminski et al. (Kaminski and Blinowska, 1991)

$$DTF_{ij}(f) = \frac{H_{ij}(f)}{\sqrt{H_i^{\,h}(f) H_i(f)}}$$

Where h is the Hermitian transpose and H is the transfer function.

We can observe that DTF uses the elements of the transfer function matrix H while PDC uses those of $\overline{A}(f)$. Since, unlike DTF calculation, the computation of PDC does not involve any matrix inversion, it is computationally more efficient and more robust than DTF. Furthermore, PDC is normalized with respect to the total inflow of information, whereas DTF is normalized with respect to the total outflow of information.

4.3   Results

4.3.1.   Robustness tests

The test of robustness depends on the system itself and on its functions. These two points must be uniquely designed to avoid any risk of error or false data. We can therefore proceed to the verification of their ability to make correctly the calculations in an uncertain domain. This analysis involves essentially the test of noise effect and sample length.

4.3.1.1 Noise effect

To test the noise effect we use a simple 3-Dimensional linear system (LS) defined as:

$$x_1(n) = 0.5x_1(n-1) + 0.3x_2(n-1) + 0.4x_3(n-1) + \varepsilon_1(n)$$
$$x_2(n) = -0.5x_1(n-1) + 0.3x_2(n-1) + 1.0x_3(n-1) + \varepsilon_2(n)$$
$$x_3(n) = -0.3x_2(n-1) - 0.2x_2(n-1) + \varepsilon_3(n)$$

Where $\varepsilon_i(n)$ are non zero-mean uncorrelated white processes with identical variances. We can observe that only $x_3(n)$ in not influenced explicitly by the past state of $x_1(n)$.

We firstly tested the influence of an additive noise on the good connectivity detection. For this reason, Gaussian white noises with different signal to noise ratio (SNR) have been added to the LS.

The different steps for the noise effect analysis can be described as following:

- PDC values are computed directly on the parameters of the LS described above and called 'reference PDC values'.
- Compute the maximum values of PDC's (to obtain one value for each two channels called PDC$_{max}$).
- Simulate MVAR process using 'Direct-Form II Transpose Filter'.
- Add noise with different SNR ratio, estimate the AR coefficients and compute the PDC values.
- Comparing the original model order and estimated one to obtain the '**Good detection of model order'**.
- Comparison between reference and estimated PDC$_{max}$ is computed and called the **'% of Good connectivity'.**
- Repeat these steps for N (1000) times for each SNR values and averaging over the N values to obtain mean 'Good detection of model order' and mean '% of Good connectivity'.
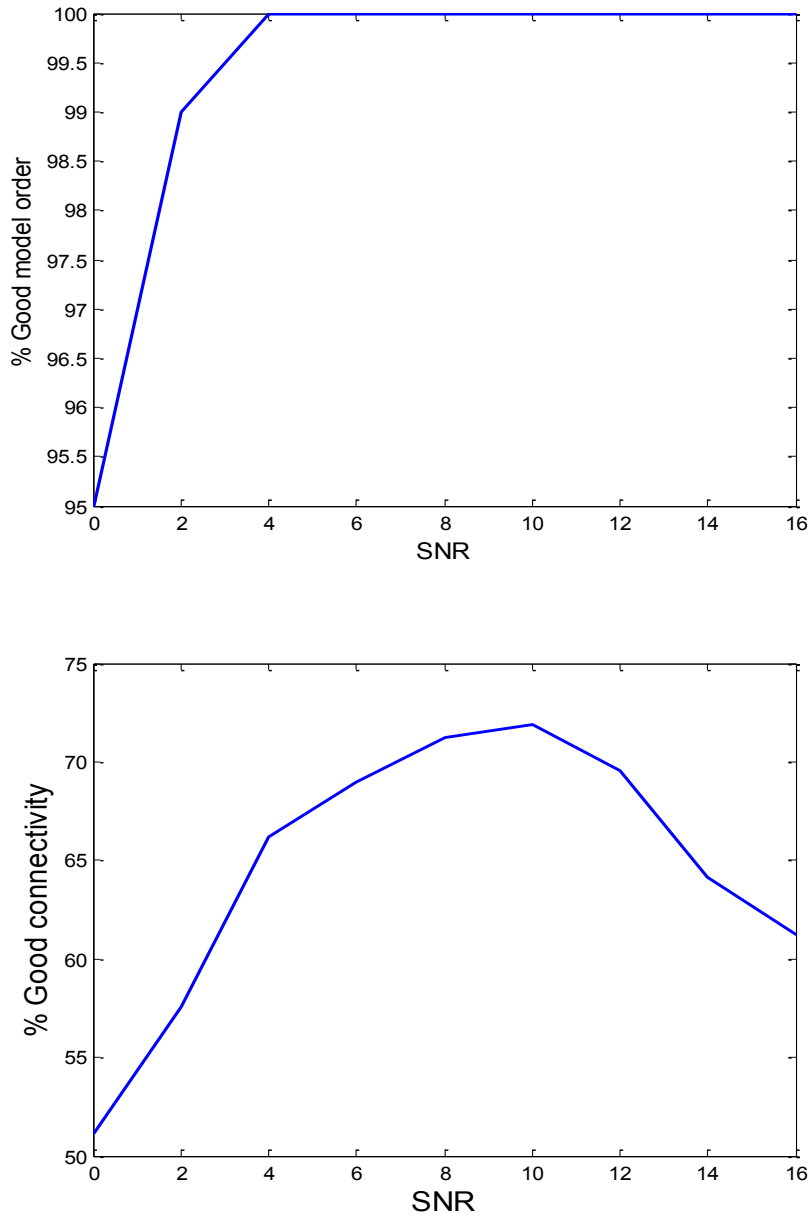
Figure 4.1: (Top) Evolution of the Good detection of the order model with the SNR values (Bottom) Evolution of the good detection of connectivity with the SNR values.

Figure 4.1 presents the evolution of the good order detection and the good connectivity with the SNR values. We can notice that the order model is well detected with 95% with the lowest SNR; the connectivity is also detected in general with a good rate (range of 50%-73%).

4.3.1.2   Signals length effect

By the same way, we also tested the performance of the MVAR model with different signal's length by using the same LS used above. We noticed from **Figure** 4.2 that whatever the number of samples, the percentage of good connectivity remains around 63%.
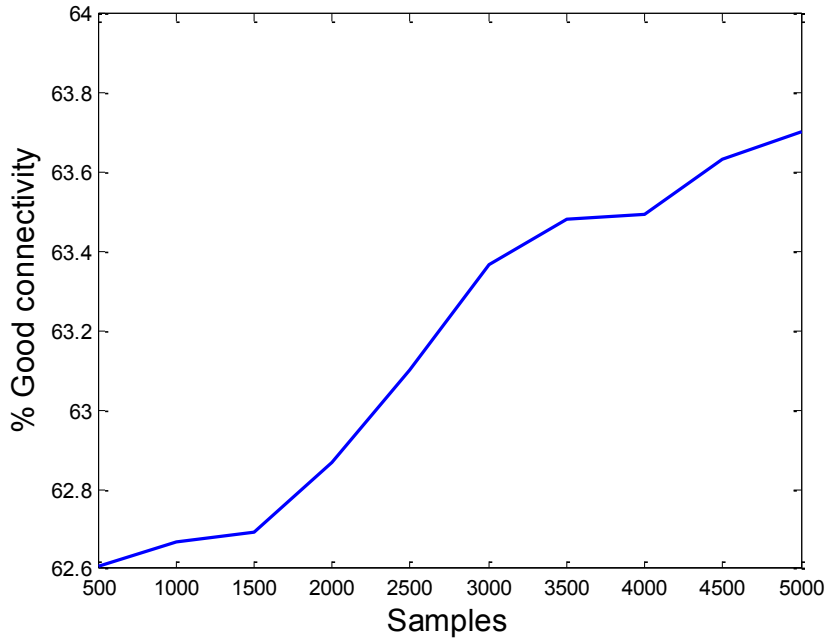
Figure 4.2: Evolution of the detection of good connectivity with the number of samples

4.3.1.3   Testing MVAR on different synthetic signals

In this part we will test the capacity of MVAR model to detect connectivity between signals in different situations such as:

   a) Linear stationary signals (LS)
   b) Nonlinear stationary signals (NLS)
   c) Linear nonstationary signals (LNS)

The aim of this part is to cover all the possible characteristics that can be presented when applying MVAR on real signals.

4.3.1.3.1   Linear Stationary (LS)

By construction MVAR is made to detect relationships between stationary signals. Several studies have been done to prove the efficiency of MVAR to perfectly detect this kind of connectivities. Inspired by what have been done by Baccala et al. (Baccala and Sameshima, 2001b), we use a five dimensional linear stationary simulations defined as:

$$x_1(n) = 0.95\sqrt{2}x_1(n-1) - 0.9025x_1(n-2) + \varepsilon_1(n)$$

$$x_2(n) = -0.5x_1(n-1) + \varepsilon_2(n)$$

$$x_3(n) = 0.1x_1(n-4) - 0.4x_2(n-2) + \varepsilon_3(n)$$

$$x_4(n) = -0.5x_3(n-1) + 0.25\sqrt{2}x_4(n-1)$$

$$+ 0.25\sqrt{2}x_5(n-1) + \varepsilon_4(n)$$

$$x_5(n) = -0.25\sqrt{2}x_4(n-1) + 0.25\sqrt{2}x_5(n-1) + \varepsilon_4(n)$$

Results of PDC and DTF are presented **Figure** 4.3. DTF presents nonzero values whenever there is some signal pathway that goes from structure j to structure i in the structural graphs that describe the model. While DTF marks the existence of signal pathways connecting structures either directly or indirectly, PDC resolves the existence of direct connection between pairs of structure.
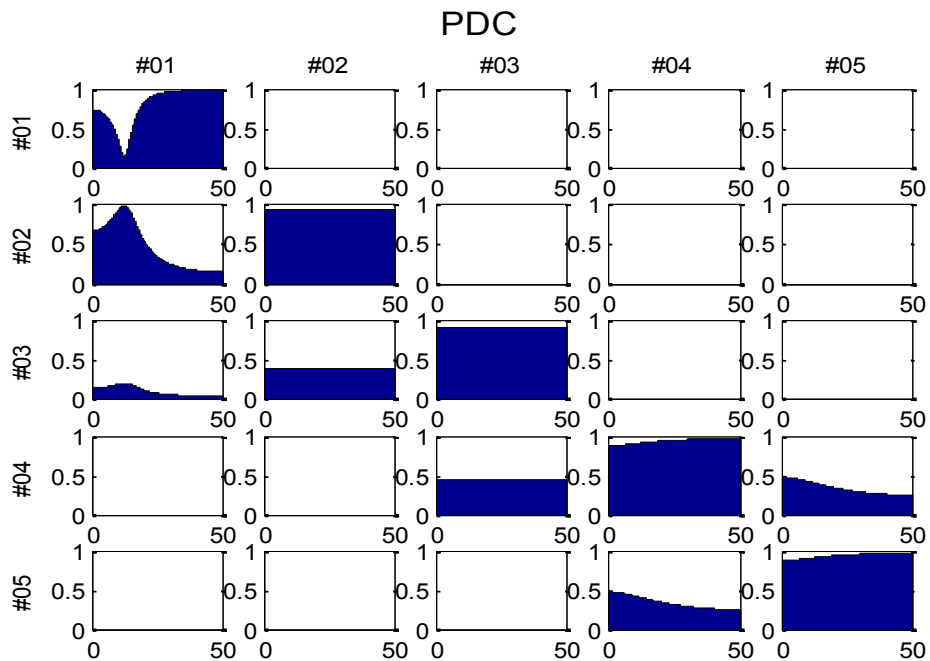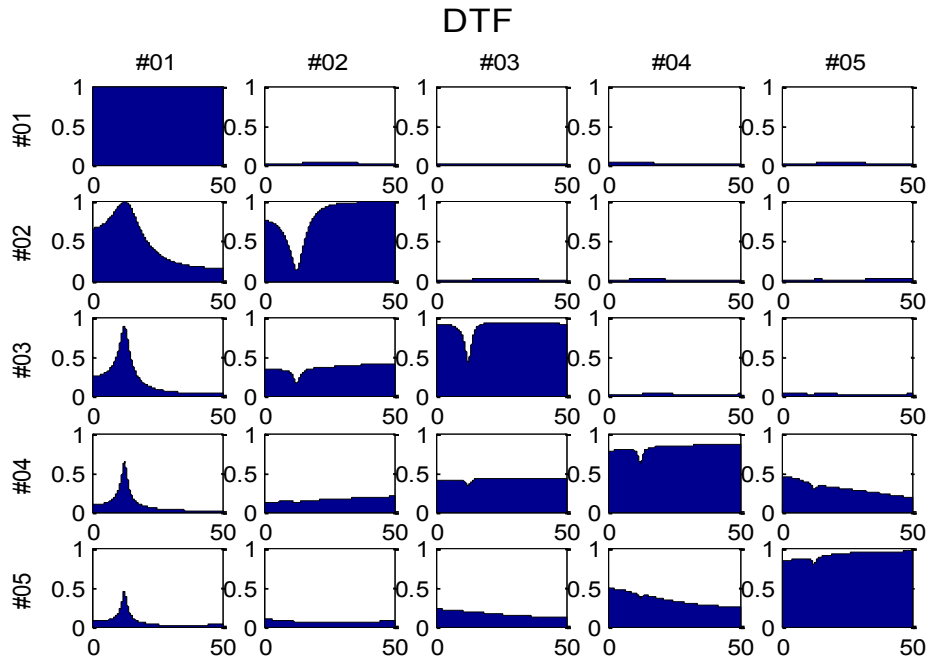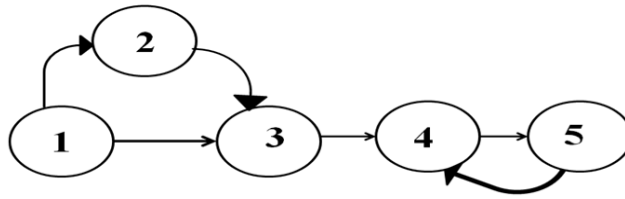
Figure 4.3: (Top) linear simulated model: (middle) DTF results, (bottom) PDC results

4.3.1.3.2   Nonlinear stationary signals

An additional challenge expected in applications to time series representing neural signal transfer is a possible nonlinearity of the processes. At least weakly nonlinear dynamic systems must not lead immediately to wrong results when applying multivariate linear analysis techniques.

We use here a nonlinear Rössler system with four dimensional defined as

$$
\begin{pmatrix} X_j \\ Y_j \\ Z_j \end{pmatrix} = \begin{pmatrix} -\Omega_j Y_j - Z_j + [\sum_i k_{ji}(X_i - X_j)] + \eta_j \\ \Omega_j X_j + a Y_j \\ b + (X_j - c)Z_j \end{pmatrix}
$$

With *i,j=1,2,3,4*

We choose the parameters used in (Winterhalder et al., 2005) with Ω_1 =1.01, Ω_2 =0.99, Ω_3 =0.97 and Ω_4 =1.03. The parameters of the oscillators have been set to a =0.15, b =0.2, and c =10. The stochastic influence is given by a Gaussian distributed white noise η_j .

In the following, the coupling parameters have been set to k_{21}=0.04, k_{31}=0.04, k_{32}=0.04 and k_{42}=0.04. The remaining couplings strengths have been set to zero.

The nonlinear stochastic system has been simulated by using an Euler method with an integration step of 0.004, a sampling step of 0.1 and N = 50000 data points. The time series analysis techniques have been applied to X-components of the Rössler system in the following way.
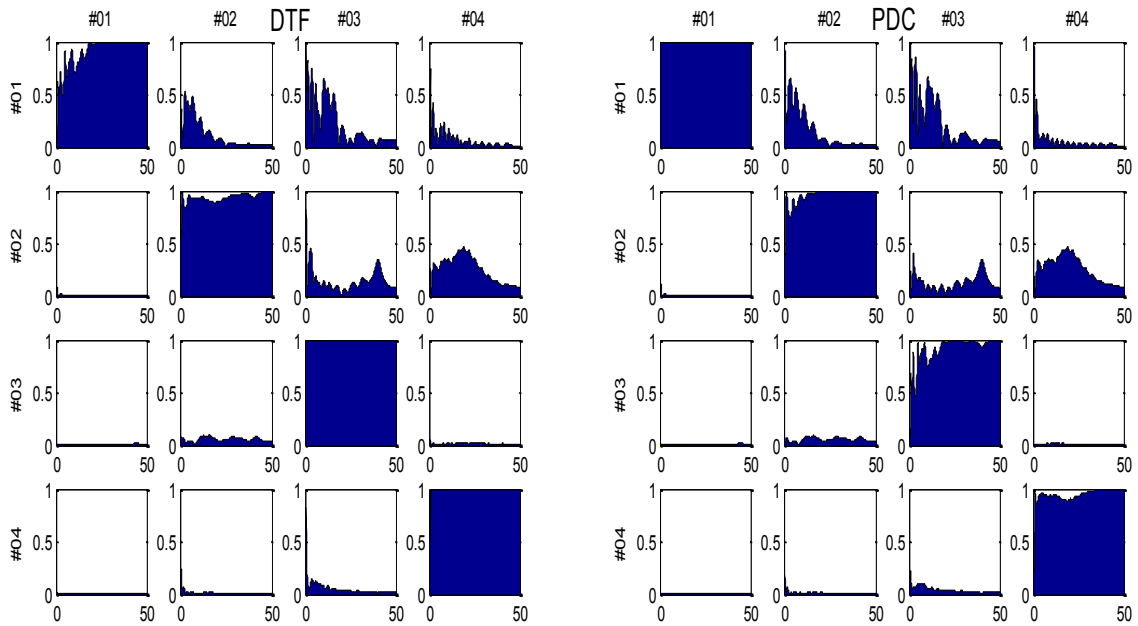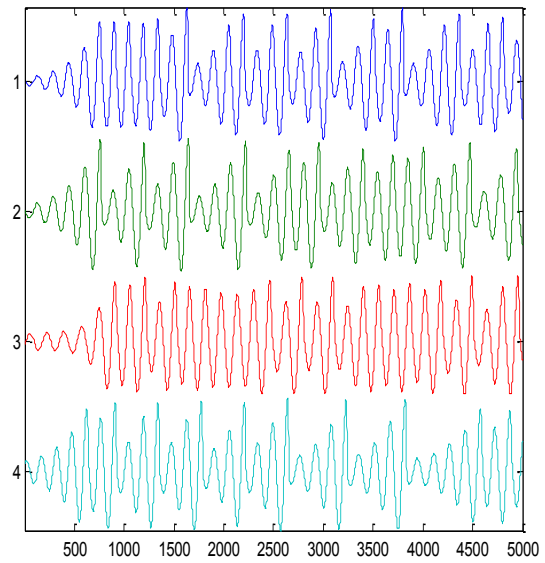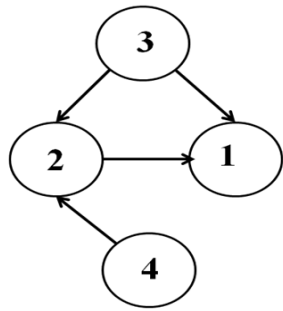
Figure 4.4: Results of application of DTF and PDC model on Rössler nonlinear system.

Figure 4.4 C and D present the results of the application of DTF and PDC to the simulated coupling scheme summarized in the graph **Figure** 4.4A, with an example of the simulated signals **Figure** 4.4B. The results of DTF and PDC are quite similar. Both methods detect coupling between 2→1, 3→1, 4→1 and 3→2. They both also present nonzero values while no coupling exists between channels such as coupling from 4→1.

MVAR permits to detect the relationships between signals even if the systems are nonlinear, but with less performance than for linear systems,. Results may depend of different Rössler system parameters and coupling factors.

4.3.1.3.3 Linear nonstationary signals

The main characteristic we want to test here is the sensitivity of the methods to the nonstationarity of the signals. We generated a simulated process that contains linear non-stationary (LNS) relationships between the signals. We used a modified version of three-dimensional MVAR processes (Sarkela et al., 2002; Winterhalder et al., 2005) with time-varying parameters:

$$x_1(t) = 0.5x_1(t-1) + 0.7x_1(t-2) + y(t)x_2(t-1) + y(t)x_3(t-1) + \varepsilon_1(t)$$
$$x_2(t) = 0.7x_2(t-1) - 0.5x_2(t-2) + 0.2x_1(t-1) + z(t)x_3(t-1) + \varepsilon_2(t)$$
$$x_3(t) = 0.8x_1(t-1) + \varepsilon_3(t)$$

With

$$y(t) = \begin{cases} 0.4 & if \ t \le 7000 \\ 0 & else \end{cases}$$

which represents the influence from x_2 to x_1 and x_3 to x_1, modeling thus an abrupt breakdown of the influence after 70% of the simulation period, and

$$z(t) = \begin{cases} 0.5\dfrac{t}{5000} & if \ t \le 5000 \\ 0.5\dfrac{10000 - t}{5000} & else \end{cases}$$

representing the unidirectional influence from $x3$ to $x2$, modeling a positive triangular function with maximum value of 0.5 in the middle of the simulation period.

To show the performance of the MVAR model on this kind of system, we choose to use the GCI method as it is a time depend method and costs less computational time than DTF and PDC.
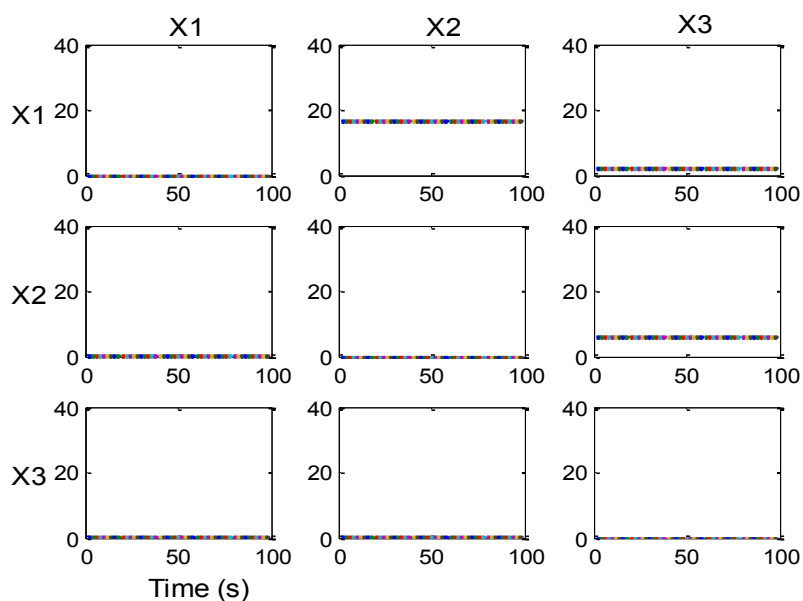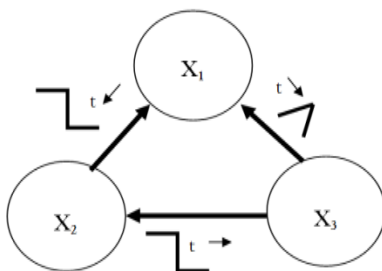
Figure 4.5: Results of application of GCI, estimated by MVAR model on linear nonstationary system

Figure 4.5 shows that MVAR totally failed to detect the relationships between nonstationary signals. The results indicated constant relationships along the time, which is not the case for the simulations. These results are expected as the MVAR suppose the stationarity of the analyzed signals. We think that the solution is to use a time-varying MVAR that could take into account the nonstationary characteristics of the analyzed signals.

4.2.4 Time-varying MVAR

The MVAR suppose that signals are stationary, which is not realistic in the majority of biosignals such as EHG. Several methods have been proposed in the literature to solve this problem. We can cite here the work of Zou et al. to extend a time invariant (TIV) model order search criterion, named the optimal parameter search algorithm (OPS), for identification of time varying TV autoregressive AR called TVOPS (Zou and Chon, 2004; Zou et al., 2003) .

However, all the proposed algorithms for adaptive AR have inconvenient and have been developed for specific applications. We aim in this work to start with the simplest and the most classical way to estimate time-varying AR parameters, and to respect as much as possible the specific characteristics of the EHG signals.

We thus propose a segmentation based approach to take into account the nonstationarity of the signals. In this case, the data are first divided into short segments and the AR parameters are then estimated from each segment. The result is a time-evolution of the AR parameters that describes the time-varying characteristics of the process. The segment length determines the accuracy of the estimated parameters and defines the resolution in time.

A balance has to be maintained between time resolution (limited by stationarity) and the statistical properties of the fitted model. As a rule of thumb, the segment/window length should possess a few times more data points than the number of estimated model parameters. Here, we choose a window length of 6s, with 50% overlap, and a data length (synthetic and real) equal to 100s, which permit a good temporal resolution and low estimation error.

4.2.4.1   MVAR vs. WMVAR

In this section we present the results obtained by the application of GCI on the LNS system described above. The coefficients are estimated using first the MVAR then the W-MVAR (windowed MVAR). The LNS system is described in **Figure** 4.5. A rectangular connectivity pattern is simulated between signal $x_2 \rightarrow x_1$ and $x_3 \rightarrow x_1$ and a triangular connectivity pattern is simulated between $x_3 \rightarrow x_1$. **Figure** 4.6 shows the obtained results. As we observed above, the **Figure** indicates no change in the estimator values along time for all the signals, which means that MVAR cannot detect the relationships between the signals when a nonstationary characteristic is present. Whereas the connectivities are well detected by the W-MVAR model.
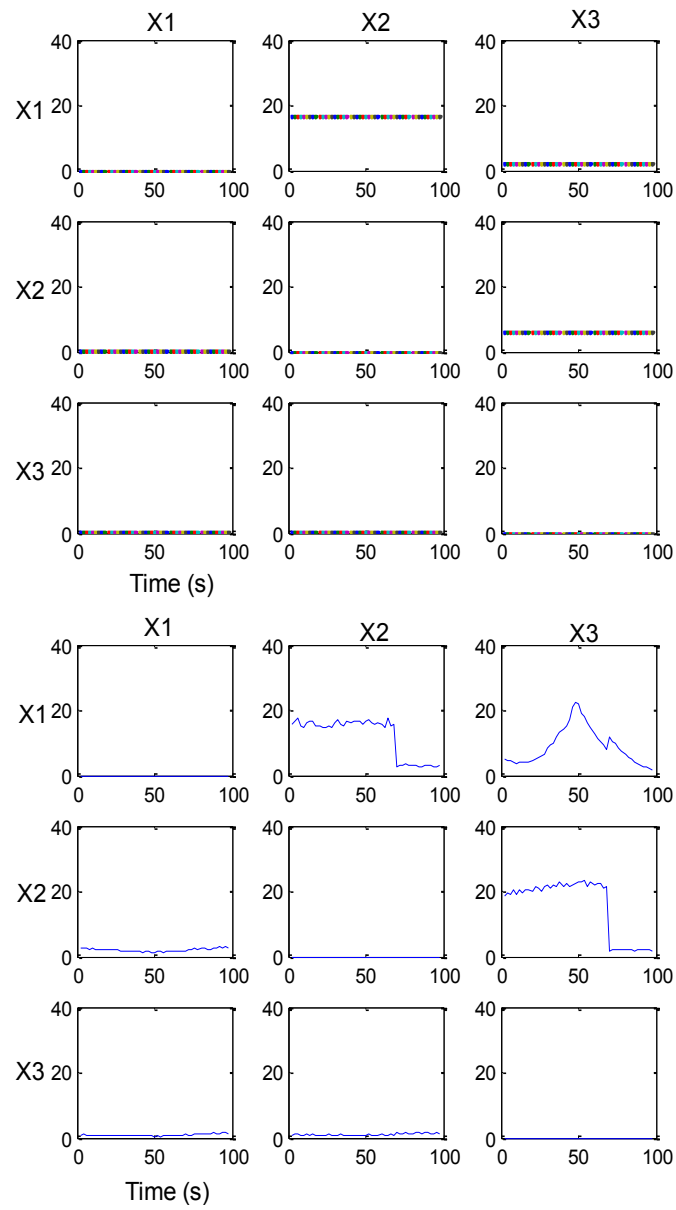
Figure 4.6: (Top) GCI results using MVAR and (Bottom) GCI results using W-MVAR

4.2.4.2 W-MVAR: DTF vs. PDC

We use here the system presented the same LNS system and compare the connectivity estimation by DTF and PDC. **Figure** 4.7 represents the obtained results.
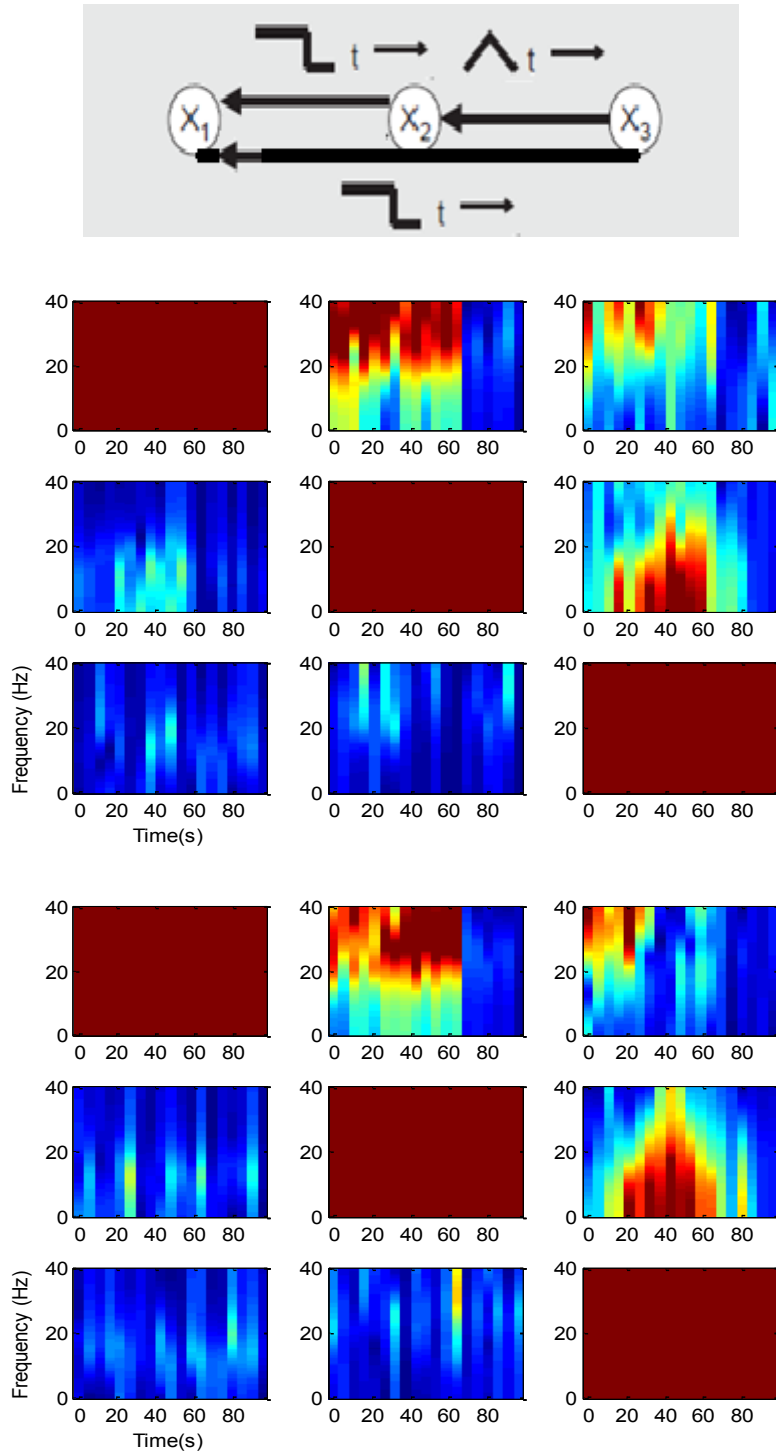
Figure 4.7: (Top) Description of the LNS system; (Middle) DTF results; (Bottom) PDC results

There is no clear difference between time-frequency PDC and DTF performances. Both methods detect the true connectivity between the signals described in the LNS model.

4.2.4.3   On real signals

A very important step is the choice of the model order. The model order of the real signals, computed by SBC, was about 35. We found nearly the same value when using the Final Prediction Error (FPE) as another order estimation criterion.

Even if the comparison between the two methods PDC and DFT did not indicate any difference in their performances in detecting the connectivity between synthetic signals, the results of Baccala et al. (Baccala and Sameshima, 2001b) indicated that PDC is more powerful than DTF to analyze signals relationships, when tested on several synthetic simulations and EEG real signals. We thus choose to apply PDC to the EHG signals. The main aim of this study is to define a quantitative criterion that could differentiate signals recorded during pregnancy from signals recorded during labor.
The quantitative criterion estimated from PDC is computed as follows:

- Computation of the evolution of PDC on the 12 bipolar EHG signals to obtain 12x12 matrices for each contraction.
  - Compute the maximum values of PDC (to represent the relation between two channels by only one value) we then obtain a matrix with 12x12 values.
- Computation of the mean value of the matrix. This mean value is the quantitative value representing each contraction for the following classification procedure.

We compute this criterion by estimating the coefficients using MVAR and W-MVAR. **Table** 4.1 illustrates the classification results of pregnancy and labor bursts by both methods. The results present the mean and standard deviation of PDC values. We can notice that MVAR in unable to classify the labor and nonlabor bursts (p=0.12), while the signals are better classified by the W-MVAR (p<0.01). The pregnancy values are similar with MVAR and W-MVAR while the difference is clear for the labor bursts. This can be explained by the fact that labor signals present more nonstationary characteristics than the pregnancy ones. There characteristics are taken into account by the W-MVAR and not by the MVAR.

	MVAR	W-MVAR
Pregnancy	0.045±0.03	0.05±0.045
Labor	0.067±0.04	0.12±0.07
P *(two tailed student test)*	0.12	<0.01

Table 4.1 Comparison between MVAR and W-MVAR to classify pregnancy and labor bursts

4.4 Discussion

In this paper we have proposed a time varying version of the multivariate autoregressive model to investigate the connectivity between nonstationary signals. The proposed model was tested on synthetic signals as well as real signals. On the synthetic signals, W-MVAR exhibited better performances for the detection of relationships between signals when non-stationary characteristics are present in the signals.

The application of the MVAR and W-MVAR on EHG signals clearly demonstrated that W-MVAR is very good in differentiating pregnancy and labor signals, whereas MVAR not. The successful estimation of PDC depends however on the reliability of the fitted MVAR model, since all the necessary information are derived from the estimated model parameters.

The main problems to solve here are the choice of an optimal model order and an optimal window length. If the model order is too low, the model will not capture the essential dynamics of the data set. Whereas if the model order is too high, it will capture the unwanted component (i.e. noise), leading to over-fitting and instability (Pereda et al., 2005).

The window length is also an important issue because it determines the resolution in the time- and frequency domain. Here, window length for W-MVAR was chosen empirically and as appropriate for the EHG signals. We think that additional work is needed to be done to define an automatic criterion for the optimal window length choice. This will make the application more general and useful for other biomedical signals, will permit its comparison to other existing methods.

4.5 General conclusions about all relationships methods

In chapter 3 and 4 we presented the application of different methods that detect relationships between signals on the EHG. These methods can be summarized as:

1. Amplitude Correlation : nonlinear correlation coefficient (h^2)

2. Phase Synchronization (PS): mean phase coherence and phase entropy

3. Generalized Synchronization (GS): three methods based on the embedding space and information theory

4. Multivariate Autoregressive (MVAR) methods: Granger Causality Index (GCI), Directed Transfer Function (DTF) and Partial Directed Coherence (PDC)

All these methods have been applied on EHG signals during pregnancy and labor in view of classification between these two categories and for labor detection.

The used database was about 30 pregnancy bursts and 30 labor bursts. The results show a difference in the capacity of each method to detect labor. They can be summarized as follow:

1. All the methods except phase synchronization show more correlation during labor than pregnancy.

2. The higher correlation noticed during labor is associated with a progressive increase in the correlation with the progress of gestation.

3. Observations 1 and 2 could be related to the increase in Gap Junctions number before delivery, which is the only available hypothesis about the better organization of the uterus from pregnancy to labor.

4. The relationships methods performed better than some of the classical frequency methods used in the literature.

5. A drawback of the GS method is the computational time costs which make it not very useful for clinical application and real time analysis, even if the methods show good results in the classification of pregnancy and labor signals.

6. The PS methods indicated a decrease in the synchronization from pregnancy to labor. The explanation of this observation is still not clear and could be simply related to the shifting toward high frequencies during labor, which decreases the 'chance' of phase synchronization. For this reason, care should be taken when applying PS methods to analyze uterine signals. It has been related on synthetic signals to an increase in signal complexity, which has also been evidenced on EHG signals from pregnancy to labor.

7. The MVAR method is an interesting tool for EHG analysis. The preliminary results show a good capacity to distinguish pregnancy and labor bursts especially with the

time varying version. MVAR have a very important characteristic which is to take into account the whole multichannel set of data, and not only two channels as the classical bivariate methods. However, as the method is based on the estimated coefficients and depends on several parameters (such as model order and window length), the adaptation of the different parameters is still a big challenge. Also the time cost is very high and could create a problem for real time or clinical application.

8. Nonlinear correlation method has shown a good performance to separate pregnancy and labor signals as well for labor monitoring (evolution of the correlation with the week of gestation). The use of multichannel analysis improved the classification rate but efforts are still to be done to improve this rate. The use of h^2 has many advantages such as:

- Non parametric method
- Faster in term of computation time
- Detect linear and nonlinear relationships
- Asymmetry: possibile to investigate information about the directionality of the relationships

4.6   What is the next to do?

All the methods mentioned above have been applied on bipolar signals as they are less noisy than the monopolar ones and present higher signal to noise ratio. The main aim was the classification of pregnancy and labor signals and the evolution of the correlation with the term. The results were good and encouraging but still not ready for clinical application mainly due to different factors such as:

- The small used database (30 pregnancy bursts and 30 labor bursts): the solution is the increase in this database. This problem has already started to be solved in our team by new recordings of EHG signals. We think that the application of the methods on larger database may improve the classification rate.

- The choice of the optimal parameters for each method: we tried to adapt the different method parameters to EHG signals. Efforts could be done in this way to define in an automatic way the noise effect, signals lengths…

- The use of bipolar signals could be a factor that can affect the performance of the different methods as the bipolar signals are created by the differentiation between neighboring channels. The differentiation affects the directionality analysis, in terms of correlation

direction and localization of the higher correlation zone, in order to localize the source of uterine electrical activity. In addition, bipolar signals can be a factor that decreases the classification rate.

These problems could be solved by using monopolar signals. These monopolar signals being corrupted by so much noise that their SNR is not suitable for signal characterization, a specific denoising tool has to be defined as a pre-processing step. The development of this denoising tool for the monopolar signals is the objective of the next chapter. This chapter introduces a novel denoising algorithm suitable for monopolar EHG signals. It then presents the preliminary results obtained by using monopolar signals for correlation analysis.

Chapter 5   Denoising monopolar EHG signals

5.1   **Why do we need monopolar signals?**

In all the previous chapters, analysis has been done on bipolar signals created from the 4x4 matrix, as the monopolar signals are very noisy and corrupted by different artifacts. Bipolar signals performed when we used only one bipolar channel, located on the median vertical axis of the uterus (supposed to be the reference position). In the second chapter, we started to analyze the relationship between the signals from separate locations on the uterus by using different methods. When analyzing the classification of pregnancy and labor signals and the longitudinal evolution along gestation of the correlation, bipolar signals show good performance and we did not observe noticeable effects of the use of bipolar signals on the interpretation of the results.

The study and the clinical use of the propagation of the uterine electrical activity are our main concern. We are therefore interested in analyzing the evolution of the propagation with term, the difference in propagation between pregnancy and labor, the direction of the propagation as well as the localization of the source of uterine electrical activity.

The classification of pregnancy and labor signals and the evolution of the propagation with term have been done by using the bipolar signals and have given consistent results. These results can be summarized as: the presence of more propagation is observed during labor than during pregnancy; an increase in the propagation of uterine electrical activity is observed with the term. The logical next step is analyzing the direction of the propagation, estimating the speed of propagation and then detecting the possible zone of sources of the propagation. For that purpose, the main disadvantages of the bipolar signals are: (i) Lower spatial resolution (12 signals instead of 16 with the same device) which reduces the spatial precision of the propagation analysis (ii) Influence on the directionality analysis as bipolar signals are the difference between adjacent electrodes, which creates 'a priori' information about the direction of the relationships between the signals.

More precisely the limitations of the bipolar signals can be described as following:

- It is fairly obvious for surface EMG signals that the monopolar signals have better spatial resolution than bipolar ones, as the signals coming from two adjacent electrodes are subtracted one from each other. For example, a 4x4 electrode matrix with d inter-electrode distance permits to record 16 monopolar signals, with d as spatial resolution. It permits to obtain either 12 bipolar signals that are artificially correlated through the differentiation, with d as spatial resolution (if we re-use one electrode for 2 adjacent bipolar signal generation); or 8 uncorrelated bipolar signals only, with 2d spatial resolution (if we do not).

- Here, in the case of the EHG signals, bipolar signals reduced the number of available signals (12 signals instead of 16). As our aim is to analyze the propagation of the uterine electrical activity, the more signals with the better resolution would be the best. Furthermore, by using monopolar signals, we record signals that are only correlated through propagation phenomenon, not by the differentiation effect.

- The computation of the bipolar signals (which is the difference between two neighbor electrodes) may create an external bias which affect the analysis of the correlation between signals and specially when analyzing the direction of the correlation (causality) of the relationships between signals.

- This differentiation of signals is also known to affect the frequency content (high pass filter). And, as in uterine signals, the part of the signals that appeared to be mostly propagated is the lower frequency band, using bipolar signals introduces a bias in the whole signal propagation analysis.

The possible solution is to use monopolar signals. However, the EHG is often corrupted by electronic and electromagnetic noise, as well as by movement artifacts, skeletal EMG and electrocardiogram from both the mother and the fetus. The interfering signals are sporadic and/or have spectra overlapping the spectral content of the signals of interest, rendering classical filtering ineffective. In the absence of good methods for denoising the monopolar EHG signal, bipolar methods are usually used to make sense of this noisy signal, as done in the previous chapters. In this chapter, we propose a novel combination of Blind Source Separation using Canonical Correlation Coefficient (BSS_CCA) and Empirical Mode Decomposition (EMD) methods to denoise monopolar EHG. We first extract the uterine bursts by using BSS_CCA. Then, the biggest part of any residual noise is extracted from the bursts by EMD. Our algorithm, called CCA_EMD, was compared with wavelet and independent component analysis (ICA) Filtering. We also compared CCA_EMD with the corresponding bipolar signals to demonstrate that the new method gives signals that have not

been detariorated by the filtering method. The proposed method indeed successfully removed artifacts from the signal without altering the underlying uterine activity when compared to bipolar methods. The CCA_EMD algorithm performed considerably better than the other methods.

5.2   State of the art

The EHG is a problematic signal that has very low frequency and is of very low amplitude when compared to various sources of contaminating noise. In this chapter we describe a large step in helping to isolate the signal from noise and thus to overcome important barriers that have prevented to use monopolar signal to provide information on the genesis and evolution of human labor. During recordings, the EHG is frequently corrupted by different artifacts which may often complicate the interpretation of the EHG. The typical types of noise in the EHG are maternal and fetal electrocardiograms (ECG), abdominal muscle electromyogram (EMG), maternal and fetal movement artifacts, power artifacts and electronic noise from the surrounding electronic devices.

The EHG is a noisy signal even recorded by bipolar electrodes that are fairly close together. Wavelet filtering has been successfully used on bipolar EHG for removing maternal and fetal ECG as well as stationary electric noises (Leman and Marque, 2000). Most techniques of wavelet filtering assume that the noise is of low amplitude and stationary when compared to the signal of interest. However, the noise in monopolar EHG is not stationary and usually of high amplitude when compared to the signal of interest. In addition, many sources of noise have main frequency components that are close to the frequency of the signal. Indeed EHG has most of its energy in the frequency band of 0.1 to 1.5 Hz whereas the bandwidths are typically for maternal cardiac frequency (around 1.2 Hz), maternal respiration (around 0.2 Hz) and fetal ECG (around 1 Hz). As the noise is in the same frequency bands and/or is of high amplitude and sporadic, it cannot be rejected by classical filters.

Recently, researchers have focused their efforts on multichannel EHG hopping that propagation analysis will permit to predict preterm labor. The work done on signals recorded by our team in Iceland during the last few years, from a 16 electrode matrix, is one of these approaches (Karlsson et al., 2007). All the related studies have been done by using bipolar signals to reduce noise effect (Hassan et al., 2009, 2010e; Terrien et al., 2010). Bipolar measurements of electric phenomena are basically a way to reject the part of the signal that is

common on both electrodes and keeping only the part that is dissimilar between the two electrodes (common noise rejection). The assumption underlying this technique is that the "local" electrical activity is dissimilar under the two electrodes and that the common part is from further afield and thus not relevant. It is highly uncertain that this holds for the case of the EHG. It is therefore likely that important information is lost by using bipolar signals, due to the low frequency content of the signal that may induce a large wave length, and thus a common part of this lower activity recorded by both electrodes.

Blind Source Separation (BSS) methods such as Independent Component Analysis (ICA) and Principal Component Analysis (PCA) are increasingly being used in biomedical signal processing involving analysis of multivariate time series data such as EEG (James and Gibson, 2003; LeVan et al., 2006).

Recently, a new method for muscle artifact elimination in scalp EEG has been developed that does not have some of the disadvantages of ICA (De Clercq et al., 2006). The method is based on the statistical Canonical correlation analysis (CCA) method applied as a blind source separation (BSS) technique, called as BSS_CCA. This method has demonstrated considerably better performance than ICA in some applications (De Clercq et al., 2006; De Vos et al., 2007).

In this chapter the aim of CCA is the extraction of the uterine bursts, based on the hypothesis that the bursts have higher autocorrelation coefficients than the noise. Thus they should be extracted by CCA. The bursts obtained after applying CCA only, contain fewer artifacts than the original signals but still contain the artifacts that have high autocorrelation. Empirical mode decomposition (EMD) was chosen as a second step to completely remove the remaining noise. EMD technique was introduced by Huang et al. (Huang et al., 1998) to analyze nonstationary and nonlinear signals. EMD has become a very important tool to analyze biomedical signals. The use of EMD for analyzing esophageal manometric data in gastro esophageal reflux disease provided good performance in removing different kind of artifacts (respiratory, motion...) from electrogastrogram (EGG) signals (Liang et al., 2005; Liang et al., 2000). The EMD approach also proved efficiency in removing artifacts from ECG signals (Blanco-Velasco et al., 2008). For EEG data, EMD algorithm has also been employed (Looney et al., 2007). This work demonstrated how reconstruction, by using the Hilbert-Huang transform, can successfully be applied to contaminated EEG data for the purposes of removing unwanted ocular artifacts. More recently, Wu and Huang have introduced a noise

assisted version of the EMD method, called Ensemble Empirical mode decomposition (EEMD) (Wu and Huang, 2009). This method has shown better performances than EMD as it extracts the IMFs in a manner so that the mode mixing disadvantage of the EMD method is corrected. We did not implement it in this work as EEMD is much slower than EMD and has not, to our knowledge, been used in real time processing for clinical application.

Wavelet transform (WT) denoising methods could also be good candidates for the second step of the processing presented here. But in this first development we chose EMD rather than the WT methods for two reasons: i) EMD is a data-driven algorithm: it decomposes the signal in a natural way without prior knowledge about the signal of interest, which not the case for the wavelet transform ii) EMD has shown a better performance than Wavelet when combined with ICA in denoising EEG signals (Mijovic et al.).

The aim of this work is thus to combine the use of BSS_CCA and EMD algorithms to design a new tool, called CCA_EMD, to remove the main interferences corrupting monopolar abdominal EHG recordings. The method was applied to real signals recorded on women during pregnancy and labor. We present here a quantitative comparison between CCA_EMD, wavelet filtering, bipolar signals (obtained in the same matrix) and ICA.

5.3   Materials and methods

5.3.1   Blind Source Separation (BSS)

5.3.1.1 Overview

Picture that you are in a room where two people are speaking simultaneously. You have two microphones pointing in different directions. The microphones give you two recorded time signals, which we could denote by $x_1(t)$ and $x_2(t)$, with x_1 and x_2 the amplitudes, and t the time index. Each of these recorded signals is a weighted sum of the speech signals emitted by the two speakers, which we denote by $s_1(t)$ and $s_2(t)$. We could express this as a linear equation:

$$x_1(t) = a_{11}s_1 + a_{12}s_2$$
$$x_2(t) = a_{21}s_1 + a_{22}s_2$$

where a_{11}, a_{12}, a_{21} and a_{22} are some parameters that depend on the distances of the microphones from the speakers. It would be very useful if you could now estimate the two original speech

signals $s_1(t)$ and $s_2(t)$, by using only the recorded signals $x_1(t)$ and $x_2(t)$. This is called the *cocktail-party problem.*

If we know the parameters a_{ij}, we could solve the linear equations described above by classical methods. The point is, however, that if we don't know the a_{ij}, the problem is considerably more difficult. One approach to solve this problem would be to use some information on the statistical properties of the signals $s_i(t)$ to estimate the a_{ii}. Actually, and perhaps surprisingly, it turns out that it is enough to assume that $s_1(t)$ and $s_2(t)$, at each time instant t, are *statistically independent.*

5.3.1.2 **Independent Component Analysis (ICA)**

The first proposed method to estimate the a_{ij} is the Independent Component Analysis (ICA) based on the information of their independence, which allows to separate the two original sources signals $s_1(t)$ and $s_2(t)$ from their mixtures $x_1(t)$ and $x_2(t)$ (Comon, 1994; Jutten and Herault, 1991). The key to estimate ICA model is the nongaussianity. Without nongaussianity the estimation is not possible at all. This is probably the main reason for the rather late emergence of ICA research: in most of classical statistical theory, random variables are assumed to have gaussian distributions, thus precluding any methods related to ICA. The Central Limit Theorem, a classical result in probability theory, tells that the distribution of a sum of independent random variables tends toward a gaussian distribution, under certain conditions. Thus, a sum of two independent random variables usually has a distribution that is closer to a gaussian than the distribution of any of the two original random variables.

To solve the BSS problem, the first main idea of ICA is to maximize the nongaussianity, it means to estimate the sources as nongaussian as possible (Comon and Jutten, 2010). To quantify the nongaussianity, several methods have been used such as the kurtosis or the fourth-order cumulant. The negentropy, based on the information theoretic quantification of differential entropy, gives better results than the kurtosis (Comon, 1994). Another approach for ICA estimation, inspired by information theory, is the minimization of mutual information and the estimation of the ICA model by maximization of likelihood estimation.

BSS methods have been implemented successfully, and give important results that meet clinical needs in terms of diagnosis on various electrophysiological signals:

(i)   Electrocardiogram (ECG): BSS has been used to reduce the artifacts of the ECG signal (Hon and Lee, 1963), the detection of fetal cardiac activity (Cox and Medgyesi-Mitschang, 1969) and the extraction of the fetal ECG signal from a

mixing containing maternal ECG signal (De Lathauwer et al., 2000; Reza et al., 2007; Zarzoso and Nandi, 2001).

(ii)   Electroencephalogram (EEG): BSS has been widely applied to EEG signals for different applications such as the removal of different kind of artifacts corrupting the EEG signal like electro-oculogram artifacts (EOG), EMG, ECG…(Barros et al., 2000; Jung et al., 2000; LeVan et al., 2006; Shackman et al., 2009; Vigario, 1997); the separation of evoked potentials induced by stimulation of different types (Vigario et al., 2000); localization of the brain activities (McMenamin et al., 2010). Magneto-encephalogram (MEG) has been also analyzed by means of BSS (Vigario et al., 2000).

(iii)   Electromyogram (EMG): The main application of BSS on the EMG was proposed by Farina et al. to test the efficiency of the BSS to analyze EMG signals (Farina et al., 2004). The study of Garcia et al. permitted to identify, from the surface EMG collected on a muscle, the activities corresponding to each motor unit of the muscle under investigation (García et al., 2003).

As we can see, BSS_ICA has been widely applied in biosignals. The main inconvenient of the ICA method are: we cannot determine the order of the independent components, which makes the automatic detection of the source of interest very difficult or maybe impossible; the choice of sources is limited to only visual inspection.

However, we first were interested in the BSS methods to develop an 'automatic tool' to denoise the monopolar signals. By applying ICA we find that the sources of interest (corresponding to the uterine activity) are randomly located from one subject to another, which renders any automatic detection impossible. We therefore excluded ICA from our possible development tools.

Recently, a new way to estimate sources has been introduced based on the Canonical Correlation Analysis (CCA) applied to BSS (Friman et al., 2002). As we noticed that the majority of the artifacts corrupting the EHG signals have low autocorrelation, and as the CCA method maximized the autocorrelation (instead of gaussianity in the case of ICA), we believe that it is possible to construct a 'semi' or 'fully' automatic algorithm to denoise the EHG signals. The BSS_CCA method is described in the next parts.

5.3.1.3 Canonical Correlation Analysis (CCA)

In BSS approach, the observed multichannel signals are assumed to reflect a linear combination of several sources which are associated with underlying physiological processes,

artifacts and noise. The BSS approach aims to recover a set of unobserved source signals using only a set of observed mixtures of sources. The observed time series $X(t) = [x_1(t); x_2(t); . . .; x_K(t)]^T$, is the result of an unknown mixture of a set of unknown source signals $S(t) = [s_1(t); s_2(t); . . . ; s_K(t)]^T$ with $t = 1; . . .;N,$ where N the number of samples, K the number of sensors and T is the transpose operator. The mixing is assumed to be linear, thus reducing the mixing to a matrix multiplication

$$X(t) = AS(t)$$

where A is the unknown mixing matrix. The aim is to estimate the mixing matrix and recover the original source signals $S(t)$. This could be done by introducing the de-mixing matrix W such that it approximates the unknown source signals in $S(t)$, by a scaling factor:

$$Z(t) = WX(t)$$

Ideally, W is the inverse of the unknown mixing matrix A, up to scaling and permutation. There are many ways to solve the BSS problem depending on the definition of a contrast function. The ICA method tries to make the estimated sources as non-Gaussian as possible. However, in PCA and most of the ICA algorithms, the temporal correlations are not taken into consideration for solving contrast functions. CCA solves this BSS problem by forcing the sources to be maximally autocorrelated and mutually uncorrelated, while the mixing matrix is assumed to be square (Friman et al., 2002).

Ordinary correlation analysis quantifies the relation between two signals $x(t)$ and $y(t)$ by means of a correlation coefficient :

$$\rho = \frac{COV(x, y)}{\sqrt{Var(x)Var(y)}}$$

where COV is the covariance and Var is the variance. CCA is a multivariate extension of ordinary correlation analysis.

Consider the observed data matrix $X(t)$ and its temporally delayed version $Y(t) = X(t-1)$. The CCA method obtains two sets of basis vectors, one for x and the other for y, such that the correlations between the projections of the variables onto these basis vectors are mutually maximized.

Consider the linear combinations of the components in X and Y:

$$u = w_{x_1}x_1 + \ldots + w_{x_k}x_k = w_x^T X$$

$$v = w_{y_1}y_1 + \ldots + w_{y_k}y_k = w_y^T Y$$

CCA find the weight vectors w_x and w_y that maximize the correlation ρ between u and v by solving the following maximization equation:

$$\max_{w_x, w_y} \rho(u,v) = \frac{E(uv)}{\sqrt{E(u^2)E(v^2)}} = \frac{w_x^T C_{xy} w_y}{\sqrt{(w_x^T C_{xx} w_x)(w_y^T C_{yy} w_y)}}$$

with C_{xx} and C_{yy} are the variance matrices from X and Y respectively and C_{xy} is the covariance matrix from X and Y.

The canonical correlation between X and Y can be calculated by solving these equations with respect to w_x and w_y:

$$C_{xx}^{-1}C_{xy}C_{yy}^{-1}C_{yx}\ w_x = \rho^2\ w_x$$

$$C_{yy}^{-1}C_{yx}C_{xx}^{-1}C_{xy}\ w_y = \rho^2\ w_y$$

with the canonical correlation coefficient ρ as the square root of the eigen-value, and w_x and w_x as eigenvectors. Since the solutions are related, only one of the eigen-value equations needs to be solved to get the demixing matrix w. The CCA gives the source signals that are uncorrelated with each other, maximally autocorrelated, and ordered by decreasing autocorrelation.

When BSS-CCA is applied to the EHG and the sources contributing to the EHG are derived, the artifacts can be removed by setting the columns representing the activations of the artifactual sources equal to zero in the reconstruction $X_{Denoised}(t)$:

$$X_{Denoised}(t) = A_{Denoised}Z(t)$$

with $Z(t)$ are the sources obtained by BSS-CCA, and $A_{Denoised}$ the mixing matrix with the columns representing activations of the artifactual sources, set to zero.

5.3.2 Empirical Mode Decomposition (EMD)

The empirical mode decomposition (EMD) was proposed by Huang et al. as a new signal decomposition method for nonlinear and nonstationary signals (Huang et al., 1998). The EMD decomposes a signal into a collection of oscillatory modes, called intrinsic mode functions

(IMF), which represent fast to slow oscillations in the signal. Each IMF can be viewed as a subband of a signal. Therefore, the EMD can be viewed as subband signal decomposition.

Given a signal $x(t)$, the effective algorithm of EMD can be summarized as follows(Huang et al., 1998):

1. Identify all extrema of $x(t)$
2. Interpolate along the point of $x(t)$ estimated in the first step in order to form an upper $e_{max}(t)$ and lower envelope $e_{min}(t)$.
3. Compute the mean $m(t)=(e_{min}(t) + e_{max}(t))/2$
4. Extract the detail $d(t)=x(t)-m(t)$
5. Iterate on the residual $m(t)$

In practice, the above procedure has to be refined by a *sifting* process (Huang et al., 1998) which amounts to first iterating steps 1 to 4 upon the detail signal $d(t)$, until this latter can be considered as zero-mean according to some stopping criterion. Once this is achieved, the detail is referred to as an *Intrinsic Mode Function* (IMF), the corresponding residual is computed and step 5 applies. By construction, the number of extrema is decreased when going from one residual to the next, and the whole decomposition is guaranteed to be completed with a finite number of modes.

Many factors have to be fixed when applying EMD. We use here the defaults parameters proposed by Flandrin and al. (Rilling et al., 2003) and developed as a free tool on his website such as the *cubic splines* method for the interpolation and the stopping criteria for sifting proposed in (Rilling et al., 2003).

Several methods have been proposed for automatically denoising signals using EMD, such as partial reconstruction based on the IMF energy to eliminate noise components proposed by Flandrin et al. (Flandrin et al., 2005). The algorithm did not work properly in our case. It could be due to the fact that the artifacts are not always fractional Gaussian as supposed by the algorithm. Otherwise, three algorithms methods have been proposed by Weng et al., (Weng and Barner, 2008). These algorithms are based on the linear weighting of the IMFs and need a reference signal that is very difficult to get in the real case. Similar to wavelet threshold, Kopsinis et al. proposed soft/hard threshold applied to EMD decomposition (Kopsinis et al., 2009). The methods show strong variability and can be easily affected by several parameters such as signal length, threshold factor…

Usually, denoising by EMD is in general carried out by partial signal reconstruction, which is based on the fact that noise components lie in the first several IMFs. Here, based on visual inspection, partial reconstruction is applied by removing the first three IMFs that we consider to be high frequency noise.

5.3.3 CCA/EMD combination

We assume that the BSS is the best way to extract the uterine bursts, based on the hypothesis that the sources of uterine bursts have higher autocorrelation than the sources corresponding to the artifacts. We thus choose the CCA method as a way to extract the uterine bursts and in the same time to eliminate all the low autocorrelated noises. The sources of device noise (electronic artifacts) are highly autocorrelated and then it is not possible to remove them by using only the CCA method. It was demonstrated that EMD has high performance to remove this kind of noise (Liang et al., 2005). For this reason, we used EMD as a complementary tool to remove the electronic noise. We called this combination the CCA_EMD algorithm.

5.3.4 Comparative study

For evaluation purpose, the proposed technique is compared with two other techniques that have already been used for denoising EHG signals in our group.

- *Wavelet filtering*: The specific algorithm which is based on the redundant wavelet packet transform was developed by Leman et al. and has already been used to remove artifacts from bipolar EHG signal. By applying this algorithm, the corrupting ECG seems to be totally removed while all other artifacts (fetal movements, electronic noise) are still presented (Leman and Marque, 2000).
- *FastICA*: which is the most popular and faster ICA algorithm (Hyvarinen and Oja, 1997). The selection of the ICA components accounting for the artifact removing was based on visual inspection and the signal was reconstructed, excluding the components related to the artifact.

For a quantitative comparison between the different methods, signal to noise (SNR) was used as a criterion. For each contraction and each EHG channel, the SNR was estimated by computing the energy of the base lines present before and after the EHG burst, and the energy of the burst. The SNR obtained by CCA_EMD were compared with those obtained with bipolar signal (vertical differentiation), ICA and the wavelet method. For statistical comparison, we used the two tailed sign test with a minimal significant level of 0.05.

5.4 Results

5.4.1 On labor signals

Figure 5.1A shows a typical example of raw monopolar EHG signals recorded from a woman during labor. The canonical components (CC) obtained by applying the BSS_CCA method are shown in **Figure** 5.1B. The fetal movements pump spikes (located in the 16th CC) and part of electronic noises (located in the 14th and the 15th CC) are well distinguished from the components related to the uterine activity.

A very important step to take into account here is the choice of the CCs corresponding to the artifacts, in order to remove them before signal reconstruction. We should detect the threshold corresponding to the transition from 'uterine activity' components to 'noise activity' components.
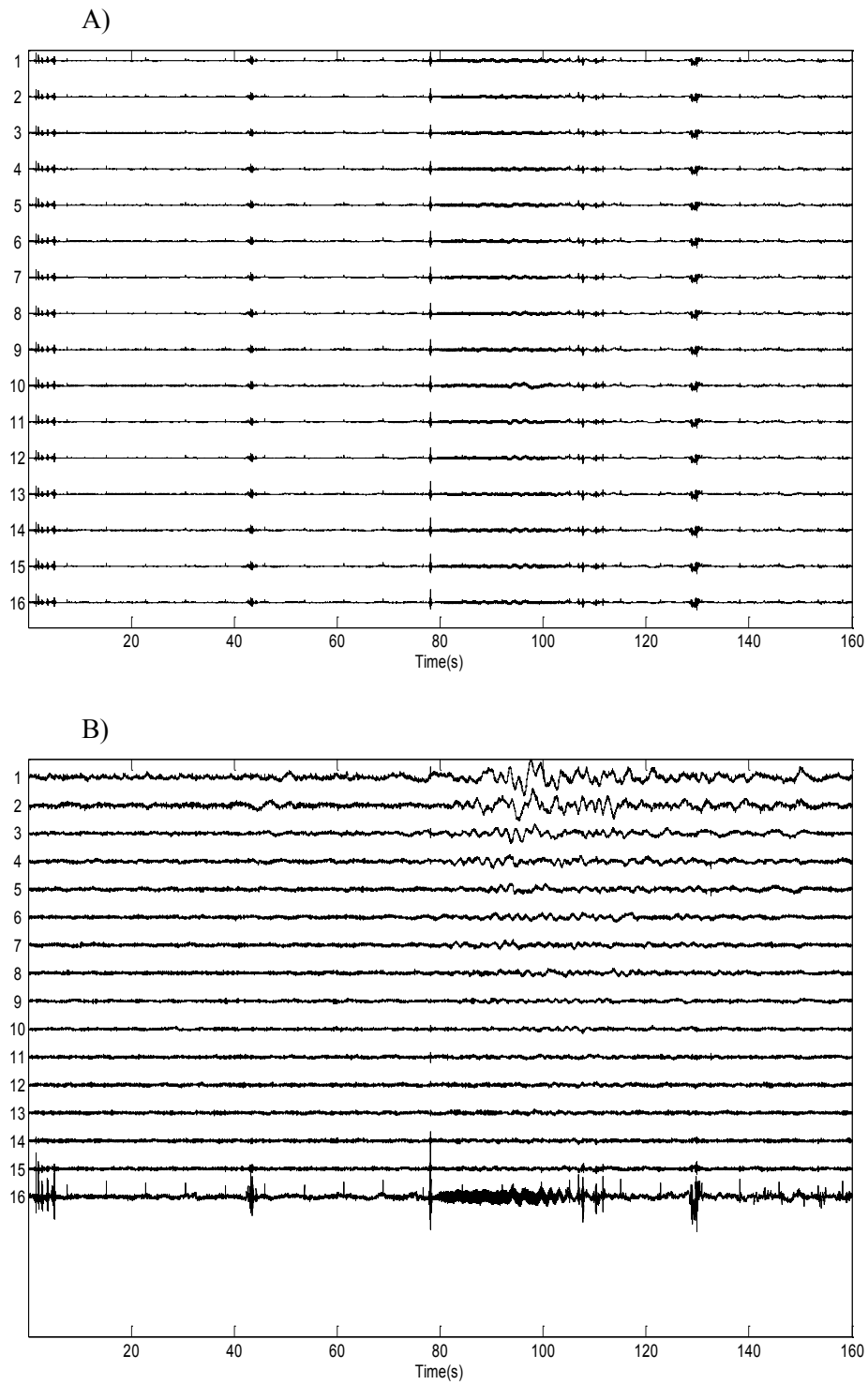
Figure 5.1: A) Original raw signals from a woman in labor B) Corresponding CCA components.
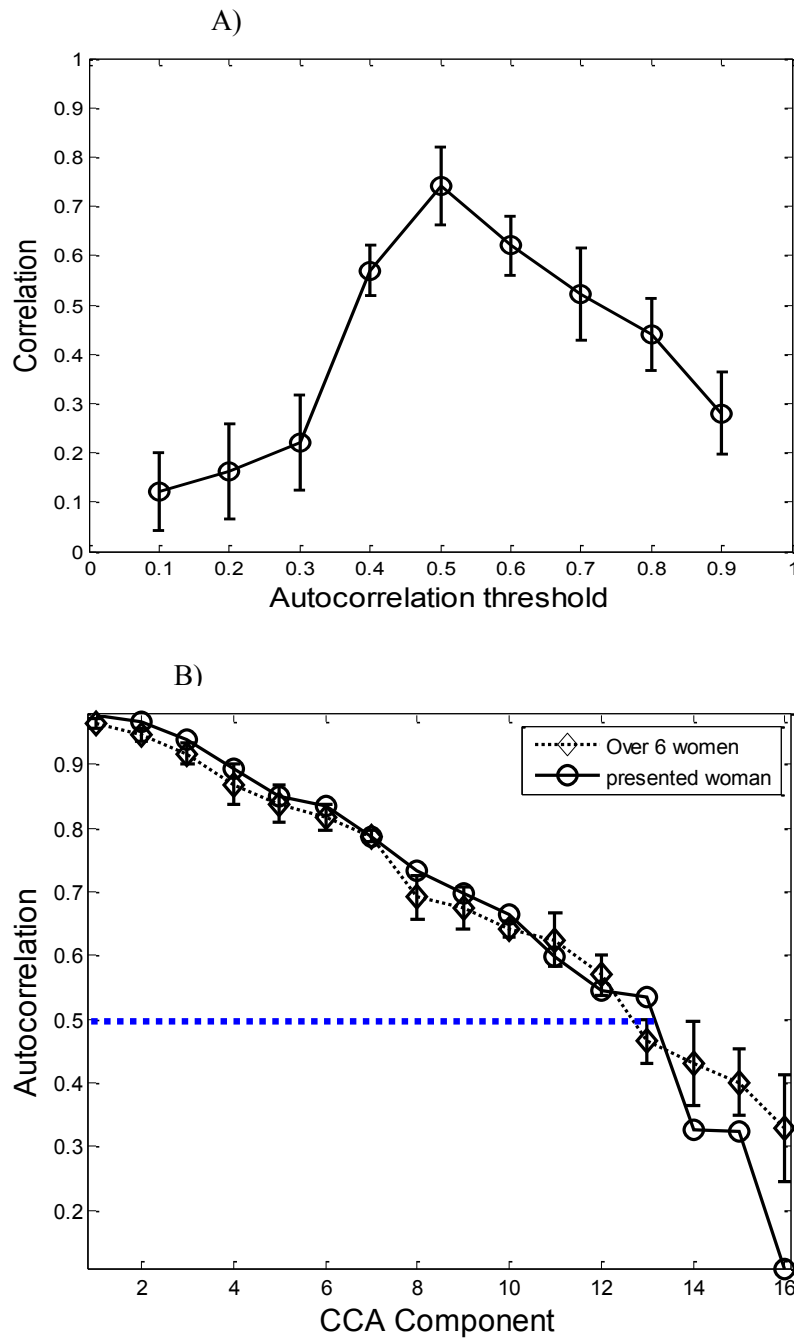
Figure 5.2: A) The correlation coefficient between Bip Org (raw bipolar signal) and Bipden (processed bipolar signal) in function of the autocorrelation threshold; B) Solid curve: autocorrelation coefficients from the contraction shown in **Figure**s 5.1. Dashed curve: averaged autocorrelation curve obtained from the 6 women in labor. The horizontal dashed line represents the threshold value.

The methodology we propose to choose the optimal threshold value can be described as following:

- Calculate the CCA components and the associated autocorrelation coefficients.
- Choose a threshold ranging between 0 and 1 (with 0.1 steps), then remove the CCs below this value and reconstruct the signals.
- Compute the original bipolar signals (BipOrg) from two raw channels X and Y, and the bipolar signal obtained from the same channels after the two preceding processing steps (BipDen). We thus get two versions of the bipolar signals, one created from the raw signals directly (BipORG) and the other by eliminating all the CCs below the given threshold of autocorrelation on each monopolar signal used for the bipolar one (BipDen).
- Compute the correlation between BipOrg and BipDen.
- Repeat these steps for 20 contractions from six women and then calculate the average and standard deviation at each autocorrelation value, for each given threshold.

The curve in **Figure** 5.2A indicates that 0.5 is the optimal threshold value for eliminating noisy CCs as we got the highest correlation between BipOrg and BipDen for this value. Computation of the mean square error (MSE) instead of the correlation confirms this, as the lowest MSE is also observed for a threshold equal to 0.5 (results not shown).

Figure 5.2B presents the autocorrelation coefficients curve computed for 20 contractions obtained from six women during labor, and the autocorrelation coefficients curve for the CC of the contraction presented **Figure** 5.1. The threshold (presented as a dashed horizontal line) is fixed at 0.5. All the CCs below this value are excluded. For the presented contraction (solid line) we reject the last three CCs. We can notice that this threshold corresponds to the last four CCs on the curve representing the autocorrelation coefficients averaged over the 6 women during labor (**Figure** 5.2 B dashed curve).

By using a threshold value equal to 0.5 and removing, before reconstruction of the EHG, the components below this value, we obtain the intermediate denoised EHGs shown in **Figure** 5.3. Notice that all the fetal movements, maternal/fetal ECG and part of electronic noises have been removed from the original signal. After BSS_CCA denoising, some noise remains that presents high autocorrelation coefficient (specially the electronic noise coming from the infusion devices). These artifacts are not completely removed by BSS_CCA. To remove this noise we apply EMD to the signals previously denoised by BSS_CCA.
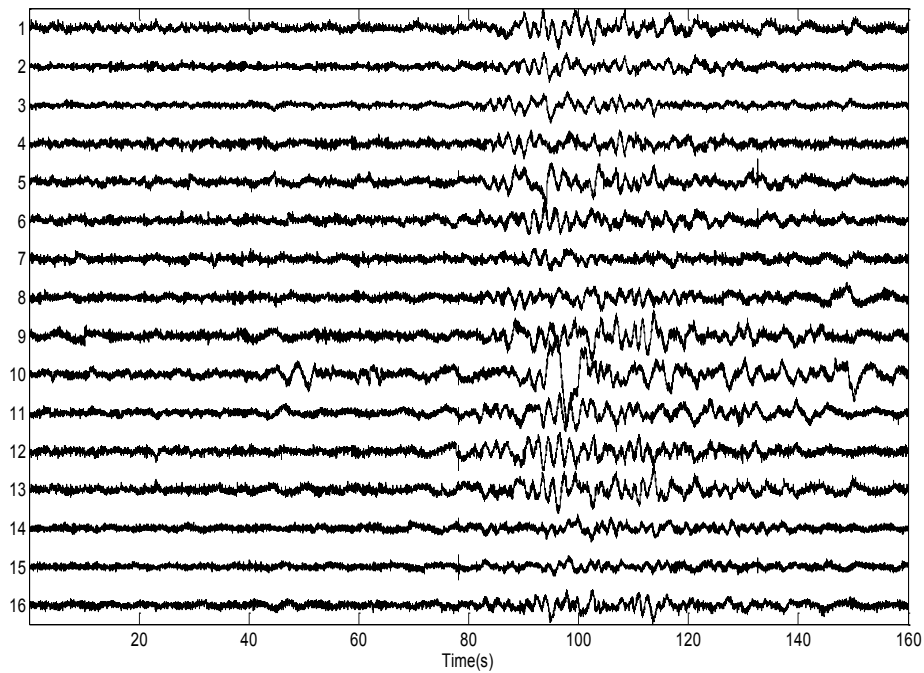
Figure 5.3: 16 signals recorded during one uterine burst denoised by CCA only.

Figure 5.4 shows the final signals after CCA_EMD. Here, based on visual inspection, partial reconstruction is applied by removing the first three IMFs that we consider to be high frequency noise. In **Figure** 5.4, we can clearly differentiate between the baseline and the uterine bursts, which will greatly ease the segmentation of uterine bursts.

Figure 5.5 presents an example of one of the channels extracted from the signals shown in **Figure**s 5.1, 5.3 and 5.4, in order to better evidence the way each step of CCA_EMD improves the signal, from a very noisy monopolar signal with various types of artifacts, to a clearly visible uterine burst. This result is based on a threshold autocorrelation value of 0.5 as described above.
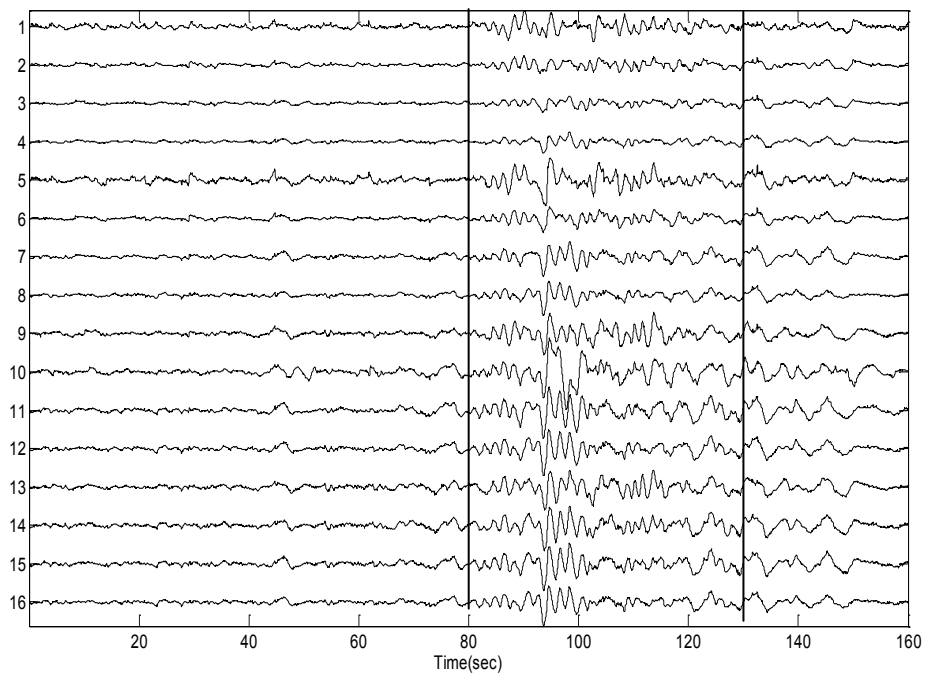
Figure 5.4: Same signals as in **Figure** 5.3 denoised by using CCA _EMD. The two vertical lines indicate the start and the end of the uterine bursts based on the TOCO signal.
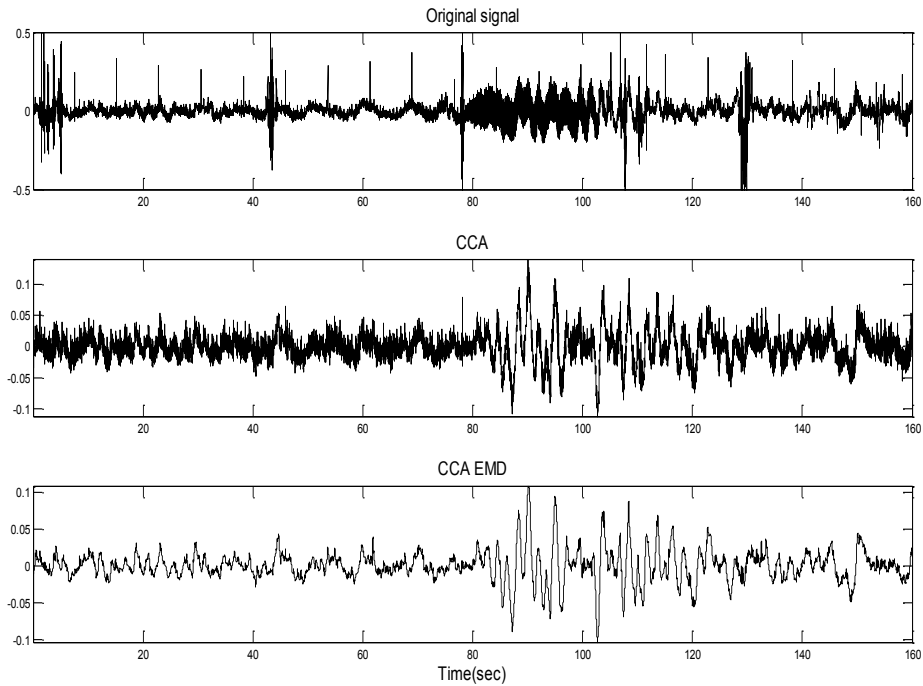
Figure 5.5: (Top): Original signal, (Middle): extracted burst by CCA and (Bottom): denoised signal after CCA_EMD.

Some residual noise from pump spikes and high frequency electronic noise is clearly visible on the middle panel of **Figure** 5.5. This residual noise is then completely removed from the burst by applying the EMD method (**Figure** 5.5 bottom). As the bipolar signal is our only available reference, we then compare the raw bipolar signal (computed as the difference between the raw channel-1 and raw channel-2, BipOrg) and the denoised bipolar signal (computed as the difference between denoised channel-1 and denoised channel-2, BipDen).

Figure 5.6 presents a typical example that indicates how CCA_EMD enhances the uterine activity information at least as well as the bipolar method. The two bipolar signals (original and denoised) are quite similar and there is no distortion (RMS error=10^{-4}, correlation coefficient=0.74). Time-frequency representations (Scalograms) show that the CCA_EMD has not visibly affected the uterine burst frequency content when compared to bipolar signals.
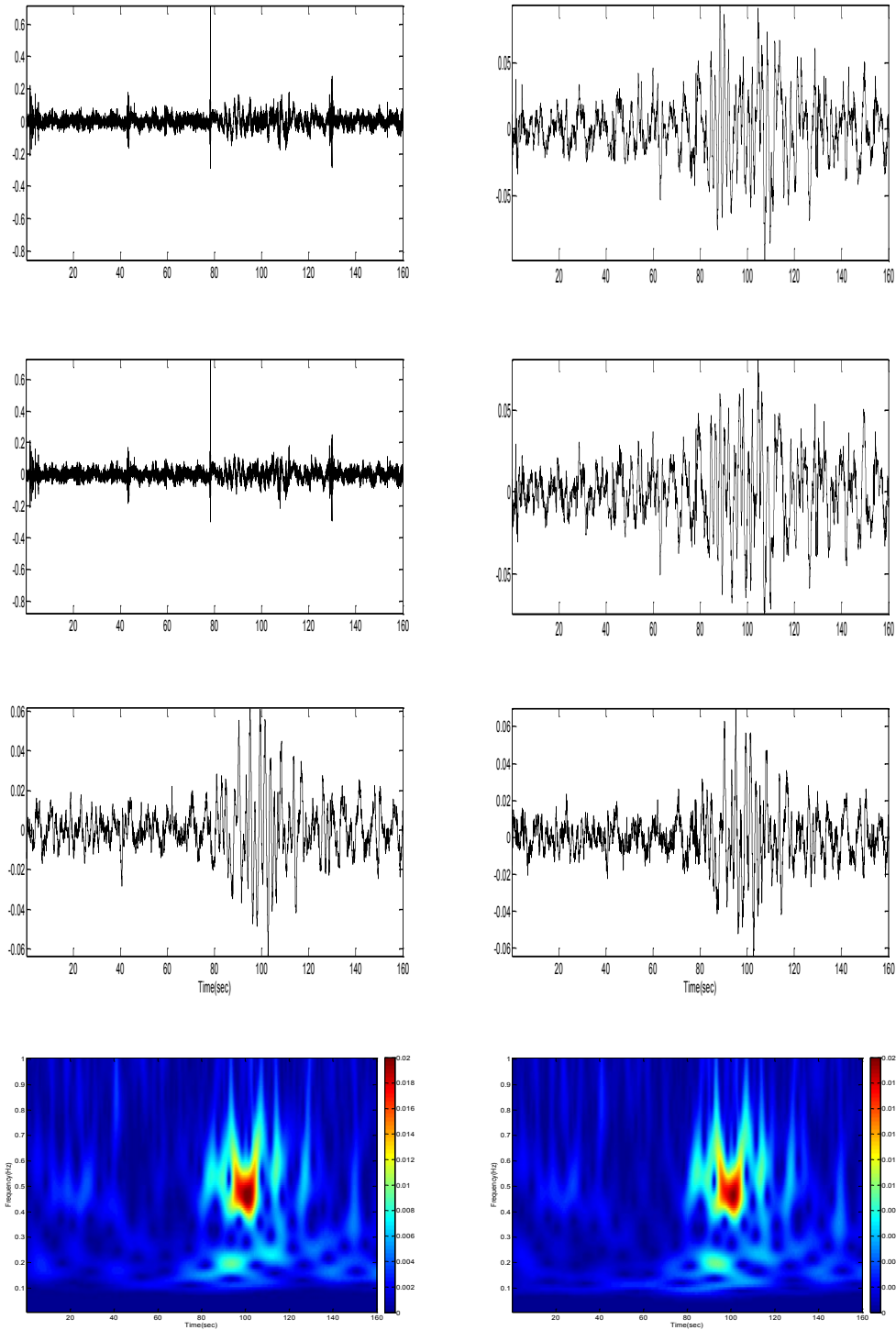
Figure 5.6: From top to bottom: monopolar channel-1, monopolar channel-2, corresponding bipolar signal and scalogram of the bipolar signal. (Left): Original data (Right): Denoised data.

Figure 5.7 shows the quantitative difference between the SNR of monopolar, bipolar, CCA_EMD, FastICA and the Wavelet algorithm described in (Leman and Marque, 2000). The values represent the median of SNR over the 16 channels for the six women during labor.

The monopolar raw signals present a poor SNR (median SNR = -3.4 dB). The results indicate clearly that CCA_EMD has the highest median SNR equal to 6.74 dB compared to 3.16 dB for wavelet, 5.02 dB for FastICA and 5.2 dB for bipolar signals.
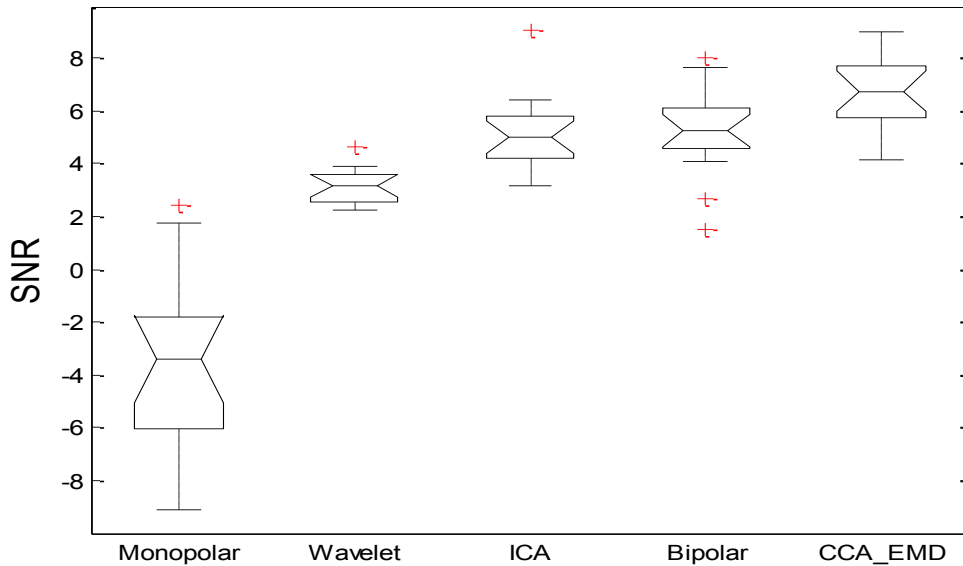
Figure 5.7: SNR computed for monopolar signals, and then after denoising by wavelet, ICA, bipolar and CCA_EMD methods.

5.4.2   **On pregnancy signals**

All the results illustrated above are for measurements on women during labor. The main differences between pregnancy and labor recordings are (i) during pregnancy there is no infusion pump noise (which is used to medicate women only during labor) (ii) during pregnancy we have fewer movement artifacts than during labor. We use the same technique for the signals during pregnancy. An example of the results obtained on pregnancy signals is illustrated **Figure** 5.8.

The results in **Figure** 5.8 confirm the feasibility of CCA_EMD algorithm to denoised labor signals as well as pregnancy signals.
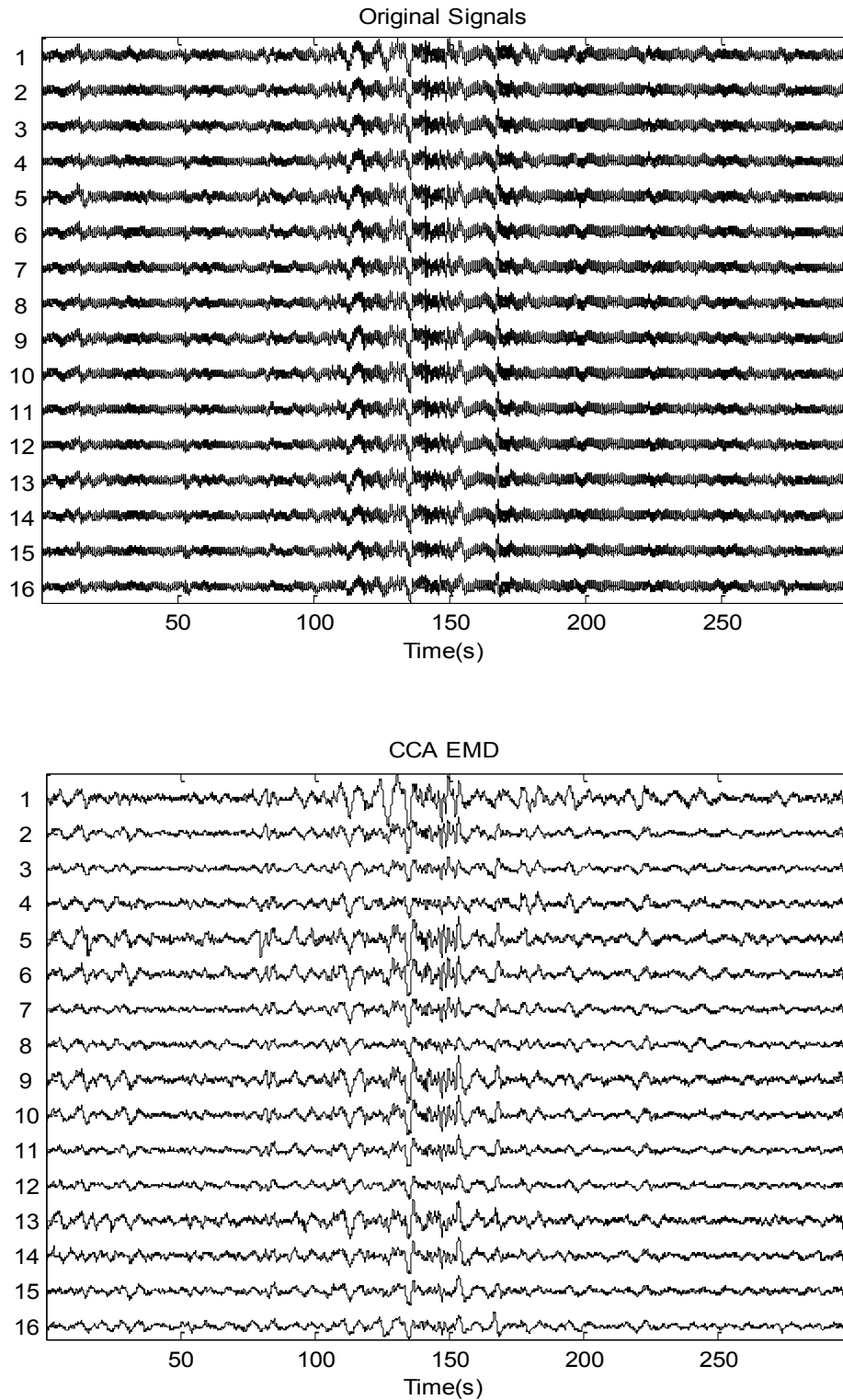
Figure 5.8: (Top) Typical example of pregnancy noisy signals; (Bottom) Signals denoised by

CCA_EMD

5.5   After denoising

In this section we present the preliminary results of the analysis of the monopolar signals to investigate the propagation of the uterine electrical activity. We used signals from the same subject (W1) than presented in Chapter 3. We compute the h^2 matrices for the three different times of gestation as described previously.

The results presented in **Figure** 5.9 present three main characteristics:

1. An increase in the correlation between the uterine burst along term, which can be explained by an increase of the propagation with the term. This observation is similar to the one made from the bipolar signals analysis. It can add a weight to the confidence about efficiency of the CCA_EMD algorithm.

2. The values are higher than the bipolar ones. This increase in the h^2 values can be explained by the fact that during differentiation of the adjacent electrodes, in order to compute bipolar signals, it is likely that we remove a large part of the time synchronization. It means that we remove all the common noise but we also remove at the same time synchronized patterns over the channels.

3. In term of localization of uterine activity sources, the matrices in **Figure** 5.9 show that at G1 (33 WG) the high correlation values are dispersed and not localized in special region. At G2 (35WG) the high values start to be concentrated in lines parallel to the diagonal. The highest values at G3 (37 WG) are then clearly located in two lines parallel to the diagonal (maximum correlation) one. These lines correspond to electrodes arranged horizontally in the 4x4 matrix. We can conclude that when we draw near the labor, the whole uterus becomes more synchronized and a preferred horizontal direction of the highest correlation values can be observed.

155
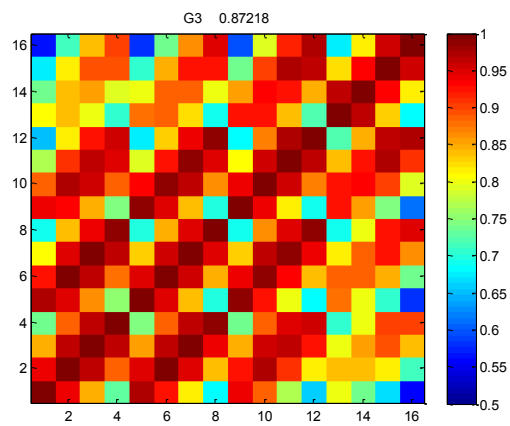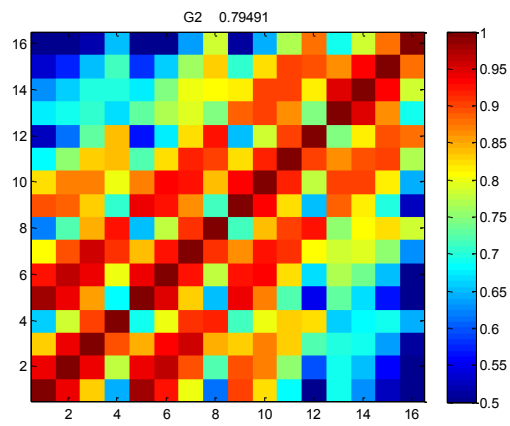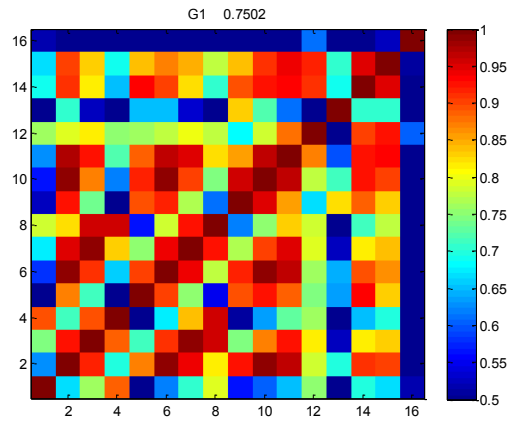
Figure 5.9 Evolution of the h^2 matrix along term for W1 33WG $\rightarrow$ 35WG $\rightarrow$ 37WG.

5.6 Discussion and Conclusion

In this work a novel combination of two important methods has been made in an effort to completely remove artifacts from a monopolar EHG signal. The method consists of two steps. First, BSS_CCA was used to extract the uterine bursts in the presence of high intensity noise in the same frequency band as the signal. Then, the signals are given a final 'cleaning' by applying EMD.

In addition, the method described here is fast and computationally economical. It can be used as a preprocessing step to facilitate segmentation of uterine EMG bursts. Furthermore, the noise activities (fetal movements…) are present in the least autocorrelated CCA components, which indicate that it is possible with this technique to separate noise sources (small autocorrelation), compared to the uterine activity that presents higher autocorrelation.

Concerning the CCA method, in this work, we have proposed a method that analyses the autocorrelation coefficient curve to estimate the right number of coefficient to remove for denoising purpose. In addition, the estimation of the threshold value by using criteria such as Akaike Information Criteria could be an important parallel way to optimize the threshold selection.

The removal of artifacts by EMD was based on visual inspection of the IMFs. For this method to be useful in real time, and/or in a clinical setting, the selection of the proper IMFs has to be done automatically. This is still a limit of the method and work has to be continued on this direction.

This chapter introduces the first combination between CCA and another method applied to a signal. In future work comparison between CCA_EMD and other combination possibilities could be interesting as well, as the use of wavelet transform or EEMD instead of EMD, as well as comparison with other existing combination such as ICA_EMD or ICA_Wavelet…

The preliminary results obtained by using denoised monopolar signals to investigate the uterine correlation along the week of gestation are then presented in this chapter. These results show the first observation of possible localization and directionality of the uterine electrical activity propagation. They also show a better characterization of monopolar propagation analysis. Monopolar signals provide a better spatial resolution and do not bias the measured propagation directions, as bipolar methods do. The next step will be to compare the use of bipolar and monopolar EHG signal to investigate the propagation of the uterine electrical

activity. The investigations are open to confirm these preliminary observations by more data and a larger sample.

Finally, we conclude that this work has opened the door for the use of monopolar EHG recordings to investigate uterine contractions. This will, in our opinion, have important applications in studying the genesis and evolution of human labor and to develop ways of predicting preterm labor.

Chapter 6 Conclusions and perspectives

We have presented in this thesis several novel approaches to analyzing uterine contractions in view of a future clinical application. Our approach is based on the analysis of the propagation of the uterine electrical activity to first understand this phenomenon and then, from this understanding, to extract tools than can be used in labor detection or/and prediction of preterm labor.

The idea of using the externally detected electrical activity of the uterus (electrohysterogram or EHG) to predict preterm labor is not new and lot of work has already been put into it. The innovative approach in this work is to make sense of the signals coming from a matrix of electrodes permitting to give us a much more complete picture of the organization and operation of the uterus, as pregnancy reaches its conclusion. In addition, longitudinal recordings from the same women at different times of gestation have been recorded which is rarely done in the literature and can give new information about the possible use of our methods for pregnancy monitoring.

The first approach to the analysis of this complicated signal was to investigate the nonlinear characteristics of the EHG signals. Then we proposed the analysis of the propagation of the EHG signals by using different methods (bivariate or multivariate) detecting the relationships between signals. Finally, the thesis finished by solving one of the main obstacles to analyzing the propagation represented by the contamination of monopolar signals by noise.

In general, the work demonstrates variable performances of the different methods of nonlinear analysis and propagation parameters to distinguish pregnancy and labor contractions.

In the nonlinear analysis, a comparison between three nonlinear methods (approximate entropy, correntropy and time reversibility) was done on linear, nonlinear stationary and nonlinear nonstationary synthetic signals in order to choose the best method to apply on real EHG signals. Indeed the EHG signals are thought to exhibit non linear as well as non stationary characteristics. The comparison demonstrated the clear superiority of time reversibility in the detection of linearity and nonlinearity of the different signals.

We thus tested EHG signals for their time reversibility property. The results indicate that uterine contractions during pregnancy are reversible, whereas labor contractions are temporally irreversible. The obtained results demonstrated that time reversibility could become a powerful tool to differentiate between pregnancy and labor contractions.

It should be pointed out that this nonlinearity measure, just like other statistical nonlinearity measures, is based on comparison with surrogate data. It is not a standalone measure, as it needs the generation of appropriate surrogates, and could therefore fail if the generation of proper surrogates fails for some reason.

The results of our limited study indicate that this can be very powerful method for EHG analysis. Although we need to confirm this on more data, we think that the time reversibility characteristic may by clinically useful in detecting contractions leading to term or preterm labor. Ultimately, these findings may have a considerable relevance in helping to prevent preterm labor.

As examples of further work possible in this direction we suggest:

- Apply Time reversibility on a larger database, which can give a clear idea about the possible use of *Tr* in clinical application.

- Investigate the nonlinearity with other nonlinear methods such as Lyapunov exponents, correlation dimension… especially as these methods have shown good performances in other domains (such as EEG analysis) without the need for surrogate data.

- Even if the *Tr* has shown high capacity to classify pregnancy and labor signals, we think that methods that do not need surrogates data could be better for real time clinical purposes as the take much less time to compute.

Our study of the relationships between EHG recorded at different locations on the abdomen indicates that a difference exists between the values provided by the different used methods in pregnancy and labor. All the methods (except phase synchronization) indicated more

pronounced amplitude relationship between the signals during labor than during pregnancy and an increase in this relationship with term. From this body of observations we feel confident to conclude that the electrical activity of the uterus presents more organization during labor than prior to labor. The fact that phase synchronization decreases with term is also a common observation made from different methods. This observation has to be now related to physiological interpretation.

Further work can be done in different ways:

- Improving the classification rate of the propagation parameters such as to take into account of the effects of noise, the signal stationarity, the use of monopolar signals…

- Localization of the source of uterine electrical activity by using monopolar signals which can give a view of higher correlation zones which may be related to pacemaker zones.

- Another fundamental aspect in the characterization of the relationship between signals may be the subject of further work is the notion of directionality (asymmetry) of the coupling. This information can be very useful in the study of the dynamics of pregnancy and labor, such as the determination of the direction of EHG propagation.

- Test these methods on a larger database for clinical purpose (pregnancy monitoring, preterm labor detection)

In the last part, we proposed a novel combination of two recent methods in order to completely remove artifacts from a monopolar EHG signal. The method consists of two steps. First, BSS_CCA is used to extract the uterine bursts in the presence of high intensity noise with overlapping frequency band with EHG. Then the signals are given a final 'cleaning' by applying EMD. The method described is fast and computationally economical and can be used as a preprocessing step to facilitate segmentation of uterine EMG bursts and propagation analysis.

Concerning the CCA method, we have in this work proposed a method that analyses the autocorrelation coefficient curve to estimate the ones that have to be eliminated, based on a similarity to a reference signal (bipolar one).

The removal of artifacts by EMD was based on visual inspection of the IMFs. For this method to be useful in real time and/or in a clinical setting, the selection of the proper IMFs has to be automated based also on the use of some computable criterion.

This part has introduced the first combination between CCA and another method applied to a biological signal. In future work, comparison between CCA_EMD and other combination method could be interesting.

Further work that derives straight from this part of the thesis is the comparison of bipolar and denoised monopolar EHG signals in investigating the propagation of the uterine electrical activity. The preliminary results presented in the denoising chapter shows the advantage of monopolar analysis as it has better spatial resolution and it does not bias the measure of propagation directions as bipolar methods inevitably do.

We only applied the CCA_EMD algorithm to a small part of our database to demonstrate the efficiency of the algorithm to denoise the uterine signals. However, an essential future work is the application of the denoising algorithm to the entire available database to investigate the possibility of improving the classification rate of pregnancy and labor contractions by using monopolar signals.

Finally, we think that the advances made in denoising the signal have opened the door for the use of monopolar EHG recordings to investigate uterine contractions. This will, in our opinion, have important implications in studying the genesis of human labor and to develop ways of predicting preterm labor.

Résumé

A) Prétraitement: Elimination des artéfacts qui contaminent les signaux EMG utérins multicanaux

Le signal électrique utérin, electrohysterographique (EHG), est fortement contaminé par plusieurs sources de bruit qui rendent l'exploitation du signal brut quasi impossible. L'artefact de mouvement, le signal cardiaque du fœtus et de la mère, les bruits électroniques et le bruit des pompes à injection (utilisées durant l'accouchement) sont les principales sources de bruit. Une combinaison originale entre la Séparation aveugle de sources fondée sur la corrélation canonique (BSS_CCA) et la Décomposition en Mode Empirique (EMD) **a été développée pour éliminer ces bruits contaminant le signal EHG** (Hassan et al., 2011). Cette approche a été quantitativement et qualitativement analysée. La méthode se décompose en deux étapes : tout d'abord, l'algorithme BSS_CCA a été utilisé pour extraire les bouffées utérines en présence de bruit non corrélé de forte intensité dans la même bande de fréquence que le signal utile. Ensuite, les signaux ont été débruités en appliquant la méthode EMD. Les résultats ont montré que cet algorithme est très efficace pour éliminer les différentes sources de bruit contaminant les signaux EHG. Ce volet de la thèse a permis **d'ouvrir plusieurs perspectives** en matière de traitement des signaux «EHG monopolaires».

B) Analyse de la propagation de l'activité électrique utérine

Des méthodes permettant l'analyse des **dépendances statistiques linéaires et non linéaires entre signaux** ont été testées/développées. L'application de ces méthodes pour étudier la différence de connectivité entre la grossesse et le travail, ont montré que les signaux durant l'accouchement sont plus corrélés que les signaux obtenus au cours de la grossesse (Hassan et al., 2009, 2010e; Terrien et al.; Terrien et al., 2009; Terrien et al., 2008). L'utilisation des enregistrements multicanaux, lors de l'analyse de cette connectivité, a démontré une plus grande efficacité des méthodes traitant conjointement tous les canaux comparativement à l'utilisation d'un seul des canaux (Hassan et al., 2010b). Des méthodes qui expliquent les relations entre les contractions utérines dans **le domaine temps-fréquence** ont été testées/développées aussi qu'une méthode basée sur les 'surrogates' pour évaluer la significativité de la relation détectée (Hassan et al., 2010a; Hassan et al., 2010d; Terrien et al., 2008). Les résultats ont montré une connectivité plus forte dans les basses fréquences que dans les hautes fréquences du spectre des signaux EHG, appuyant l'hypothèse que les activités basses fréquences ont un lien plus étroit avec la propagation de l'activité électrique utérine que les activités hautes fréquences (Hassan et al., 2010c). Une autre dimension a été ajoutée à notre étude : l'analyse multi-variée des signaux multicanaux utérins. Un modèle (nommé W-MVAR) fondé sur les **modèles autorégressifs multivariés classiques** (MVAR) a été proposé. Il prend en compte la **nonstationnarité du signal** EHG. L'application des modèles MVAR et W-MVAR sur les signaux EHG a clairement démontré que le modèle W-MVAR est beaucoup plus efficace dans la différenciation des signaux de grossesse et d'accouchement que le modèle MVAR. **La conclusion de cette partie est que l'utérus devient beaucoup plus synchronisé et organisé lorsqu'on approche de l'accouchement.**

Conclusion **:** La thèse a permis de définir **une nouvelle approche** pour l'analyse des contractions utérines en vue d'une **future application clinique**. L'approche est basée sur l'analyse de la **connectivité utérine** pour, tout d'abord comprendre ce phénomène et ensuite, à partir de cette compréhension, développer des outils qui pourraient être utilisés dans le suivi du travail d'accouchement et / ou la **prédiction de l'accouchement prématuré**. Les résultats ont montré que les méthodes de détection de relation entre les signaux sont des outils très puissants pour distinguer les contractions de grossesse et d'accouchement aussi que pour suivre l'évolution de la grossesse.

REFERENCES

(2009). Center for Disease Control and Prevention and National Center for Health Statistics data. (United States, U.S. Departement of health and human services).

Akaike, H. (1969). Fitting autoregressive models for prediction. Annals of the Institute of Statistical Mathematics *21*, 243-247.

Akaike, H. (1974). A new look at the statistical model identification. IEEE Trans. Autom. Control *AC19*, 716-723.

Akaike, H. (1979). A Bayesian Extension of the Minimum AIC Procedure of Autoregressive Model Fitting. Biometrika *66*, 237-242.

Akay, M. Nonlinear biomedical signal processing, Vol II (New York: IEEE Inc.).

Ansari-Asl, K., Senhadji, L., Bellanger, J.-J., and Wendling, F. (2006). Time-frequency characterization of interdependencies in nonstationary signals: application to epileptic EEG. IEEE Trans Biomed Eng *52*, 1218-1226.

Arnhold, J., Grassberger, P., Lehnertz, K., and Elger, C.E. (1999). A robust method for detecting interdependences: application to intracranially recorded EEG. Physica D: Nonlinear Phenomena *134*, 419-430.

Aysegul, G., and Jose, C.P. (2009). Correntropy as a novel measure for nonlinearity tests. Signal Process. *89*, 14-23.

Babloyantz, A., and Lourenco, C. (1996). Brain chaos and computation. Int J Neural Syst *7*, 461-471.

Babloyantz, A., Salazar, J.M., and Nicolis, C. (1985). Evidence of chaotic dynamics of brain activity during the sleep cycle. Physics Letters A *111*, 152-156.

Baccala, L.A., and Sameshima, K. (2001a). Overcoming the limitations of correlation analysis for many simultaneously processed neural structures. Prog Brain Res *130*, 33-47.

Baccala, L.A., and Sameshima, K. (2001b). Partial directed coherence: a new concept in neural structure determination. Biol Cybern *84*, 463-474.

Baggish, M., Valle, R., and Guedj, H. (2007). Hysteroscopy: Visual Perspectives of Uterine Anatomy, Physiology & Pathology, 3rd Edition, 3rd edn (Lippincott Williams & Wilkins).

Barros, A.K., Vigario, R., Jousmaki, V., and Ohnishi, N. (2000). Extraction of event-related signals from multichannel bioelectrical measurements. IEEE Trans Biomed Eng *47*, 583-588.

Bendat, J.S., and Piersol, A.G. (2000). Random Data Analysis and Measurement Procedures. Measurement Science and Technology *11*, 1825.

Berryman, M.J., Coussens, S.W., Pamula, Y., Kennedy, J.D., Lushington, K., Shalizi, C.R., Allison, A.G., Martin, A.J., Saint, D.A., and Abbott, D. (2005). Nonlinear aspects of the EEG during sleep in children. In Fluctuations and noise in biological, biophysical, and biomedical systems III (Austin, Texas, SPIE - International Society for Optical Engineering), pp. 40-48.

Bhattacharya, J. (2001). Reduced degree of long-range phase synchrony in pathological human brain. Acta Neurobiol Exp (Wars) *61*, 309-318.

Blanco-Velasco, M., Weng, B., and Barner, K.E. (2008). ECG signal denoising and baseline wander correction based on the empirical mode decomposition. Computers in Biology and Medicine *38*, 1-13.

Boashash, B. (1992). Interpreting and estimating the instantaneous frequency of a signal-Part 1: Fundamentals. In Proc. IEEE, pp. 520-538.

Bode, O. (1931). Das elektrohysterogramm. Arch. Gyndk *28*, 123-128.

Borgnat, P., and Flandrin, P. (2009). Stationarization via surrogates. Journal of Statistical Mechanics: Theory and Experiment *2009*, P01001.

Brazier, M.A. (1968). Studies of the EEG activity of limbic structures in man. Electroencephalogr Clin Neurophysiol *25*, 309-318.

Brazier, M.A., and Casby, J.U. (1952). Cross-correlation and autocorrelation studies of electroencephalographic potentials. Electroencephalogr Clin Neurophysiol *4*, 201-211.

Buhimschi, C., Boyle, M.B., and Garfield, R.E. (1997). Electrical activity of the human uterus during pregnancy as recorded from the abdominal surface. Obstet Gynecol *90*, 102-111.

Buhimschi, C., Boyle, M.B., Saade, G.R., and Garfield, R.E. (1998). Uterine activity during pregnancy and labor assessed by simultaneous recordings from the myometrium and abdominal surface in the rat. Am J Obstet Gynecol *178*, 811-822.

Buhimschi, C., and Garfield, R.E. (1996). Uterine contractility as assessed by abdominal surface recording of electromyographic activity in rats during pregnancy. Am J Obstet Gynecol *174*, 744-753.

Buresti G., L.G. (1999). Application of Continuous Wavelet Transform to the Analysis of Experimental Turbulent Velocity Signals. In Turbulence and Shear Flow Phenomena, B.H. Inc., ed. (Santa Barbara (U.S.A.)), p. 762.

Burioka, N., Miyata, M., Cornelissen, G., Halberg, F., Takeshima, T., Kaplan, D.T., Suyama, H., Endo, M., Maegaki, Y., Nomura, T.*, et al.* (2005). Approximate entropy in the electroencephalogram during wake and sleep. Clin EEG Neurosci *36*, 21-24.

Caldeyro-barcia, R., and Poseiro, J.J. (1960). Physiology of the uterine contraction. Clin. Obstet. Gynecol. *3*, 386-408.

Cao, L. (1997). Practical method for determining the minimum embedding dimension of a scalar time series. Physica D: Nonlinear Phenomena *110*, 43-50.

Coleman, H.A., and Parkington, H.C. (1990). Hyperpolarization-activated channels in myometrium: a patch clamp study. Prog Clin Biol Res *327*, 665-672.

Comon, P. (1994). Independent component analysis, A new concept? Signal Processing *36*, 287-314.

Comon, P., and Jutten, C. (2010). Handbook of Blind Source Separation Independent Component Analysis and Applications (Academic Press).

Cox, D. (1981). Statistical analysis of time series: some recent developments. Scandinavian Journal of Statistics *8*, 93-115.

Cox, J.R., Jr., and Medgyesi-Mitschang, L.N. (1969). An algorithmic approach to signal estimation useful in fetal electrocardiography. IEEE Trans Biomed Eng *16*, 215-219.

Csapo, A.I. (1962). Smooth muscle as a contractile unit. Physiol Rev Suppl *5*, 7-33.

Daubechies, I. (1990). The wavelet transform time-frequency localization and signal analysis. IEEE Trans. Inform. Theory *36*, 961-1004.

De Clercq, W., Vergult, A., Vanrumste, B., Van Paesschen, W., and Van Huffel, S. (2006). Canonical correlation analysis applied to remove muscle artifacts from the electroencephalogram. IEEE Trans Biomed Eng *53*, 2583-2587.

De Lathauwer, L., De Moor, B., and Vandewalle, J. (2000). Fetal electrocardiogram extraction by blind source subspace separation. IEEE Trans Biomed Eng *47*, 567-572.

De Vos, M., Vergult, A., De Lathauwer, L., De Clercq, W., Van Huffel, S., Dupont, P., Palmini, A., and Van Paesschen, W. (2007). Canonical decomposition of ictal scalp EEG reliably detects the seizure onset zone. Neuroimage *37*, 844-854.

Denney, J.M., Culhane, J.F., and Goldenberg, R.L. (2008). Prevention of preterm birth. Womens Health (Lond Engl) *4*, 625-638.

Devedeux, D., Marque, C., Mansour, S., Germain, G., and Duchene, J. (1993). Uterine electromyography: a critical review. Am J Obstet Gynecol *169*, 1636-1653.

Diks, C., Van Houwelingen, J.C., Takens, F., and DeGoede, J. (1995). Reversibility as a criterion for discriminating time series. phys.Lett. A *201*, 221-228.

Doret, M., Bukowski, R., Longo, M., Maul, H., Maner, W.L., Garfield, R.E., and Saade, G.R. (2005). Uterine electromyography characteristics for early diagnosis of mifepristone-induced preterm labor. Obstet Gynecol *105*, 822-830.

Duchêne, J., Marque, C., and Planque, S. (1990). Uterine EMG signal : Propagation analysis. In Annual International Conference of the IEEE EMBS, pp. 831-832.

Dyson, D.C., Danbe, K.H., Bamber, J.A., Crites, Y.M., Field, D.R., Maier, J.A., Newman, L.A., Ray, D.A., Walton, D.L., and Armstrong, M.A. (1998). Monitoring women at risk for preterm labor. N Engl J Med *338*, 15-19.

Elbert, T., Ray, W.J., Kowalik, Z.J., Skinner, J.E., Graf, K.E., and Birbaumer, N. (1994). Chaos and physiology: deterministic chaos in excitable cell assemblies. Physiol Rev *74*, 1-47.

Elger, C.E., Widman, G., Andrzejak, R., Arnhold, J., David, P., and Lehnertz, K. (2000). Nonlinear EEG analysis and its potential role in epileptology. Epilepsia *41 Suppl 3*, S34-38.

Eswaran, H., Govindan, R.B., Furdea, A., Murphy, P., Lowery, C.L., and Preissl, H.T. (2009). Extraction, quantification and characterization of uterine magnetomyographic activity--a proof of concept case study. Eur J Obstet Gynecol Reprod Biol *144 Suppl 1*, S96-100.

Eswaran, H., Preissl, H., Wilson, J.D., Murphy, P., Robinson, S.E., and Lowery, C.L. (2002). First magnetomyographic recordings of uterine activity with spatial-temporal information with a 151-channel sensor array. Am J Obstet Gynecol *187*, 145-151.

Euliano, T.Y., Marossero, D., Nguyen, M.T., Euliano, N.R., Principe, J., and Edwards, R.K. (2009). Spatiotemporal electrohysterography patterns in normal and arrested labor. Am J Obstet Gynecol *200*, 54 e51-57.

Euliano, T.Y., Nguyen, M.T., Marossero, D., and Edwards, R.K. (2007). Monitoring contractions in obese parturients: electrohysterography compared with traditional monitoring. Obstet Gynecol *109*, 1136-1140.

Farina, D., Fevotte, C., Doncarli, C., and Merletti, R. (2004). Blind separation of linear instantaneous mixtures of nonstationary surface myoelectric signals. IEEE Trans Biomed Eng *51*, 1555-1567.

Faure, P., and Korn, H. (2001). Is there chaos in the brain? I. Concepts of nonlinear dynamics and methods of investigation. C R Acad Sci III *324*, 773-793.

Fele-Zorz, G., Kavsek, G., Novak-Antolic, Z., and Jager, F. (2008). A comparison of various linear and non-linear signal processing techniques to separate uterine EMG records of term and pre-term delivery groups. Med Biol Eng Comput *46*, 911-922.

Flandrin, P., Goncalves, P., and Rilling, G. (2005). EMD Equivalent Filter Banks, from Interpretation to Applications. In Hilbert-Huang Transform and Its Applications,, N.E.H.a. S.S.P, ed. (World Scientific), pp. 57-74.

Franaszczuk, P.J., Bergey, G.K., and Kaminski, M.J. (1994). Analysis of mesial temporal seizure onset and propagation using the directed transfer function method. Electroencephalogr Clin Neurophysiol *91*, 413-427.

Friman, O., Borga, M., Lundberg, P., and Knutsson, H. (2002). Exploratory fMRI analysis by autocorrelation maximization. Neuroimage *16*, 454-464.

Furdea, A., Eswaran, H., Wilson, J.D., Preissl, H., Lowery, C.L., and Govindan, R.B. (2009). Magnetomyographic recording and identification of uterine contractions using Hilbert-wavelet transforms. Physiol Meas *30*, 1051-1060.

García, G.A., Nishitani, R., Okuno, R., and Akazawa, K. (2003). Independent component analysis as preprocessing tool for decomposition of surface electrode-array electromyogram. In 4th International Symposium on Independent Component Analysis and Blind Signal Separation (Nara, Japan).

Garfield, R.E. (1994). Role of cell-to-cell coupling in control of myometrial contractility and labor. In: R.E. Garfield and T.N. Tabb, Editors, Control of uterine contractility (Florida).

Garfield, R.E., Chwalisz, K., Shi, L., Olson, G., and Saade, G.R. (1998a). Instrumentation for the diagnosis of term and preterm labour. J Perinat Med *26*, 413-436.

Garfield, R.E., and Hayashi, R.H. (1981). Appearance of gap junctions in the myometrium of women during labor. Am J Obstet Gynecol *140*, 254-260.

Garfield, R.E., and Maner, W.L. (2007). Physiology and electrical activity of uterine contractions. Semin Cell Dev Biol *18*, 289-295.

Garfield, R.E., Maner, W.L., MacKay, L.B., Schlembach, D., and Saade, G.R. (2005). Comparing uterine electromyography activity of antepartum patients versus term labor patients. American Journal of Obstetrics and Gynecology *193*, 23-29.

Garfield, R.E., Maul, H., Maner, W., Fittkow, C., Olson, G., Shi, L., and Saade, G.R. (2002). Uterine electromyography and light-induced fluorescence in the management of term and preterm labor. J Soc Gynecol Investig *9*, 265-275.

Garfield, R.E., Maul, H., Shi, L., Maner, W., Fittkow, C., Olsen, G., and Saade, G.R. (2001). Methods and devices for the management of term and preterm labor. Ann N Y Acad Sci *943*, 203-224.

Garfield, R.E., Saade, G., Buhimschi, C., Buhimschi, I., Shi, L., Shi, S.Q., and Chwalisz, K. (1998b). Control and assessment of the uterus and cervix during pregnancy and labour. Hum Reprod Update *4*, 673-695.

Garfield, R.E., Sims, S., and Daniel, E.E. (1977). Gap junctions: their presence and necessity in myometrium during parturition. Science *198*, 958-960.

Gautama, T., Mandic, D.P., and Van Hulle, M.M. (2003). A differential entropy based method for determining the optimal embedding parameters of a signal In IEEE international conference on Acoustics, Speech, and Signal Processing, pp. 29-32.

Gautama, T., Mandic, D.P., and Van Hulle, M.M. (2004). The delay vector variance method for detecting determinism and nonlinearity in time series. Physica D: Nonlinear Phenomena *190*, 167-176.

Grassberger, P., and Procaccia, I. (1983). Measuring the strangeness of strange attractors. Physica D: Nonlinear Phenomena *9*, 189-208.

Grinsted A., Moore J. C., and S., J. (2004). Application of the cross wavelet transform and wavelet coherence to geophysical time series. Nonlinear Processes in Geophysics *11*, 561-566.

Hannan, E.J., and Quinn, B.G. (1979). The Determination of the Order of an Autoregression. Journal of the Royal Statistical Society. Series B (Methodological) *41*, 190-195.

Hassan, M., Alexandersson, Á., Terrien, J., Karlsson, B., and Marque, C. (2010a). Wavelet phase synchronization between EHGs at different uterine sites: comparison of pregnancy and labor contractions. In XII Mediterranean Conference on Medical and Biological Engineering and Computing 2010 (Springer Berlin Heidelberg), pp. 21-24.

Hassan, M., Boudaoud, S., Terrien, J., Karlsson, B., and Marque, C. (2011). Combination of canonical correlation analysis and empirical mode decomposition applied to denoising the labor electrohysterogram. IEEE Transactions on Biomedical Engineering, *58*, 2441-2447.

Hassan, M., Terrien, J., Alexandersson, A., Marque, C., and Karlsson, B. (2010b). Improving the classification rate of labor vs. normal pregnancy contractions by using EHG multichannel recordings. In Annual International Conference of the IEEE Engineering in Medicine and Biology Society, pp. 4642-4645.

Hassan, M., Terrien, J., Karlsson, B., and Marque, C. (2009). Spatial analysis of uterine EMG signals: evidence of increased in synchronization with term. In Conf Proc IEEE Eng Med Biol Soc, pp. 6296-6299.

Hassan, M., Terrien, J., Karlsson, B., and Marque, C. (2010c). Application of wavelet coherence to the detection of uterine electrical activity synchronization in labor. IRBM *31*, 182-187.

Hassan, M., Terrien, J., Karlsson, B., and Marque, C. (2010d). Interactions between uterine EMG at different sites investigated using wavelet analysis: comparison of pregnancy and labor contractions. EURASIP Journal on Advances in Signal Processing *2010*, 17.

Hassan, M., Terrien, J., Karlsson, B., and Marque, C. (2010e). Interactions between Uterine EMG at Different Sites Investigated Using Wavelet Analysis: Comparison of Pregnancy and Labor Contractions. EURASIP Journal on Advances in Signal Processing *2010*, 9.

Hesse, W., Moller, E., Arnold, M., and Schack, B. (2003). The use of time-variant EEG Granger causality for inspecting directed interdependencies of neural assemblies. J Neurosci Methods *124*, 27-44.

Hon, E.H., and Lee, S.T. (1963). Noise Reduction in Fetal Electrocardiography. Ii. Averaging Techniques. Am J Obstet Gynecol *87*, 1086-1096.

Hornero, R., Escudero, J., Fernandez, A., Poza, J., and Gomez, C. (2008). Spectral and nonlinear analyses of MEG background activity in patients with Alzheimer's disease. IEEE Trans Biomed Eng *55*, 1658-1665.

Huang, N.E., Shen, Z., Long, S.R., Wu, M.C., Shin, H.H., Zheng, Q., Yen, N.C., Tung, C.C., and Liu, H.H. (1998). The Empirical Mode Decomposition and the Hilbert spectrum for nonlinear and non-stationary time series analysis. Proc. Royal Soc. *454*, 903-995.

Hyvarinen, A., and Oja, E. (1997). A fast fixed-point algorithm for independent component analysis. Neural Computation *9*, 1483–1492.

Iams, J.D. (2003a). Prediction and early detection of preterm labor. Obstet Gynecol *101*, 402-412.

Iams, J.D. (2003b). What have we learned about uterine contractions and preterm birth? The HUAM Prediction Study. Semin Perinatol *27*, 204-211.

Iams, J.D., Goldenberg, R.L., Meis, P.J., Mercer, B.M., Moawad, A., Das, A., Thom, E., McNellis, D., Copper, R.L., Johnson, F., and Roberts, J.M. (1996). The length of the cervix and the risk of spontaneous premature delivery. National Institute of Child Health and Human Development Maternal Fetal Medicine Unit Network. N Engl J Med *334*, 567-572.

James, C.J., and Gibson, O.J. (2003). Temporally constrained ICA: an application to artifact rejection in electromagnetic brain signal analysis. IEEE Trans Biomed Eng *50*, 1108-1116.

Jung, T.P., Makeig, S., Humphries, C., Lee, T.W., McKeown, M.J., Iragui, V., and Sejnowski, T.J. (2000). Removing electroencephalographic artifacts by blind source separation. Psychophysiology *37*, 163-178.

Jutten, C., and Herault, J. (1991). Blind separation of sources, part I: An adaptive algorithm based on neuromimetic architecture. Signal Processing *24*, 1-10.

Kalitzin, S.N., Parra, J., Velis, D.N., and Lopes da Silva, F.H. (2007). Quantification of unidirectional nonlinear associations between multidimensional signals. IEEE Trans Biomed Eng *54*, 454-461.

Kaminski, M.J., and Blinowska, K.J. (1991). A new method of the description of the information flow in the brain structures. Biol Cybern *65*, 203-210.

Kao, C.Y., and McCullough, J.R. (1975). Ionic currents in the uterine smooth muscle. J Physiol *246*, 1-36.

Karlsson, B., Terrien, J., Guðmundsson, V., Steingrímsdóttir, T., and Marque, C. (2007). Abdominal EHG on a 4 by 4 grid: mapping and presenting the propagation of uterine contractions. In 11th Mediterranean Conference on Medical and Biological Engineering and Computing (Ljubljana, Slovenia), pp. 139-143.

Kitlas, A., Oczeretko, E., Swiatecka, J., Borowska, M., and Laudanski, T. (2009). Uterine contraction signals--application of the linear synchronization measures. Eur J Obstet Gynecol Reprod Biol *144 Suppl 1*, S61-64.

Kopsinis, Y., Aboutanios, E., Waters, D.A., and McLaughlin, S. (2009). Development of EMD-based Denoising Methods Inspired by Wavelet Thresholding. IEEE Trans. on Signal Processing, 1351-1362.

Korzeniewska, A., Kasicki, S., Kaminski, M., and Blinowska, K.J. (1997). Information flow between hippocampus and related structures during various types of rat's behavior. J Neurosci Methods *73*, 49-60.

Kreuz, T., Andrzejak, R.G., Mormann, F., Kraskov, A., Stogbauer, H., Elger, C.E., Lehnertz, K., and Grassberger, P. (2004). Measure profile surrogates: a method to validate the performance of epileptic seizure prediction algorithms. Phys Rev E Stat Nonlin Soft Matter Phys *69*, 061915.

Kus, R., Kaminski, M., and Blinowska, K.J. (2004). Determination of EEG activity propagation: pair-wise versus multichannel estimate. IEEE Trans Biomed Eng *51*, 1501-1510.

Lachaux, J.P., Lutz, A., Rudrauf, D., Cosmelli, D., Le Van Quyen, M., Martinerie, J., and Varela, F. (2002). Estimating the time-course of coherence between single-trial brain signals: an introduction to wavelet coherence. Neurophysiol Clin *32*, 157-174.

Lachaux, J.P., Rodriguez, E., Martinerie, J., and Varela, F.J. (1999). Measuring phase synchrony in brain signals. Hum Brain Mapp *8*, 194-208.

Lamberts, J., van Den Broek, P.L., Bener, L., van Egmond, J., Dirksen, R., and Coenen, A.M. (2000). Correlation dimension of the human electroencephalogram corresponds with cognitive load. Neuropsychobiology *41*, 149-153.

Lammers, W.J., Mirghani, H., Stephen, B., Dhanasekaran, S., Wahab, A., Al Sultan, M.A., and Abazer, F. (2008). Patterns of electrical propagation in the intact pregnant guinea pig uterus. Am J Physiol Regul Integr Comp Physiol *294*, R919-928.

Lehnertz, K., Andrzejak, R.G., Arnhold, J., Kreuz, T., Mormann, F., Rieke, C., Widman, and Elger, C.E. (2001). Nonlinear EEG analysis in epilepsy: its possible use for interictal focus localization, seizure anticipation, and prevention. J Clin Neurophysiol *18*, 209-222.

Lehnertz, K., Widman, G., Andrzejak, R., Arnhold, J., and Elger, C.E. (1999). Is it possible to anticipate seizure onset by non-linear analysis of intracerebral EEG in human partial epilepsies? Rev Neurol (Paris) *155*, 454-456.

Leman, H., and Marque, C. (2000). Rejection of the maternal electrocardiogram in the electrohysterogram signal. IEEE Trans Biomed Eng *47*, 1010-1017.

Leman, H., Marque, C., and Gondry, J. (1999). Use of the electrohysterogram signal for characterization of contractions during pregnancy. IEEE Trans Biomed Eng *46*, 1222-1229.

LeVan, P., Urrestarazu, E., and Gotman, J. (2006). A system for automatic artifact removal in ictal scalp EEG based on independent component analysis and Bayesian classification. Clin Neurophysiol *117*, 912-927.

Li, X., Yao, X., Fox, J., and Jefferys, J.G. (2007). Interaction dynamics of neuronal oscillations analysed using wavelet transforms. J Neurosci Methods *160*, 178-185.

Liang, H., Lin, Q.H., and Chen, J.D. (2005). Application of the empirical mode decomposition to the analysis of esophageal manometric data in gastroesophageal reflux disease. IEEE Trans Biomed Eng *52*, 1692-1701.

Liang, H., Lin, Z., and McCallum, R.W. (2000). Artifact reduction in electrogastrogram based on empirical mode decomposition method. Med Biol Eng Comput *38*, 35-41.

Linhart, J., Olson, G., Goodrum, L., Rowe, T., Saade, G., and Hankins, G. (1998). Pre-term labor at 32 to 34 weeks' gestation: effect of a policy of expectant management on length of gestation. Am. J. Obstet. Gynecol. *178*.

Lockwood, C.J. (2001). Biochemical predictors of prematurity. Front Horm Res *27*, 258-268.

Lodge, S., and Sproat, J.E. (1981). Resting membrane potentials of pacemaker and non pacemaker areas in rat uterus. Life Sci *28*, 2251-2256.

Looney, D., Li, L., Rutkowski, T.M., Mandic, D.P., and Cichocki, A. (2007). Artifacts Removal from EEG Using EMD. In International Conference on Cognitive Neurodynamics. ICCN (Springer Netherlands).

Lucovnik, M., Maner, W.L., Chambliss, L.R., Blumrick, R., Balducci, J., Novak-Antolic, Z., and Garfield, R.E. (2011). Noninvasive uterine electromyography for prediction of preterm delivery. Am J Obstet Gynecol *204*, 228 -238

Lutkepohl, H. (1985). Comparison of criteria for estimating the order of a vector autoregressive process. Time. Ser. Anal *6*, 5-52.

Maner, W.L., and Garfield, R.E. (2007). Identification of human term and preterm labor using artificial neural networks on uterine electromyography data. Ann Biomed Eng *35*, 465-473.

Maner, W.L., Garfield, R.E., Maul, H., Olson, G., and Saade, G. (2003). Predicting Term and Preterm Delivery With Transabdominal Uterine Electromyography. Obstet Gynecol *101*, 1254-1260.

Mansour, S., Devedeux, D., Germain, G., Marque, C., and Duchene, J. (1996). Uterine EMG spectral analysis and relationship to mechanical activity in pregnant monkeys. Med Biol Eng Comput *34*, 115-121.

Marple, and S, L. (1999). Computing the discrete-time analytic signal via FFT, Vol 47 (New York, NY, United States: Institute of Electrical and Electronics Engineers).

Marque, C. (1987). Analyse de la dynamique des contractions uterines par électromyographie abdominale. In Génie biomédical (Compiègne, Université de Technologie de Compiègne).

Marque, C., and Duchene, J. (1989). Human abdominal EHG processing for uterine contraction monitoring. In Applied sensors (Boston: Butterworth), pp. 187-226.

Marque, C., Duchene, J.M., Leclercq, S., Panczer, G.S., and Chaumont, J. (1986). Uterine EHG processing for obstetrical monitoring. IEEE Trans Biomed Eng *33*, 1182-1187.

Marque, C., Terrien, J., Rihana, S., and Germain, G. (2007). Preterm labour detection by use of a biophysical marker: the uterine electrical activity. BMC Pregnancy and Childbirth *7(Suppl. 1)*.

Mars, N.J., and Lopes da Silva, F.H. (1983). Propagation of seizure activity in kindled dogs. Electroencephalogr Clin Neurophysiol *56*, 194-209.

Maul, H., Maner, W.L., Olson, G., Saade, G.R., and Garfield, R.E. (2004). Non-invasive transabdominal uterine electromyography correlates with the strength of intrauterine pressure and is predictive of labor and delivery. J Matern Fetal Neonatal Med *15*, 297-301.

McMenamin, B.W., Shackman, A.J., Maxwell, J.S., Bachhuber, D.R.W., Koppenhaver, A.M., Greischar, L.L., and Davidson, R.J. (2010). Validation of ICA-based myogenic artifact correction for scalp and source-localized EEG. Neuroimage *49*, 2416-2432.

Meeren, H.K., Pijn, J.P., Van Luijtelaar, E.L., Coenen, A.M., and Lopes da Silva, F.H. (2002). Cortical focus drives widespread corticothalamic networks during spontaneous absence seizures in rats. J Neurosci *22*, 1480-1495.

Merkwirth, C., Parlitz, U., Wedekind, I., and Lauterborn, W. (2002). OpenTSTOOL http://www.dpi.physik.uni-goettingen.de/tstool/.

Mijovic, B., De Vos, M., Gligorijevic, I., Taelman, J., and Van Huffel, S. Source separation from single-channel recordings by combining empirical-mode decomposition and independent component analysis. IEEE Trans Biomed Eng *57*, 2188-2196.

Miller, S.M., Garfield, R.E., and Daniel, E.E. (1989). Improved propagation in myometrium associated with gap junctions during parturition. Am J Physiol *256*, C130-141.

Miyoshi, H., Boyle, M.B., MacKay, L.B., and Garfield, R.E. (1998). Gap junction currents in cultured muscle cells from human myometrium. Am J Obstet Gynecol *178*, 588-593.

Mormann, F., Kreuz, T., Andrzejak, R.G., David, P., Lehnertz, K., and Elger, C.E. (2003). Epileptic seizures are preceded by a decrease in synchronization. Epilepsy Res *53*, 173-185.

Mormann, F., Lehnertz, K., David, P., and E. Elger, C. (2000). Mean phase coherence as a measure for phase synchronization and its application to the EEG of epilepsy patients. Physica D: Nonlinear Phenomena *144*, 358-369.

Nichols, J.M., Seaver, M., Trickey, S.T., Todd, M.D., Olson, C., and Overbey, L. (2005). Detecting nonlinearity in structural systems using the transfer entropy. Physical Review E *72*, 046217.

Ocak, H. (2009). Automatic detection of epileptic seizures in EEG using discrete wavelet transform and approximate entropy. Expert Systems with Applications *36*, 2027-2036.

Oczeretko, E., Kitlas, A., Swiatecka, J., Borowska, M., and Laudanski, T. (2005). Nonlinear Dynamics in Uterine Contractions Analysis (Fractals in Biology and Medicine: Birkhäuser Basel), pp. 215-222.

Oczeretko, E., Kitlas, A., Swiatecka, J., and Laudanski, T. (2004). Fractal analysis of the uterine contractions. Riv Biol *97*, 499-504.

Oczeretko, E., Swiatecka, J., Kitlas, A., Laudanski, T., and Pierzynski, P. (2006). Visualization of synchronization of the uterine contraction signals: running cross-correlation and wavelet running cross-correlation methods. Med Eng Phys *28*, 75-81.

Pereda, E., Gamundi, A., Rial, R., and Gonzalez, J. (1998). Non-linear behaviour of human EEG: fractal exponent versus correlation dimension in awake and sleep stages. Neurosci Lett *250*, 91-94.

Pereda, E., Quiroga, R.Q., and Bhattacharya, J. (2005). Nonlinear multivariate analysis of neurophysiological signals. Progress in Neurobiology *77*, 1-37.

Pijn, J., and Lopes Da Silva, F. (1993). Propagation of electrical activity: nonlinear associations and time delays between EEG signals. In Basic Mechanisms of the EEG (Boston: Zschocke & Speckmann).

Pijn, J.P., Velis, D.N., and Lopes da Silva, F.H. (1992). Measurement of interhemispheric time differences in generalised spike-and-wave. Electroencephalogr Clin Neurophysiol *83*, 169-171.

Pijn, J.P., Vijn, P.C., Lopes da Silva, F.H., Van Ende Boas, W., and Blanes, W. (1990). Localization of epileptogenic foci using a new signal analytical approach. Neurophysiol Clin *20*, 1-11.

Pikovsky A. , R.M., Kurths J. (2001). Synchronisation : a universal concept in nonlinear sciences. In Cambridge University Press (Cambridge).

Pincus, S.M. (1991). Approximate entropy as a measure of system complexity. Proc Natl Acad Sci U S A *88*, 2297-2301.

Planes, J.G., Morucci, J.P., Grandjean, H., and Favretto, R. (1984). External recording and processing of fast electrical activity of the uterus in human parturition. Med Biol Eng Comput *22*, 585-591.

Planque, S. (1990). Contribution à l'étude de la propagation des signaux electrohystérographiques. In Génie biomédical (Compiègne, Université de technologie de Compiègne).

Quian Quiroga, R., Kraskov, A., Kreuz, T., and Grassberger, P. (2002). Performance of different synchronization measures in real data: a case study on electroencephalographic signals. Phys Rev E Stat Nonlin Soft Matter Phys *65*, 041903.

Rabotti, C., Mischi, M., van Laar, J.O., Oei, G.S., and Bergmans, J.W. (2008). Estimation of internal uterine pressure by joint amplitude and frequency analysis of electrohysterographic signals. Physiol Meas *29*, 829-841.

Rabotti, C., Mischi, M., van Laar, J.O., Oei, G.S., and Bergmans, J.W. (2009). Inter-electrode delay estimators for electrohysterographic propagation analysis. Physiol Meas *30*, 745-761.

Ramon, C., Preissl, H., Murphy, P., Wilson, J.D., Lowery, C., and Eswaran, H. (2005). Synchronization analysis of the uterine magnetic activity during contractions. Biomed Eng Online *4*, 55.

Reza, S., Gari, D.C., Christian, J., and Mohammad, B.S. (2007). Multichannel ECG and noise modeling: application to maternal and fetal ECG signals. EURASIP J. Appl. Signal Process. *2007*, 94-94.

Rihana, S., Terrien, J., Germain, G., and Marque, C. (2009). Mathematical modeling of electrical activity of uterine muscle cells. Med Biol Eng Comput *47*, 665-675.

Rilling, G., Flandrin, P., and Gonçalvès, P. (2003). On empirical mode decomposition and its algorithms. In In Proceedings of the 6th IEEE/EURASIP Workshop on Nonlinear Signal and Image Processing (NSIP '03) (Grado, Italy).

Rissanen, J. (1983). A Universal Prior for Integers and Estimation by Minimum Description Length. The Annals of Statistics *11*, 416-431.

Romero, R., Gomez, R., and Sepulveda, W. (1992). The uterine cervix, ultrasound and prematurity. Ultrasound Obstet Gynecol *2*, 385-388.

Rosenblum, M.G., Pikovsky, A.S., and Kurths, J. (1996). Phase synchronization of chaotic oscillators. Phys Rev Lett *76*, 1804-1807.

Sanborn, B.M. (1995). Ion channels and the control of myometrial electrical activity. Semin Perinatol *19*, 31-40.

Santamaria, I., Pokharel, P.P., and Principe, J.C. (2006). Generalized correlation function: definition, properties and application to blind equalization. IEEE Trans signal Process. *54*, 2187-2197.

Sarkela, M., Mustola, S., Seppanen, T., Koskinen, M., Lepola, P., Suominen, K., Juvonen, T., Tolvanen-Laakso, H., and Jantti, V. (2002). Automatic analysis and monitoring of burst suppression in anesthesia. J Clin Monit Comput *17*, 125-134.

Schlembach, D., Maner, W.L., Garfield, R.E., and Maul, H. (2009). Monitoring the progress of pregnancy and labor using electromyography. Eur J Obstet Gynecol Reprod Biol *144 Suppl 1*, S33-39.

Schmitz, A. (2000). Measuring statistical dependence and coupling of subsystems. Physical Review E *62*, 7508.

Scho¨lkopf, B., and A., S. (2002). Learning with kernels. MIT press, Cambridge.

Schreiber, T. (1999). Interdisciplinary application of nonlinear time series methods. Physics Reports *308*, 1-64.

Schreiber, T., and Schmitz, A. (2000). Surrogate time series. Phys. D *142*, 346-382.

Schwarz, G. (1978). Estimating the Dimension of a Model. The Annals of Statistics *6*, 461-464.

Sello S, and J, B. (2000). Wavelet cross-correlation analysis of turbulent mixing from large-eddy-simulations. Physics/0003029-arxiv.org.

Shackman, A.J., McMenamin, B.W., Slagter, H.A., Maxwell, J.S., Greischar, L.L., and Davidson, R.J. (2009). Electromyogenic artifacts and electroencephalographic inferences. Brain Topogr *22*, 7-12.

Sheather, S.J. (2004). Density estimation. Statistical Science *19*, 588-597.

Shmigol, A., Eisner, D., and Wray, S. (1998). Properties of voltage-activated [Ca2+]i transients in single smooth muscle cells isolated from pregnant rat uterus. J Physiol *511*, 803-811.

Stam, C.J. (2005). Nonlinear dynamical analysis of EEG and MEG: review of an emerging field. Clin Neurophysiol *116*, 2266-2301.

Takens, F. (1981). Detecting Strange Attractors in Turbulence, Lecture Nontes in Mathematics. Springer *898*, 366-381.

Tass, P., Rosenblum, M.G., Weule, J., Kurths, J., Pikovsky, A., Volkmann, J., Schnitzler, A., and Freund, H.J. (1998). Detection of n:m Phase Locking from Noisy Data: Application to Magnetoencephalography. Physical Review Letters *81*, 3291.

Terrien, J., Hassan, M., Alexandersson, A., Marque, C., and Karlsson, B. Evolution of phase synchronization of the two frequency components of the electrohysterogram (EHG): Application to the detection of human labor. Conf Proc IEEE Eng Med Biol Soc *1*, 17-20.

Terrien, J., Hassan, M., Germain, G., Marque, C., and Karlsson, B. (2009). Nonlinearity testing in the case of non Gaussian surrogates, applied to improving analysis of synchronicity in uterine contraction. Conf Proc IEEE Eng Med Biol Soc *2009*, 3477-3480.

Terrien, J., Hassan, M., Marque, C., and Karlsson, B. (2008). Use of piecewise stationary segmentation as a pre-treatment for synchronization measures. Conf Proc IEEE Eng Med Biol Soc *2008*, 2661-2664.

Terrien, J., Steingrimsdottir, T., Karlsson, B., and Marque, C. (2010). Synchronization between EMG at Different Uterine Locations Investigated Using Time-Frequency Ridge Reconstruction: Comparison of Pregnancy and Labor Contractions. EURASIP Journal on Advances in Signal Processing *2010*, 10.

Torrence, C., and Compo, G.P. (1998). A Practical Guide to Wavelet Analysis. Bull. Amer. Meteor. Soc *79*, 61-78.

van der Heyden, M.J., Diks, C., Pijn, J.P.M., and Velis, D.N. (1996). Time reversibility of intracranial human EEG recordings in mesial temporal lobe epilepsy. Physics Letters A *216*, 283-288.

Verdenik, I., Pajntar, M., and Leskosek, B. (2001). Uterine electrical activity as predictor of preterm birth in women with preterm contractions. Eur J Obstet Gynecol Reprod Biol *95*, 149-153.

Vigario, R., Sarela, J., Jousmaki, V., Hamalainen, M., and Oja, E. (2000). Independent component approach to the analysis of EEG and MEG recordings. IEEE Trans Biomed Eng *47*, 589-593.

Vigario, R.N. (1997). Extraction of ocular artefacts from EEG using independent component analysis. Electroencephalogr Clin Neurophysiol *103*, 395-404.

Vinken, M.P., Rabotti, C., Mischi, M., and Oei, S.G. (2009). Accuracy of frequency-related parameters of the electrohysterogram for predicting preterm delivery: a review of the literature. Obstet Gynecol Surv *64*, 529-541.

Wendling, F., Bartolomei, F., Bellanger, J.J., and Chauvel, P. (2001). Interpretation of interdependencies in epileptic signals using a macroscopic physiological model of the EEG. Clin Neurophysiol *112*, 1201-1218.

Wendling, F., Bartolomei, F., and Senhadji, L. (2009). Spatial analysis of intracerebral electroencephalographic signals in the time and frequency domain: identification of epileptogenic networks in partial epilepsy. Philos Transact A Math Phys Eng Sci *367*, 297-316.

Weng, B., and Barner, K. (2008). Optimal Signal Reconstruction Using the Empirical Mode Decomposition. EURASIP Journal on Advances in Signal Processing *2008*, 12.

Widman, G., Schreiber, T., Rehberg, B., Hoeft, A., and Elger, C.E. (2000). Quantification of depth of anesthesia by nonlinear time series analysis of brain electrical activity. Phys Rev E Stat Phys Plasmas Fluids Relat Interdiscip Topics *62*, 4898-4903.

Winterhalder, M., Schelter, B., Hesse, W., Schwab, K., Leistritz, L., Klan, D., Bauer, R., Timmer, J., and Witte, H. (2005). Comparison of linear signal processing techniques to infer directed interactions in multivariate neural systems. Signal Processing *85*, 2137-2160.

Wu, D.Y., Cai, G., Yuan, Y., Liu, L., Li, G.Q., Song, W.Q., and Wang, M.B. Application of nonlinear dynamics analysis in assessing unconsciousness: a preliminary study. Clin Neurophysiol *122*, 490-498.

Wu, Z., and Huang, N. (2009). Ensemble Empirical Mode Decomposition: a Noise-Assisted Data Analysis Method. Advances in Adaptive Data Analysis *1*, 1-41.

Xu, Y., Haykin, S., and Racine, R.J. (1999). Multiple window time-frequency distribution and coherence of EEG using Slepian sequences and hermite functions. IEEE Trans Biomed Eng *46*, 861-866.

Young, R.C. (1997). A computer model of uterine contractions based on action potential propagation and intercellular calcium waves. Obstet Gynecol *89*, 604-608.

Young, R.C. (2000). Tissue-level signaling and control of uterine contractility: the action potential-calcium wave hypothesis. J Soc Gynecol Investig *7*, 146-152.

Young, R.C., and Hession, R.O. (1999). Three-dimensional structure of smooth muscle in term-pregnant human uterus. Obstet Gynecol *93*, 94-99.

Zarzoso, V., and Nandi, A.K. (2001). Noninvasive fetal electrocardiogram extraction: blind separation versus adaptive noise cancellation. IEEE Trans Biomed Eng *48*, 12-18.

Zhao, H., Cupples, W.A., Ju, K.H., and Chon, K.H. (2007). Time-varying causal coherence function and its application to renal blood pressure and blood flow data. IEEE Trans Biomed Eng *54*, 2142-2150.

Zou, R., and Chon, K.H. (2004). Robust algorithm for estimation of time-varying transfer functions. IEEE Trans Biomed Eng *51*, 219-228.

Zou, R., Wang, H., and Chon, K.H. (2003). A robust time-varying identification algorithm using basis functions. Ann Biomed Eng *31*, 840-853.